



*Horizon 2020 Work programme*

Food Security, Sustainable Agriculture and Forestry, Marine, Maritime and Inland Water Research and the Bioeconomy

*Call*

H2020-FNR-2020: Food and Natural Resources

*Topic name*

FNR-16-2020: ENZYMES FOR MORE ENVIRONMENT-FRIENDLY CONSUMER PRODUCTS

*FuturEnzyme:*

Technologies of the Future for Low-Cost Enzymes for Environment-Friendly Products

Final ID: 101000327

27/03/2024



# DATASETS OF ENGINEERED VARIANTS

DELIVERABLE NUMBER D5.6

MANUEL FERRER  
CSIC

## Document information sheet

<b>Work package:</b>	WP5, Enhancing enzymes through innovative engineering.
<b>Authors:</b>	Manuel Ferrer (mferrer@icp.csic.es), Laura Fernandez-Lopez (l.fernandez.lopez@csic.es), Peter N. Golyshin (p.golyshin@bangor.ac.uk), Patrick Shahgaldian (patrick.shahgaldian@fhnw.ch), Wolfgang Streit (wolfgang.streit@uni-hamburg.de), Pablo Pérez-García (pablo.perez.garcia@uni-hamburg.de), Karl E. Jaeger (k.-e.jaeger@fz-juelich.de), Rebecka Molitor (r.molitor@fz-juelich.de), Anne Timm (anne.timm@inofea.com), Rita Correro (rita.correro@inofea.com), Víctor Guallar (victor.guallar@bsc.es)
<b>Document version:</b>	1
<b>Date:</b>	31/03/2024
<b>WP starting date:</b>	01/08/2021
<b>WP duration:</b>	40 months
<b>WP lead:</b>	FHNW
<b>WP participant(s):</b>	FHNW, CSIC, BSC, Bangor, UHAM, UDUS, Inofea AG, BioSynth (previously EUCODIS)
<b>Deliv lead beneficiary:</b>	CSIC
<b>Dissemination Level:</b>	Confidential, only for members of the consortium (including the Commission Services)
<b>Type:</b>	Other
<b>Due date (months):</b>	34 months
<b>Contact details:</b>	Manuel Ferrer (CSIC; mferrer@icp.csic.es), Peter N. Golyshin (Bangor; p.golyshin@bangor.ac.uk), Karl E. Jaeger (UDUS; k.-e.jaeger@fz-juelich.de), Patrick Shahgaldian (FHNW; patrick.shahgaldian@fhnw.ch), Anne Timm (INOFEA; anne.timm@inofea.com), Víctor Guallar (BSC; victor.guallar@bsc.es)

1. Scope of Deliverable .....	3
2. Introduction.....	3
3. Mutants reported in Deliverables D5.3 and D5.4, updated .....	4
3.1. Multi-functional PluriZymes: ester-hydrolysis and proteolysis in one .....	5
3.2. Multi-functional PluriZymes: xylanase and ester-hydrolase in one .....	6
3.3. Multi-functional PluriZymes: ester-hydrolase and transaminase in one .....	11
3.4. A nano-pore forming protein engineered for PET degradation based on the PluriZyme concept ..	13
4. Mutants reported in Deliverable D5.2, updated .....	14
4.1. FE_Lip9 lipase engineering: for detergent and textile applications .....	14
4.2. Engineering FE_Lip5 by lid domain remodeling: for detergent applications .....	23
4.3. PEH_Paes_PE-H engineering: for textile applications .....	29
4.4. PET46 from <i>Candidatus Bathyarchaeota</i> engineering: for textile applications .....	30
4.5. Gen0105 and Kest3 engineering for detergent application .....	31
4.6. Gen0095 engineering for textile applications .....	36
4.7. TB035 engineering for textile applications.....	36
5. New mutants designed by genetic engineering and characterized .....	37
5.1. PE-H from <i>Halopseudomonas formosensis</i> (Pform_PE-H) .....	37
5.2. PE-H from <i>Halopseudomonas oceani</i> (Poce_PE-H) .....	38
5.3. Engineering of new PET44 variants .....	39
5.4. Engineering of EH <sub>37</sub> variants .....	41
5.5. Engineering of non-catalytic proteins into enzymes .....	42
6. Supramolecular engineered enzymes reported in Deliverable D5.5, updated .....	44
6.1. Fe_LipMRD9 (or Lip9) .....	45
6.2. PEH_Paes_PE-H_Y250S.....	46
6.3. EstLip_TB035 .....	46
6.4. EstLip_Dim (AT); 5. EstLip_Dim (ATH); 6. EstLip_Dim (ATP); 7. EstLip_Dim (ATB) .....	47
6.5. FE-Polur1 (AT); 9. FE-Polur1 (ATH); 10. FE-Polur1 (ATP); 11. FE-Polur1 (ATB) .....	47
6.6. EstLip_PTEST 1 (AT); 13. EstLip_PTEST (ATH); 14. EstLip_PTEST 1 (ATP); 15. EstLip_PTEST 1 (ATB)	47
6.7. CalA lipase.....	50
6.8. EH3 esterase .....	51
6.9. Laccase from <i>Trametes versicolor</i> .....	52
7. New supramolecular engineered enzymes .....	54
7.1. Lip9 protection through $\beta$ -cd supramolecular engineering .....	55
8. Conclusions and outlooks .....	61
9. Final remarks .....	62

## 1. Scope of Deliverable

As stated in the Grant Agreement, this deliverable will consist in the methodological details, detailed results and datasets informing about the performance, activity and stability of all engineered enzymes generated in the project.

## 2. Introduction

Enzyme engineering stands at the forefront of biotechnology, offering a promising avenue for tailored catalysts with diverse applications across industries. Within the framework of the FuturEnzyme project, a series of deliverables have been meticulously crafted to harness the power of enzyme manipulation, culminating in the design of engineered variants poised to revolutionize enzymatic processes in the 3 target sectors relevant to FuturEnzyme. The engineered work commences with Deliverable D5.1 (The shortlist of at least 18 enzymes nominated for engineering), where a meticulous selection process identifies a shortlist of enzymes primed for engineering. This initial phase lays the groundwork for subsequent advancements, setting the stage for targeted modifications aimed at enhancing enzyme functionality. Building upon this foundation, Deliverable D5.2 (Set of 18 mutants generated by genetic engineering) introduces a set of mutants generated through genetic engineering techniques. This pivotal step underscores the innovative approach adopted within the project, leveraging cutting-edge methodologies to sculpt enzymes with heightened performance and versatility. The concept of PluriZymes, as outlined in Deliverables D5.3 (Set of 4 PluriZymes with single activities) and D5.4 (set of 3 multi-purpose PluriZymes), represents a paradigm shift in enzyme design. By introducing additional active sites into existing enzyme scaffolds, researchers unlock a realm of possibilities, ranging from amplified catalytic efficiency to the facilitation of multi-step reactions. This approach, guided by computational insights and strategic mutagenesis, epitomizes precision engineering at the molecular level, heralding a new era of enzyme customization. Furthermore, Deliverable D5.5 (18 improved enzymes by supramolecular engineering) expands the horizon of enzyme engineering through supramolecular methodologies (enzyme immobilization and shielding) to enhance enzyme stability and functionality, paving the way for robust enzymatic systems capable of withstanding diverse environmental conditions. As we embark on Deliverable D5.6, the design of engineered variants reaches a crescendo, consolidating insights gleaned from preceding efforts while embracing new discoveries. This deliverable not only encapsulates the culmination of prior endeavors but also signifies a leap forward, with updated information and novel insights. Below, the main results and datasets are provided for the complete list of mutants engineered by genetic and supramolecular engineering techniques, using as starting point some of the enzymes selected as priority which are listed in [Table 1](#).

**Table 1.** Enzymes selected as priority targets, some been produced at large for validation purposes or are in the pipeline.

ID	Enzyme	Activity	Application <sup>1</sup>		
			D	T	C
1	Kest3	Esterase / Lipase	Yes	No	No
2.1	FE_Lip9	Esterase / Lipase / PETase	Yes	Yes (O)	No
2.2	FE_Lip9_mut	Esterase / Lipase / PETase	Yes	Yes	No
3	FE_ID 9	Esterase / Lipase	Yes	No	No
4	FE_polur1	Esterase / Lipase / PETase	Yes	Yes (O)	No
5	EstLip_Dim_#008	Esterase / Lipase	Yes	Yes (O)	No
6	EstLip_Paes_TB035	Esterase / Lipase	Yes	Yes (O)	No
7	EstLip_PtEst1	Esterase / Lipase	Yes	Yes (O)	No
8	EstLip_TBec304	Esterase / Lipase	Yes	Yes (O)	No
9	Paes_PE-H_Y250S	PETase	Yes	Yes (O)	No
10	PEH_Pbau_PE-H	PETase	Yes	Yes (O)	No
11	Pform_PE-H	PETase	Yes	Yes (O)	No
12	PEH_Poce_PE-H	PETase	Yes	Yes (O)	No
13	GEN0105	Esterase / Lipase	Yes	No	No
14	GEN0095	Cellulase	Yes	Yes	No
15	VD-V4_PL9	Hyaluronidase	No	No	Yes

16	VD_PL22	Hyaluronidase	No	No	Yes
17	VA-23_PL8A	Hyaluronidase	No	No	Yes
18	Hyal_HRDSV_2334	Hyaluronidase	No	No	Yes
19	VD-V4_GAGL	Hyaluronidase	No	No	Yes
20	VA-23_PL8B	Hyaluronidase	No	No	Yes
21	FE_EH37	Esterase / Lipase	Yes	Yes (O)	No
22	FE_Lip5	Esterase / Lipase	Yes	No	No
23	TR2E2	PluriZyme (Esterase / Transaminase)	Yes	No	No
24	EH <sub>1AB1C</sub>	PluriZyme (Esterase/Lipase/Protease)	Yes	No	No
25	X11_mut1	PluriZyme (Esterase / Xylanase)	Yes	No	No
26	[name]	Laccase	No	Yes (D)	No
27	pVec11	Peroxidase	No	Yes (D)	No
28	AB-Hyl_PL8	Hyaluronidase	No	No	Yes
29	DS-Hhyl_PL8	Hyaluronidase	No	No	Yes
30	LC1Hm_4133_PL8	Hyaluronidase	No	No	Yes
31	LC1Hm_4133_cut	Hyaluronidase	No	No	Yes
32	BCL_HA12 (3)-PL1	Hyaluronidase	No	No	Yes
33	BCL_HA12 (7)-PL1	Hyaluronidase	No	No	Yes
34	VS9_Bhyl_PL8	Hyaluronidase	No	No	Yes
35	LHYAL_HIRNI (from Leech)	Hyaluronidase	No	No	Yes
36	HYALP_HUMAN (HP-20 human sperm)	Hyaluronidase	No	No	Yes
37	APIME Hyaluronidase (bee venom)	Hyaluronidase	No	No	Yes
38	HYAL1 (hyaluronidase home sapiens)	Hyaluronidase	No	No	Yes
39	THET1 (from Thermobaculum terrenum)	Hyaluronidase	No	No	Yes
40	VS9_HylPL8	Hyaluronidase	No	No	Yes
41	VS2-Hhyl1PL8-1	Hyaluronidase	No	No	Yes
42	VS2-Hhyl1PL8-2	Hyaluronidase	No	No	Yes
43	VSALT_HhylPL8	Hyaluronidase	No	No	Yes
44	SSP_HhylPL8-1	Hyaluronidase	No	No	Yes
45	SSP_HhylPL8-2	Hyaluronidase	No	No	Yes
46	MCB-Hyl	Hyaluronidase	No	No	Yes

<sup>1</sup>Abbreviations: D, Detergents; T, Textiles; C, Cosmetics; O, Oil removal; D, Dye removal; Y, Yes; N, No.

### 3. Mutants reported in Deliverables D5.3 and D5.4, updated

- D5.3: Set of 4 PluriZymes with single activities
- D5.4: Set of 3 multi-purpose PluriZymes

Short Summary: Genetic engineering of enzymes has developed considerably over the last decades, opening great potential for applications such as greener production processes, by tuning substrate specificity and improving their catalytic properties under industrial settings. A novel approach to improve biocatalysts' performance was explored in FuturEnzyme: the addition of new active sites to already existing enzymes, or what was coined the PluriZyme strategy. The concept of PluriZyme involves the innovative design of new active sites within protein structures, including enzymes with one native active site. The process of adding artificial active sites is facilitated by the use of Protein Energy Landscape Exploration (PELE), a software tool that enables the identification of suitable regions within a protein scaffold. These regions are selected based on their potential to accommodate a specific substrate that is targeted for transformation. Once a suitable site is identified, computational analysis is employed to mutate nearby amino acids. This mutation process is crucial as it allows for the incorporation of necessary amino acids that are essential for catalysis to occur. The approach is highly strategic, focusing on the precise modification of the protein's active site to achieve desired catalytic functions. The novelty of this approach compared to state of art, can be summarized as follows: (i.) Targeted Design: Unlike traditional methods that often rely on random or semi-random mutagenesis, the PluriZyme approach uses targeted design. This specificity allows for more efficient and predictable modifications, leading to potentially higher success rates in enzyme design; (ii.) Computational Efficiency: The use of PELE software streamlines the process of identifying and modifying active sites. This

computational approach can significantly reduce the time and resources needed compared to experimental trial-and-error methods; (iii.) Precision at the Molecular Level: The ability to mutate specific amino acids for accommodating substrates offers a level of precision that is not always achievable with other methods. This can lead to the creation of enzymes with highly specialized and novel catalytic abilities; (iv.) Potential for Complex Substrate Processing: Given its precision and specificity, the PluriZyme approach could be particularly effective in designing enzymes capable of processing complex or unusual substrates, which might be challenging with traditional enzyme engineering methods; and (v.) Integration with Existing Protein Scaffolds: This method allows for the modification of existing enzyme scaffolds, which can be advantageous over designing entirely new enzymes. It leverages the stability and well-characterized nature of existing proteins while imbuing them with new functionalities

### 3.1. Multi-functional PluriZymes: ester-hydrolysis and proteolysis in one

Within FuturEnzyme, we have designed a multi-purpose PluriZyme is the PluriZyme  $\text{EH}_{1\text{AB}1\text{C}}$  that has up to three different active sites: the two ester-hydrolytic active sites (referred with the subscript A and B), and a new one (referred with the subscript C) supporting proteolytic activity. The design of such PluriZyme sought two different ends. First, designing a PluriZyme with two different functionalities, in this case, esterase and protease activities that allow two reactions in one-pot. Second, producing a catalytically-efficient protease. This second issue is important as proteases are almost as abundantly discovered in metagenomic searches as esterases, they usually find expression problems and only 1% can be efficiently produced, in juxtaposition to esterases. Proteases are instrumental for the hydrolysis of amide bonds in rich-protein materials such as food waste, and this is why these proteins are key for the formulation of detergents. However, proteases are difficult to be produced and that's why many and diverse efforts in pursuit of new proteolytic enzymes that are efficient and easily produced are being made. In brief, we have recently successfully found and designed, by introducing a few mutations, a second artificial active site (Ser-His-Asp) in an esterase containing a native site to generate a PluriZyme,  $\text{EH}_{1\text{AB}1}$ , with two efficient biological active sites for the ester hydrolysis that coexists in a close region. Compared to the natural triad (referred to as  $\text{EH}_{1\text{A}1}$ ), the newly introduced artificial site (referred to as  $\text{EH}_{1\text{B}1}$ ) is slightly more solvent exposed and located at an  $\sim 10$  Å distance. We have considered increasing the number of chemical reactions within this enzymatic design (Fig. 1A).

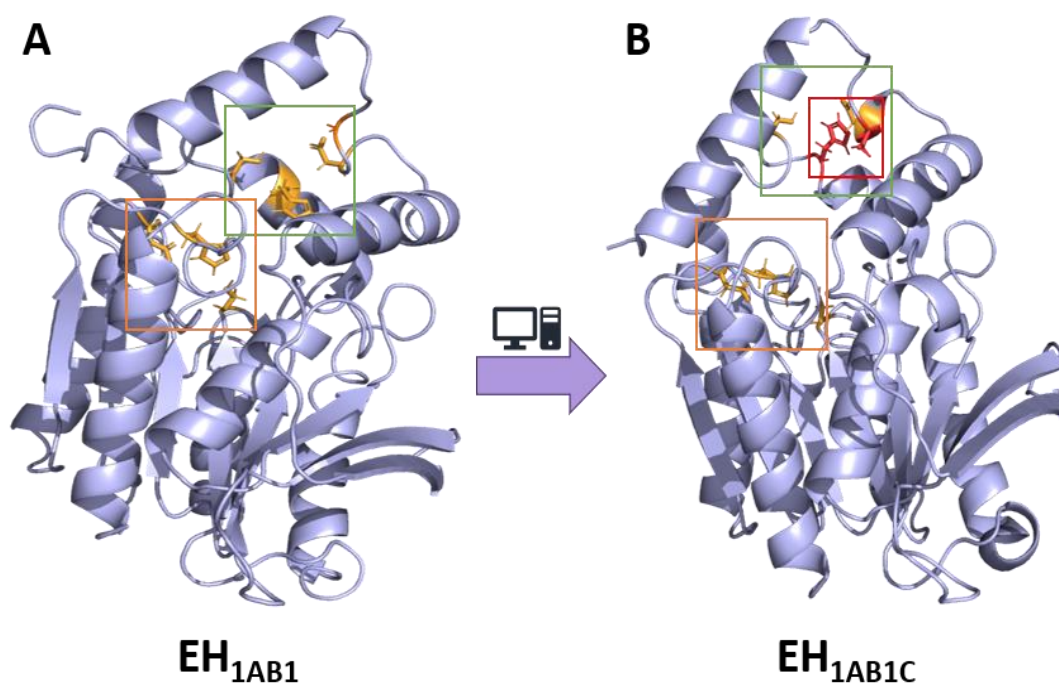


**Fig. 1.** Schematic representation of the design of a protease-esterase PluriZyme  $\text{EH}_{1\text{AB}1\text{C}}$ . A) The target was the PluriZyme  $\text{EH}_{1\text{AB}1}$ , that contained two ester hydrolyase active sites, one native ( $\text{EH}_{1\text{A}}$ , orange) and one artificially introduced ( $\text{EH}_{1\text{B}1}$ , green). B)  $\text{EH}_{1\text{AB}1\text{C}}$  was further designed by introducing catalytic residues supporting proteolytic activity in the vicinity of the artificially introduced B1 (red).

In particular, we considered the incorporation of a new active center to support another reaction, namely, proteolysis, to explore the possibility of designing an in-one protease-esterase PluriZyme. For this purpose, we performed a local PELE exploration with multiple dipeptides, namely, AH, AQ, DI, EA, FF, KA, LA, LL, NV, PF, QQ, RG, SW, TM, YN and YY. Following the inspection of the best enzyme-substrate poses, we decided to introduce the Leu24Cys variant, named EH<sub>1AB1C</sub>, which, together with the catalytic histidine of EH<sub>1B1</sub>, His214, could introduce a catalytic dyad similar to those seen in cysteine proteases, and that could hydrolyse proteins like casein and peptides. By introducing this mutation, a newly designed PluriZyme, herein referred to as EH<sub>1AB1C</sub>, included three potential sites (Fig. 1B). The first supports ester hydrolysis through a native catalytic triad (Ser161, Asp256 and His286) and an oxyanion hole (Gly88, Gly89 and Gly90), with Ser161 being the nucleophile. The second, also supporting ester hydrolysis, would employ an artificial catalytic triad (Ser211, Asp25 and His214) with Ser211 as the nucleophile and an oxyanion hole (Gly207, Tyr208 and Phe209). The third would support the protease activity through a catalytic dyad (Cys24 and His214). The resulting artificial enzyme, EH<sub>1AB1C</sub>, have been shown to efficiently hydrolyse (azo)casein at pH 6.5–8.0 and 60–70 °C. The presence of both esterase and protease activities in the same scaffold allowed also the one-pot cascade synthesis (55.0 ± 0.6% conversion, 24 h) of L-histidine methyl ester from the dipeptide L-carnosine in the presence of methanol.

The results demonstrate that active sites supporting proteolytic activity can be artificially introduced into an esterase scaffold to design easy-to-produce in-one protease-esterase PluriZymes for cascade reactions, namely, the synthesis of amino acid esters from dipeptides. It is also possible to design artificial proteases with good production yields, in contrast to natural proteases that are difficult to express. In a general sense, this also serves as a proof of concept for the design of PluriZymes with reactive groups supporting different chemistry, as well as the design of easily-expressed artificial proteases by incorporating a proteolytic active site into ester hydrolases that can be easily expressed. This proteolytic PluriZyme can be a detergent or detergent additive capable of removing protein stains. For methodological details, detailed results and datasets (open access), see [Fernandez-Lopez et al. 2022](#).

### 3.2. Multi-functional PluriZymes: xylanase and ester-hydrolase in one

We further approach building a secondary catalytic site that confers esterase activity into an extremophilic xylanase, Xyn11, from *Pseudothermotoga thermarum*. The idea is to insert an esterase catalytic triad in a xylanase to increase the rate of the enzyme due to debranching (Fig. 2). More in detail, to insert a serine, histidine, and aspartic catalytic triad to grant the enzyme with feruloyl esterase activity, and once debranched, the polymer could flow through the wild-type active site faster, enhancing the wild-type activity.

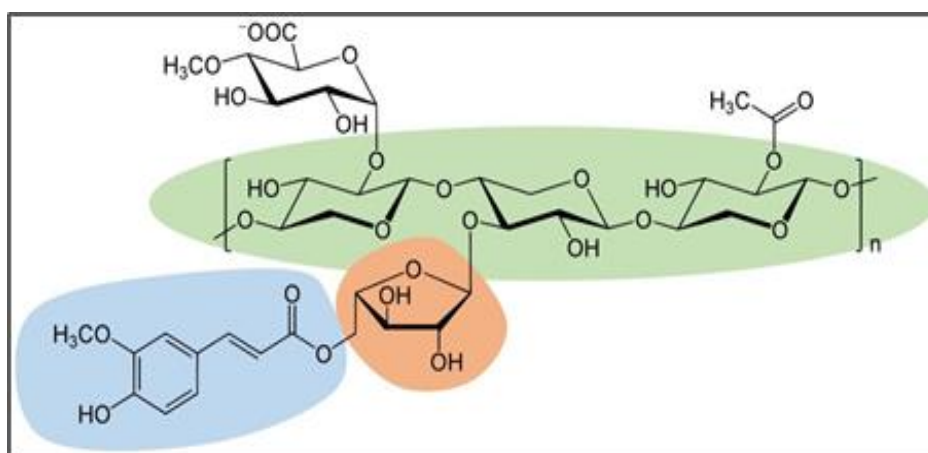


Fig. 2. Schematic representation of the xylan polymer with ramifications.

To search for suitable binding sites for the feruloyl arabinose ligand, we employed the global exploration PELE protocol. With this method, the ligand explores, with enough sampling, the entire surface, and the best binding energy minima can be identified. After the simulation, a significantly enclosed pocket was found to bind the feruloyl part of the ligand with slightly better binding energies.

At this point, as the energies did not show a significant minimum, some mutations were added to enhance the stabilization of the ligand inside the found cavity. Ten different mutants were tested with PELE simulations using the feruloyl arabinose ligand, and the one with the best binding energy minimum was selected, which is mutant 10 (Fig. 3), with the mutations V256S and K331Q.

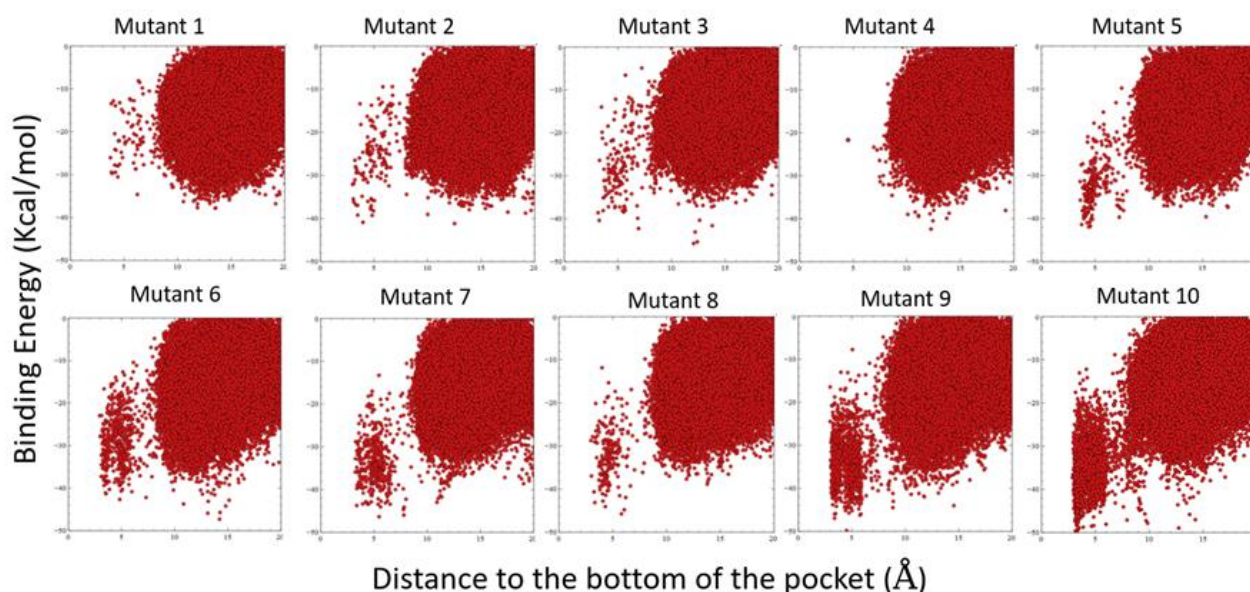


Fig. 3. PELE simulations for each of the 10 mutants proposed to accommodate the ligand in the active site.

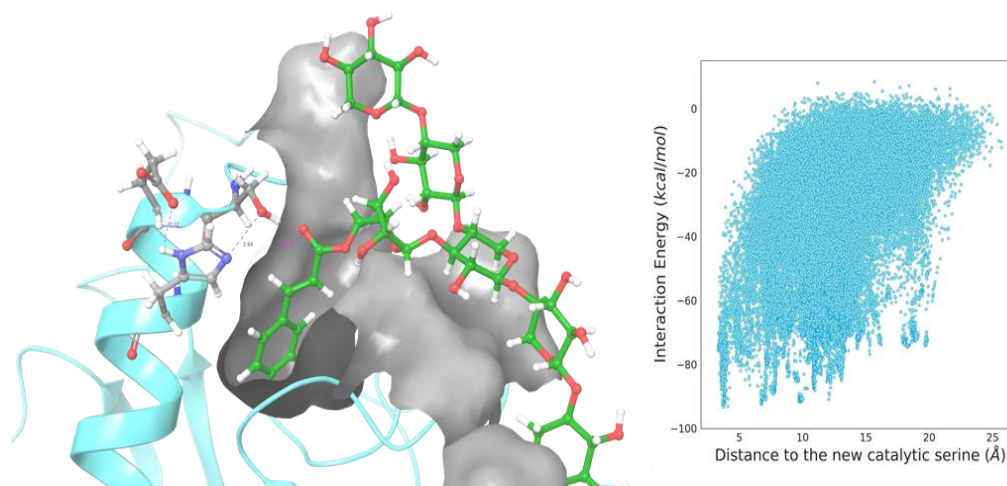
Once suitable mutations were selected to enhance the interaction energy of the ligand inside the binding site, several catalytic triads composed of Serine, Histidine, and aspartate were proposed (Table 2). All 4 triads were tested with and without the mutations of the pocket using PELE. In Fig. 4, results for the Triad 1 without Pocket mutations are shown.

Table 2. Triads proposed and tested with PELE.

	Serine	Histidine	Aspartic
Triad 1	L271S	K275H	Wild type
Triad 2	L271S	L274H	K275D
Triad 3	K331S	Q329H	Wild type
Triad 4	K331S	D325H	Q329D

PELE results were validated using MD simulations. Among all the combinations, mutants selected were L271S, K275H, called Xyn11\_mut1; L271S, K275H, V256S, L274A, K331Q, called Xyn11\_mut2, and K331S, D325H, Q329D, V256S, L274A, called Xyn11\_mut3. The best mutants were sent to CSIC to test them in experimental assays. Synthetic genes (codon-optimized) of sequences encoding three selected xylanase mutants (Xyn11\_mut1, Xyn11\_mut2 and Xyn11\_mut3) were purchased from Integrated DNA Technologies (IDT). The mutant xylanases encoding plasmids were used for transforming *E. coli* XL1 Blue and further transferred to *E. coli* Rosetta (Stratagene) for protein production. Briefly, cell crude extracts were obtained from *E. coli* cultures grown at 37 °C until reaching OD600 of 0.6 and then were induced with 1 mM IPTG at 37 °C for 5 h.

After disruption by sonication the mutants were purified by heat shot at 90°C followed by protein purification using nickel affinity chromatography. The three mutants from which we obtained the synthetic gene produce very well in *E. coli*, producing mutants at 11-25 mg per litre of culture. Stock solutions were prepared at concentrations from 1.4 to 3.2 mg/ml. Once produced, the activity tests of Xyn11\_mut1, Xyn11\_mut2 and Xyn11\_mut3 were performed. The esterase activity was firstly assessed using a pH indicator assay in 384-well plates (ref. 781162, Greiner Bio-One GmbH, Kremsmünster, Austria) at 90°C and pH 8.0 in a Synergy HT Multi-Mode Microplate Reader in continuous mode at 550 nm over 0.5-1.0 min (extinction coefficient of phenol red, 8450 M<sup>-1</sup>cm<sup>-1</sup>). The acid produced after ester bond cleavage by the hydrolytic enzyme induced a color change in the pH indicator that was measured spectrophotometrically at 550 nm. Using the pH-indicator assay (pH 8.0, 90 °C) the capacity to hydrolyse a set of 96 structurally different esters according to the Tanimoto-Combo similarity score, were tested, that include cinnamate and ferulate esters such as phenylethyl cinnamate, isobutyl cinnamate, methyl 2,5-dihydroxycinnamate, methyl cinnamate and methyl ferulate. Xyn11\_mut3 did show activity only against methyl 2,5-dihydroxycinnamate (30.8±0.9 units/g) and too much lower extent methyl ferulate (8.46±0.3 units/g). Xyn11\_mut1 showed much higher esterase activity in assays with the synthetic substrate methyl ferulate, with Km of 2.8±0.6 mM and Vmax of 1641±10 units/g). This activity is in the range of best performing esterases and lipase capable of degrading methyl ferulate, e.g., CalB (1270 U/g, pH 8.0, 30°C). Xyn11\_mut2 did not show appreciable activity under the assay conditions for any of the synthetic substrates.



**Fig. 4.** PELE exploration and binding energy profile of the 3 mutants of Xyn11 with feruloyl arabinose.

The xylanase activity was further determined. For that, the assay conditions for xylanase activity are pH 9.0 and 90°C, optimal conditions for Xyn11 wild type. Buffer is Tris HCl, 20 mM, 50 mM NaCl, pH 9.0. For the reaction with xylan used is 1% xylan in Tris ClH, 20 mM, 50 mM NaCl, pH 7.0. To prepare the xylan (100 mL suspension), 60 mL of the buffer are heated to 60°C under stirring, and then 1 g of wheat bran xylan is added, and bring to boil. The suspension is stirred overnight (cooling) and top up with water (mQ) to make up the remaining 60 mL (some evaporates) and then add the remaining 40 mL of buffer. This suspension is aliquoted and frozen before it is used in the experiments (in the fridge the xylan degrades due to the action of the fungi). For the xylanase assays, 20 µl of enzyme (1/300 dilution) + 180 µl of wheat bran xylan in Tris ClH, 20 mM, 50 mM NaCl, pH 7.0, and incubate it for 10 minutes at 90°C. The reaction is stopped on ice before adding the reactive DNS (100 µl) and boiled for 10 minutes, and the amount of reducing sugars is determined. The wild type Xyn11 showed an activity of 545 micromol reducing sugars (xylose) / min x mg enzyme. We found that Xyn11\_mut1 has higher levels of xylanase activity to Xyn11 (136 micromol reducing sugars (xylose) / min x mg enzyme), whereas Xyn11\_mut2 and Xyn11\_mut3 have much lower levels: 6 and 3 micromol reducing sugars (xylose) / min x mg enzyme, respectively. We further found that both Xyn11 wild type and Xyn11\_mut1 were unable to cut xylobiose, but were active against xylotriose, xylotetraose, xylopentaose and xylohexaose yielding mainly xylose and xylobiose.

Note that wheat bran xylan contains about 0.7% ferulic acid in its structure, and the higher degradation rate of this polymer in the presence of Xyn11\_mut1 may be due to the presence of feruloyl esterase activity in this enzyme design compared to the Xyn11 wild type that will allow the degradation of the feruloyl moieties within the xylan polymer by the artificially introduced active site, rendering the xylan backbond to be more easily degraded by the native xylanase active site. The location of the native and artificial active sites is shown in Fig. 5.

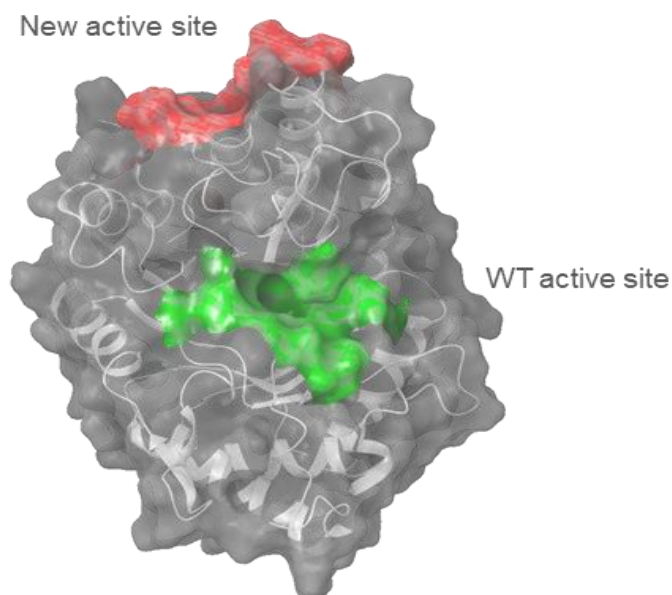
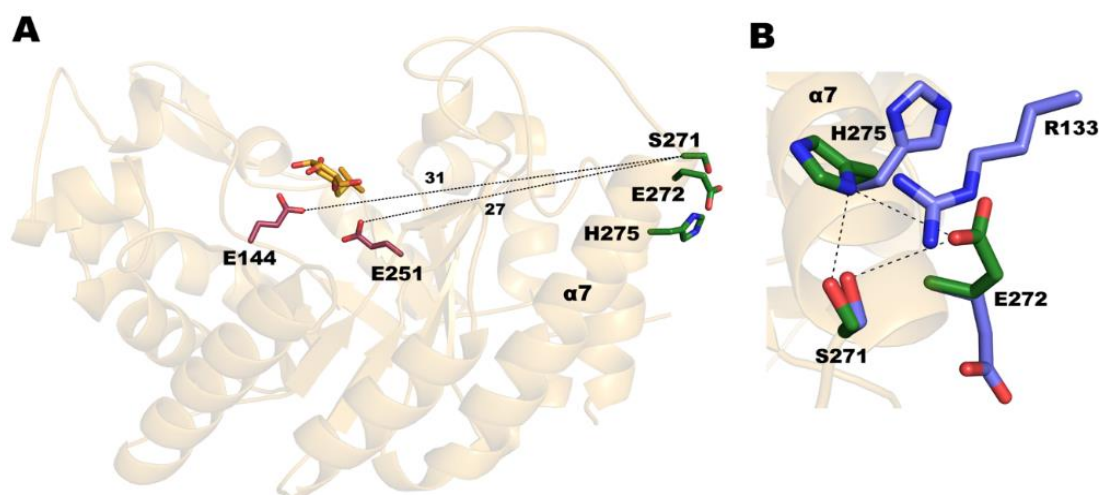


Fig. 5. Xyn11-mut1 folding with the native and artificially introduced active sites shown.

In order to unambiguously demonstrate the presence of both active sites we have solved the structure of the PluriZyme Xyn11-mut1 (8BBI - <https://www.ncbi.nlm.nih.gov/Structure/pdb/8BBI>). The crystal structure of mutant 1 of Xyn11 was obtained by X-ray diffraction at 2.1 angstrom. It shows a TIM barrel architecture typical of GH10 xylanases. The intrinsic xylanase active site, located at the axis of the barrel, is formed by the pair Glu144 and Glu251 and includes a trapped IPTG molecule. Using the software PELE allowed to create a second artificial catalytic site located on the surface of the protein at 27 Å and 31 Å from Glu251 and Glu144, respectively (Fig. 6A). Mutagenesis experiments were performed to create the double mutant (Xyn11-Mut1) L271S and K275H. The second artificial esterase catalytic triad is formed by residues Ser271, Glu272 and His275, at the beginning of  $\alpha 7$  (Fig. 6A). There are no significant structural differences upon superimposition of Xyn11 onto the Xyn11-Mut1 coordinates. However, as happened in the native crystal, Xyn11-Mut1 crystals contain two molecules in the asymmetric unit that present some conformational differences at the artificial esterase catalytic triad. Thus, only chain B presents the Ser271-Glu272-His275 triad in a proper conformation that displays the expected hydrogen bonding pattern conserved in reported esterases (Fig. 6B). In chain A, Arg133, from a symmetry related molecule, is making a hydrogen bond to Ser271 producing a shift in Glu272 and His275 side-chains.

Attempts to crystallize Xyn11-Mut1 with different irreversible inhibitors were performed, but the ligand was not captured in the crystal. Therefore, docking simulations were performed to depict the Xyn11-Mut1 artificial esterase site by using molecule B coordinates, which presents an active conformation of its catalytic triad. Ethyl 4'-hydroxy-3'-methoxycinnamate, an ethyl derivative of ferulic acid (PDB code 3PFB, in violet), was docked into molecules B using Autodock Vina, and residues underlining the catalytic site were considered flexible. Among all results obtained, the best solution shown in Fig. 7A was selected on the basis of a productive interaction of the ligand with the catalytic triad. A series of minor conformational changes are observed in the flexible residues upon ligand binding to allocate the substrate. The ligand adopts the

tetrahedral conformation typical of the intermediate of ester hydrolases where the nucleophilic serine is located under the carbonyl group to produce the attack, with the oxygen being close to two glycines that stabilize the formed oxanion (Wang et al. 2018). However, in this case, it seems that the oxygen from the carbonyl group could be stabilized by His275 from the catalytic triad Fig. 7A that, in turn, could be hydrogen linked to the catalytic Glu272. Additional hydrogen links could be establishing the ferulic moiety to Asp325 and Gln329 side-chains. Furthermore, to the best solution obtained by the docking simulations, arabinose, xylose and ferulic acid units can be manually attached to the ligand to illustrate the putative binding of xylan (Fig. 7B). As shown in the figure, the polymeric xylose chain would extend far from the protein surface therefore having no impediment to allocate its terminal ferulic moieties into the artificial esterase active site of Xyn11-Mut1.



**Fig. 6.** A) Xyn11-Mut1 folding. The intrinsic xylanase catalytic pair is shown as raspberry sticks (Glu144 and Glu251) whereas the artificial secondary esterase triad is shown as green sticks (Ser271, Glu272 and His275). The trapped IPTG molecule is shown as orange sticks. B) Superimposition of chain A (blue) and chain B (green) at the artificial esterase secondary catalytic site. The catalytic triad of molecule B shows the proper hydrogen bond pattern conserved among esterases.

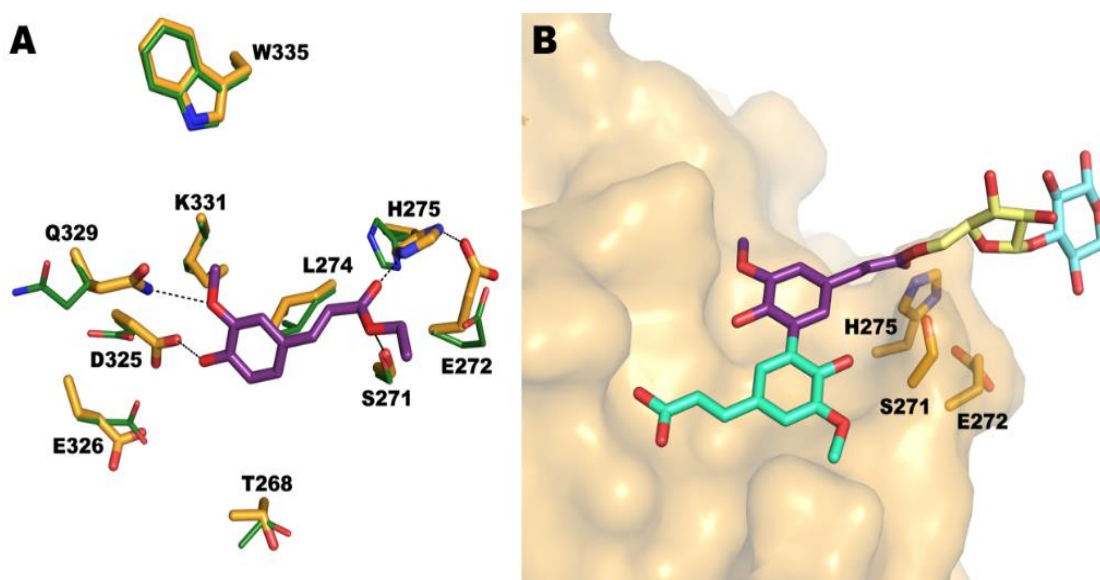


**Fig. 7.** A) Best model obtained after automatic docking of ethyl 4'-hydroxy-3'-methoxycinnamate (in violet) within the artificial esterase active site of Xyn11-Mut1. The residues considered flexible are shown as sticks (in orange), highlighting the conformational changes from the free state (in forest). Hydrogen bonds are shown as dashes while covalent bond is shown as continuous line. B) Arabinose (in yellow), xylose (in cyan) and ferulic acid (in green) units have been manually built to the automatically docked substrate to illustrate the putative binding of a xylan template. The cavity of the artificial second active site is depicted by the surface of the protein (in orange). The catalytic triad is shown as orange sticks.

The results demonstrate that active sites supporting ferulolytic activity can be artificially introduced into an xylanase scaffold to design a PluriZyme with xylanase and esterase activity. This PluriZyme mutant can be a detergent or detergent additive capable of removing plant stains. For structural datasets (open access) see Protein Data Bank number [8BBI](#).

### 3.3. Multi-functional PluriZymes: ester-hydrolase and transaminase in one

The above two examples demonstrated that the design of PluriZymes with two biologically active sites supporting different chemistries, in particular esterase and protease activities, and esterase and xylanase activities, is feasible. A third approach to design PluriZymes with different biological reactivities was undertaken. For this purpose, we select as scaffold a class III  $\omega$ -transaminase, TR<sub>2</sub>, isolated through metagenomic techniques, and added an artificial catalytic triad Ser-His-Asp supporting ester-hydrolysis. By using the PELE computational methods, a total of 20 mutants of the TR<sub>2</sub> enzyme were selected for investigations and synthesized; a priori, based on computational data, they may contain one active site supporting the original transaminase activity and a second active site with esterase activity. The mutants were produced and purified and their transaminase and esterase activity tested. Only one mutant, TR<sub>2</sub>E<sub>2</sub> (with A172S and Q173H mutations) was confirmed as having both activities. The transaminase activity of R<sub>2</sub>E<sub>2</sub> was unaffected by the mutations compared to that of the native TR<sub>2</sub>, while the introduced esterase active site astoundingly active with a wide range of chemically and structurally diverse esters. Functional and structural characterization of the native TR<sub>2</sub> and the PluriZyme TR<sub>2</sub>E<sub>2</sub> confirmed the presence and functionality of both active sites. Subsequently, TR<sub>2</sub>E<sub>2</sub> PluriZyme was successfully used in the one-step transformation of 3-oxo-4-(2,4,5-trifluorophenyl) methyl butanoate into 3-amino-4-(2,4,5-trifluorophenyl) butanoate with excellent conversion rate and enantioselectivity. Kinetic and follow-up reactions confirmed the reaction mechanism. In brief, the reaction proceeds first by the hydrolysis of the  $\beta$ -keto ester in the artificial site and then by the amination of the  $\beta$ -keto acid in the native site. The transfer of the reaction intermediates from one site to other was confirmed by mutational analysis. Furthermore, to demonstrate the versatility of this PluriZyme for cascade reactions (Fig. 8), its activity with seven other  $\beta$ -keto esters to produce  $\beta$ -amino acids was confirmed.

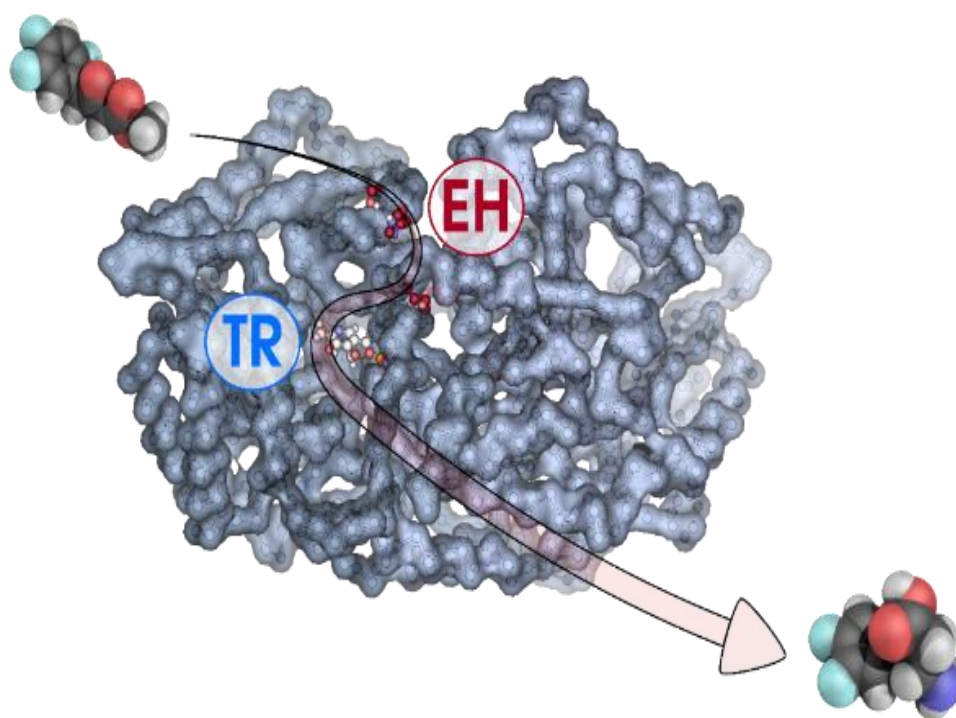


**Fig. 8.** A PluriZyme with transaminase and esterase activity that can carry out the one-pot cascade transformation of  $\beta$ -keto esters into  $\beta$ -amino acids using a single protein scaffold.

Further structural characterization of the native TR<sub>2</sub> (<https://www.ncbi.nlm.nih.gov/Structure/pdb/7QYG>) and the free PluriZyme TR<sub>2</sub>E<sub>2</sub> (<https://www.ncbi.nlm.nih.gov/Structure/pdb/7QYF>) and in complex with the inhibitor ethanolamine O-sulphate (EOS) (<https://www.ncbi.nlm.nih.gov/Structure/pdb/7QX3>) and the cofactor pyridoxal-5'-phosphate (PLP)PEP (<https://www.ncbi.nlm.nih.gov/Structure/pdb/7QX3>), confirmed the presence and functionality of both active sites. The structures of with type TR<sub>2</sub> transaminase and TR<sub>2</sub>E<sub>2</sub> PluriZyme (transaminase+esterase) are shown in Fig. 9.

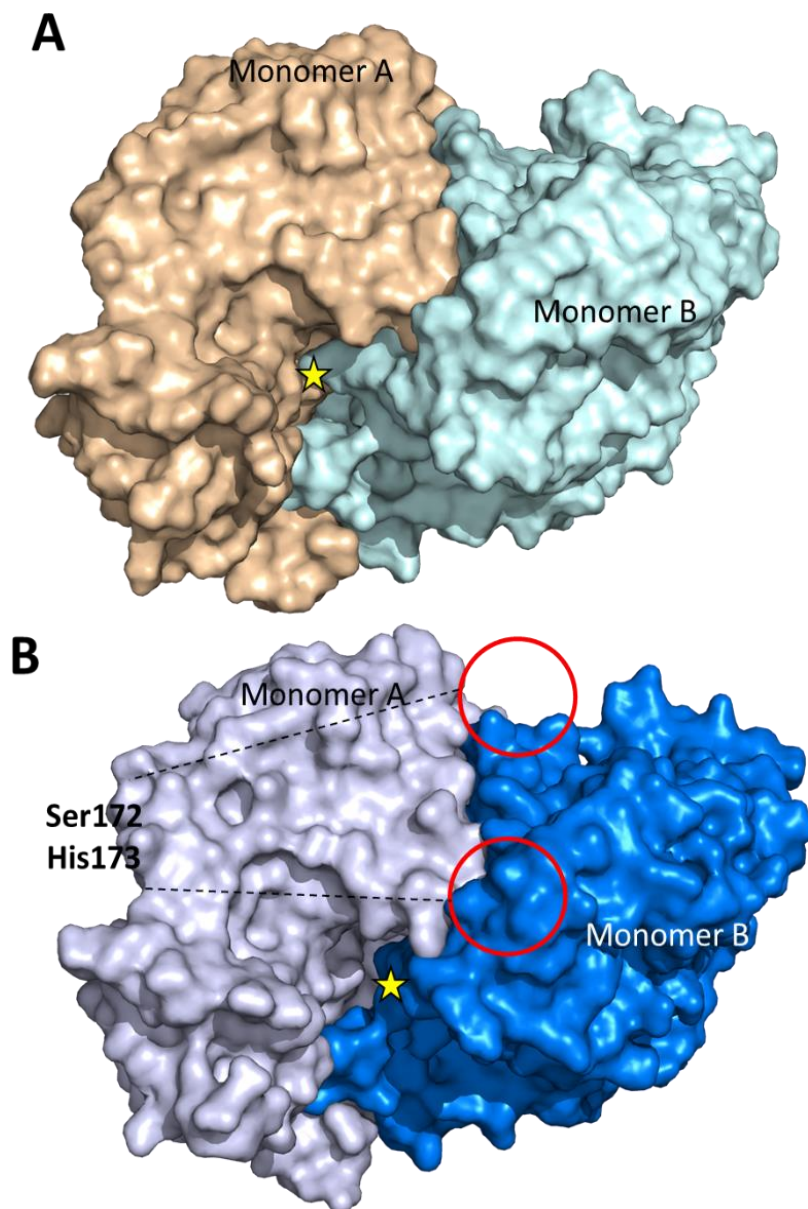


**Fig. 9.** A) Surface representation of the TR<sub>2</sub> dimer with highlighted transaminase binding site (red circle). B) Surface representation of the TR<sub>2</sub>E<sub>2</sub> dimer with a highlighted transaminase binding site (red circle). The positions of the Ser172 and His173 mutations are colored magenta. The figure was created using PyMOL Version 2.3.2.

The results demonstrate that active sites supporting esterase activity can be artificially introduced into a transaminase scaffold to design a PluriZyme with transaminase and esterase activity. This PluriZyme mutant can be relevant for applications others than those to be priority in FuturEnzyme. For methodological details, detailed results and datasets (open access), see [Roda, Fernandez-Lopez et al. 2022](#), and Protein Data Bank accession numbers [7QYG](#), [7QYF](#), and [7QX3](#).

3.4. A nano-pore forming protein engineered for PET degradation based on the PluriZyme concept

For the fourth PluriZyme designed, BSC and CSIC explored the possibility of enzymatically recycling polyethylene terephthalate (PET), particularly for the case of polyester (PES) fabrics and their macro-, micro- and nanosized particles, e.g., in waste streams during textile processing. Results on building additional sites to PETases are still not satisfactory enough, possibly indicating the difficulty to establish an open and large enough site to bind and degrade PET. Since the PluriZyme workflow, capable of building catalytic triads, can be implemented into any protein, we turned our efforts into adding triads into a protein that could trap nanoparticles of PET efficiently (Fig. 10). For this, we chose the homo-octamer membrane biological assembly crystal structure of *Fragaceatoxin C* (FraC, PDB-ID 4TSY). We selected this protein scaffold for its pore dimensions, stability, and compartmental localization in membranes. We introduced esterase catalytic activity in two newly designed active sites and finally checked that they could be applied for PET nanoparticles degradation.

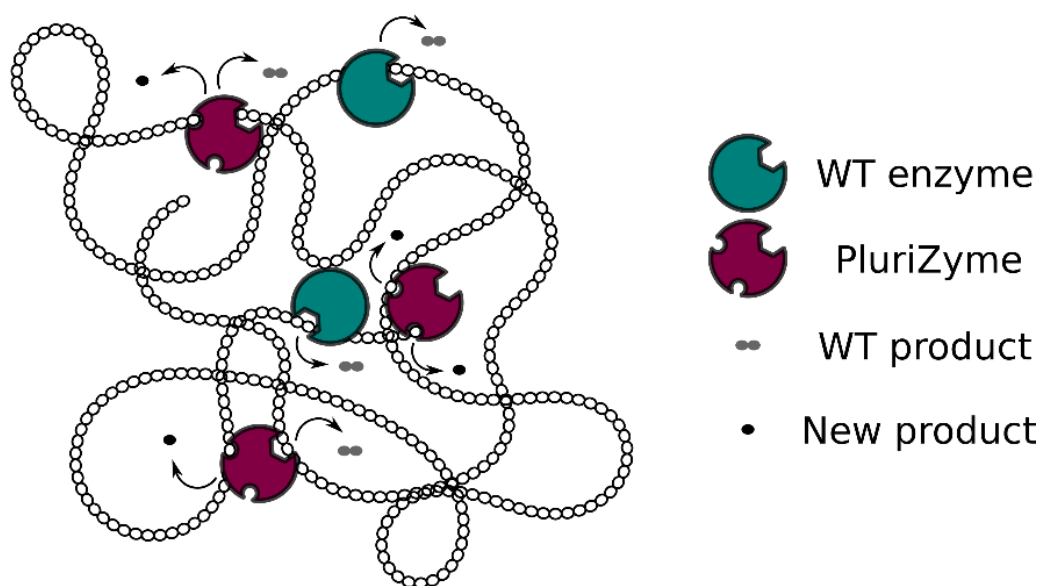


**Fig. 10.** Example of a PluriZyme design for polymer degradation. The addition of a new active site with different biochemistry to the WT enzyme scaffold can release new products of interest.

The first active designed mutant (FraC<sub>m1</sub>) located the triad in the alpha helix N terminal domain, where non-conserved polar residues face the channel cavity of the pore. We rationally inserted two mutations, K20H and T21S, in the eight monomers, creating a new enzymatic complex with eight potential different active sites. In addition, the preexistence of two acidic residues, at positions 17 and 24, increased the number of possible combinations of catalytic triad formations. The second active designed mutant (FraC<sub>m2</sub>) located the triad in an area where several acidic residues—Asp38, Glu40, and Glu173— are located; in this case, there is also a native histidine, His175; PELE simulations revealed that the Asp38Ser variant could generate a catalytic triad. Moreover, we wanted to add a mutation that could act as an oxyanion hole to stabilize the negative charge that appears during hydrolysis: Glu173Gln. Finally, a double mutant (FraC<sub>m3</sub>) combining the mutations in FraC<sub>m1</sub> and FraC<sub>m2</sub> was designed, which since contains two active sites can be referred to as a PluriZyme. As shown in Fig. 11, one could imagine that any nanoparticle (or nanoparticle protuberance such as the one shown in Fig. 11, that was obtained from molecular dynamics simulations) that gets stacked in the pore will have 8 scissors pointing at it and ready to cut the ester bonds. As a result, our FraC variants achieve one order of magnitude higher degradation rates than the current best PETases, when operating on PET nanoparticles. In addition, our constructs also hydrolyze multiple esters substrates.

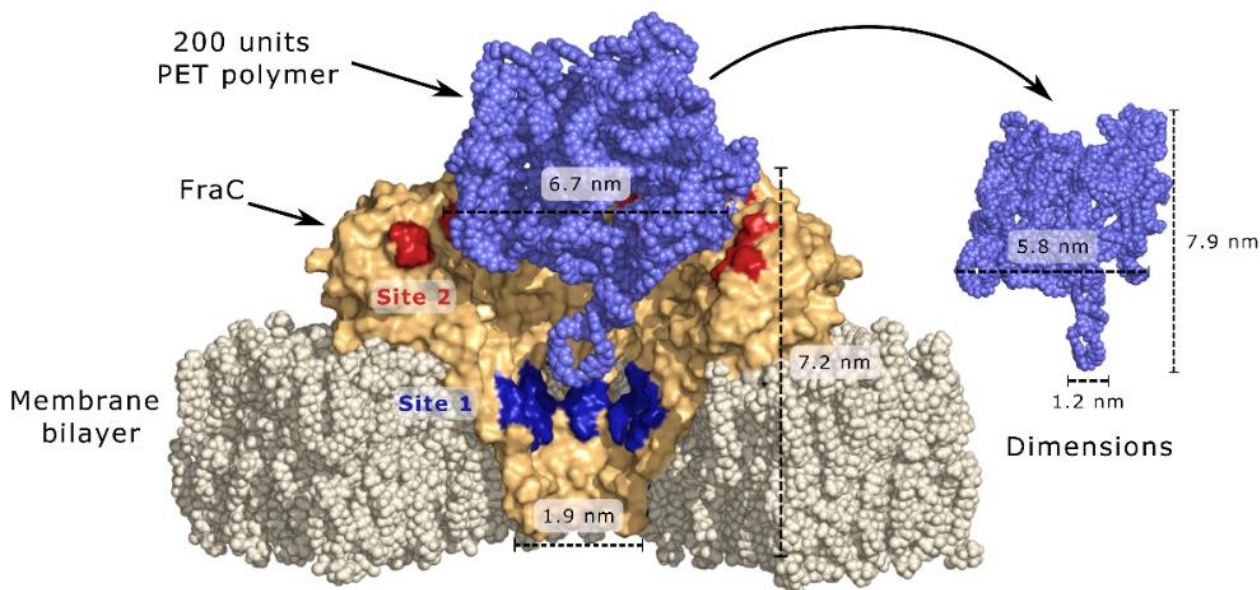


**Fig. 11.** Graphical representation of a schematic coupling between the pore and the PET particle polymer. The artificial sites 1 (FraC<sub>m1</sub>) and 2 (FraC<sub>m2</sub>) are color coded.

The results demonstrate that the methodology to design PluriZymes can be also applied to design novel biocatalytic nanopores for recycling of polyester (PES) fabrics and their macro-, micro- and nanosized particles, e.g., in waste streams during textile processing. For methodological details, detailed results and datasets (open access), see [Robles-Martín, Amigot-Sánchez, Fernández-Lopez et al. 2023](#).

**Conclusions Section 3. A novel approach to improve biocatalysts' performance, namely, the addition of new active sites to already existing enzymes, or what was coined the PluriZyme strategy, has been validated. Based on this engineering approach, to date, we have successfully generated 5 engineered enzymes: (i.) 3 PluriZymes with multipurpose-functionalities, namely, one PluriZyme with protease and esterase activity, one PluriZyme with transaminase and esterase activity, and one PluriZyme with xylanase and esterase activity; 2 engineered mutants of the pore-forming protein Fragaceatoxin C (FraC, PDB-ID 4TSY) (FraC<sub>m1</sub> and FraC<sub>m2</sub>) for the recycling polyethylene terephthalate (PET), particularly for the recycling of polyester (PES) fabrics and their macro-, micro- and nanosized particles, e.g., in waste streams during textile processing.**

#### 4. Mutants reported in Deliverable D5.2, updated

- D5.2: The set of mutants generated by genetic engineering

Short Summary: Genetic engineering of enzymes has developed considerably over the last decades, opening great potential for applications such as greener

##### 4.1. FE\_Lip9 lipase engineering: for detergent and textile applications

Lip9 was nominated for detergent and textile application as it is capable to degrade all the stained fabrics tested (pigments with oil on polyester/cotton (PC-09), mayonnaise on cotton (C-S-05S), lipstick, pink on polyester/cotton (P-S-16), fluid make-up on cotton (C-S-17), high discriminative sebum BEY on polyester/cotton (PC-S-132), beef fat on cotton (C-S-61) and butterfat on cotton (C-S-10)), showing a preference for butterfat on cotton (C-S-10) (for details see [Fig. 12](#)); it has the capacity to degrade and clean spinning oils all raw textiles (61488F1, 3X58, 67007, 61988F1, 5237-00 and E03130) (for details see [Fig. 13](#)), and do show PETase and BHETase activities, being capable of degrading polyester-based fabrics (for details see [Fig. 14](#)); T<sub>opt</sub>: 25-40°C; T<sub>d</sub>, 41.70 ± 1.29°C; pH<sub>opt</sub>, 7.0 to 10.0; t<sub>1/2</sub> in washing liquor, 3.5 h.

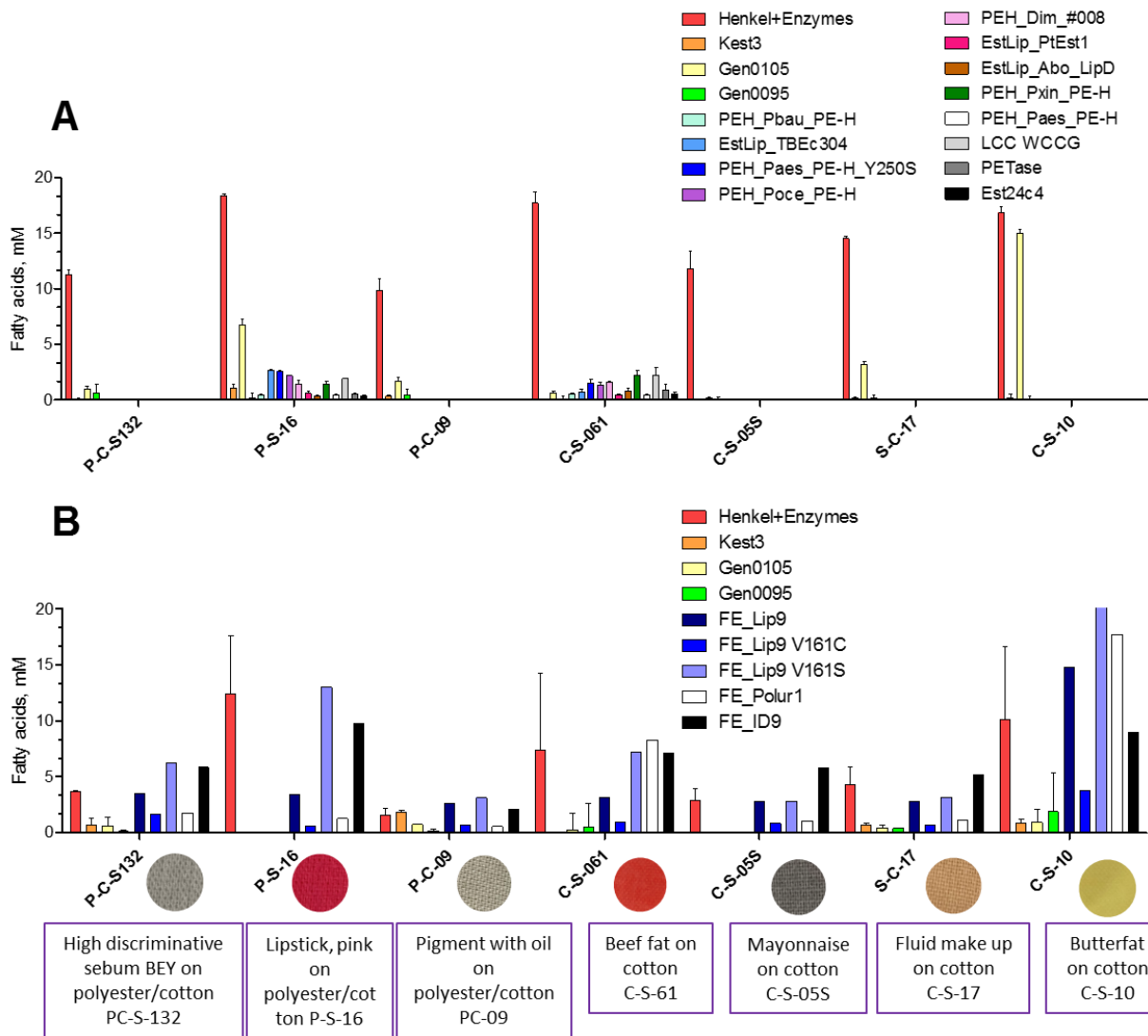


**Fig.12.** Enzymatic preparations capable of degrading stained swatches. Tests were performed as detailed in Deliverable D3.2 using a buffer (A) or washing buffer (B).

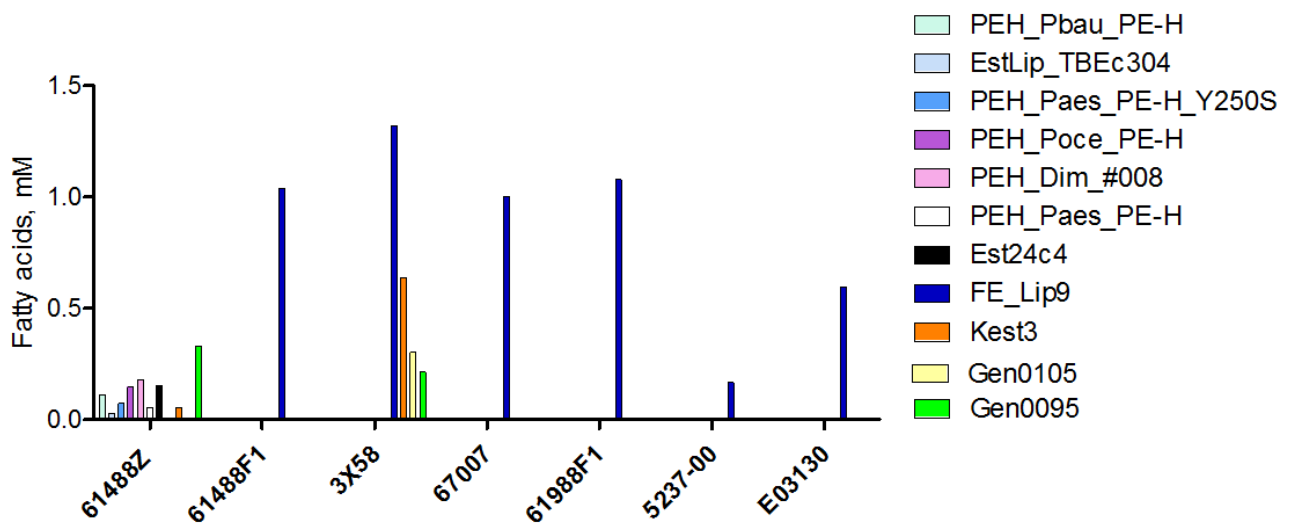


**Fig.13.** Enzymatic preparations capable of removing spinning oils from raw Schoeller fabrics. Tests performed as detailed in Deliverable D3.2.

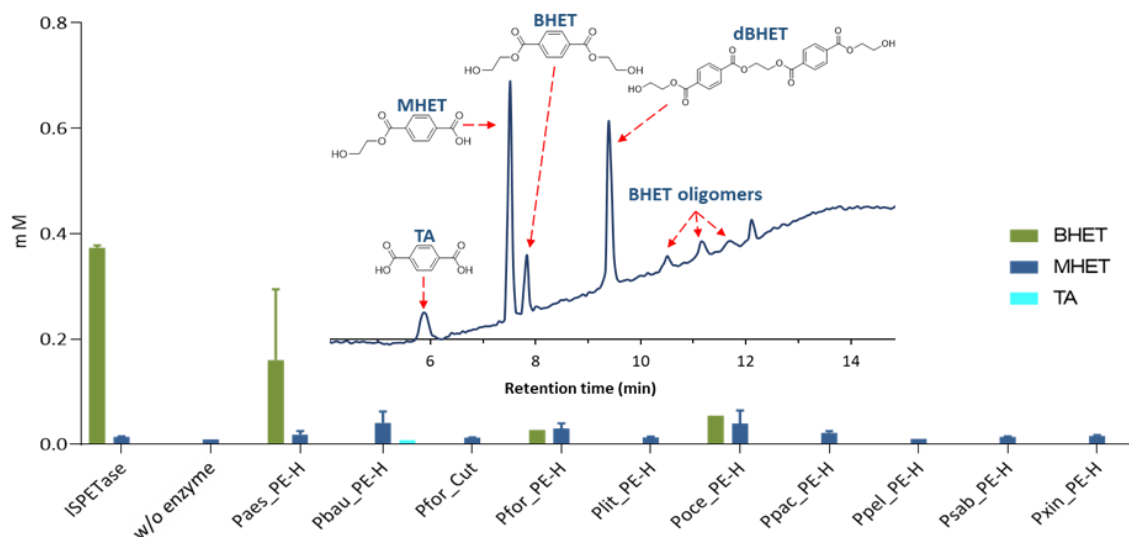


**Fig. 14.** Enzymatic preparations capable of degrading sample textile 4-b 3X58 (VORB, 100% PES 100g/m<sup>2</sup>) pretreated by alkaline boiling, provided by partner Schoeller. Inset, represent the capacity of FE\_Lip9 to degrade this fabric with the indication of the HPLC chromatograms with degradation products observed. Tests, by which the amount of degradation products (BHET, MHET and TA) could be quantified, were performed as detailed in Deliverable D3.2.

As detailed in Deliverable D5.1, FE\_Lip9 was found as having characteristics of interest for the detergent and textile sectors. Indeed, FE\_Lip9 was among the lipases most efficient at degrading dyed fabrics tested (see Deliverable D5.1, and above). After obtaining these results, a classical engineering approach was also implemented with the aim of improving their catalytic activity against these substances. The engineering of FE\_Lip9 was first approached by the analysis of functional hot spots found through hotspot wizard server (<https://loschmidt.chemi.muni.cz/hotspotwizard>), using PET<sub>4</sub> for docking with SwissDock server (<http://www.swissdock.ch/>). Two mutants, V161S and V161C, were selected because their priority positions in the hot spot ranking and proximity to catalytic pocket (see Fig. 15), synthesized, expressed and characterized, as for the wild type variant.

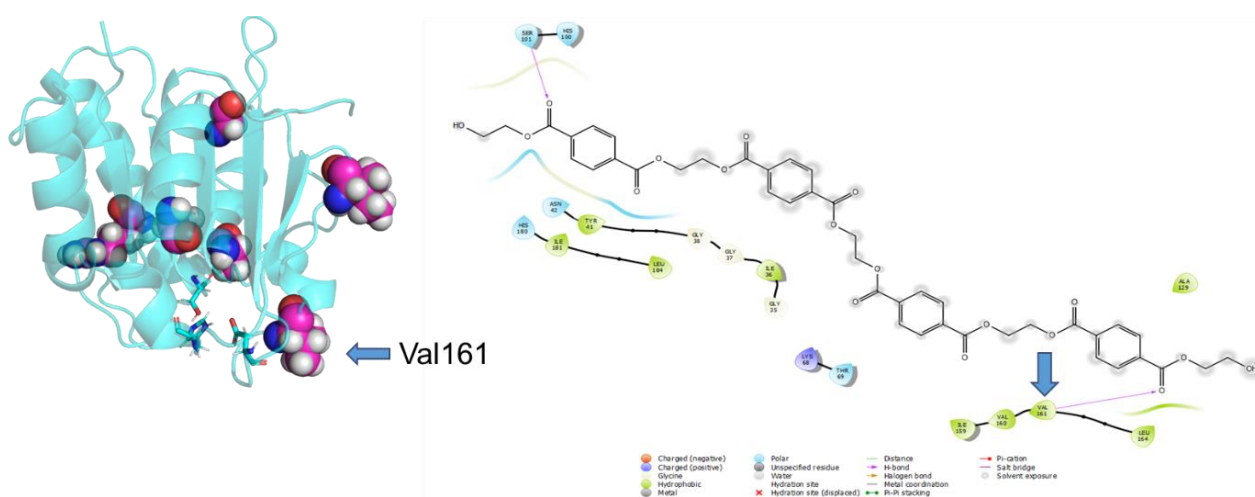


**Fig. 15.** 3D structure of FE\_Lip9 representing the main hotspots. The position of Val161 is highlighted. The target substrate used for docking, PET<sub>4</sub>, and its ligand diagram (that represent 4 Å distant residues) are shown on the right side.

We further used molecular mechanics simulations of substrate binding with the Monte Carlo code PELE to explore the active site; considering the conservation of the residues and the amino acid frequencies in related sequences, we suggested some potential mutants that could improve the activity of the lipase. For this, we

used molecular mechanics simulations of substrate binding with the Monte Carlo code PELE. We used triolein or glyceryl trioleate (TOL) and a tetramer of polyethylene terephthalate (PET4 or PET for simplification) as substrates to evaluate the affinity of the active sites for both types of substrates. Triolein was selected as a target lipid for engineering the lipase character of FE\_Lip9 for detergent application, and tetramer of polyethylene terephthalate from engineering the PETase character for textile applications. The protein structure model of Fe\_Lip9 obtained from AlphaFold 2.0 (Model 1.1.1) was prepared with PrepWizard from Maestro (Schrodinger), to check all hydrogens atoms and set the correct protonation states. We docked the substrates to the active site and selected the best pose for each protein-ligand combination, in order to have a starting pose for PELE's simulations. This selection was based on distance and Glide score. As shown in Fig. 16, there are several goods candidates that improve the energetics when compared with wild type when PELE simulations were performed. Substrates were constrained into a spherical box with a 25 Å radius to compare the affinity to the modified active sites. In brief, the designed mutants using triolein were: G11S, I12Y, I12N, N48V, H76N, H76S, A81V, A105S, L108Y, I135N, I135Y, V136F, V137C, V137S, L160A, L160F, and the double mutants I135Y/I12N and I135Y/I12Y. As shown in Fig. 17, there are several goods candidates that improve the energetics when compared with wild type when PELE simulations were performed. Substrates were constrained into a spherical box with a 25 Å radius to compare the affinity to the modified active sites. In brief, the designed mutants using triolein were: G11S, I12Y, I12N, N48V, H76N, H76S, A81V, A105S, L108Y, I135N, I135Y, V136F, V137C, V137S, L160A, L160F, and the double mutants I135Y/I12N and I135Y/I12Y.

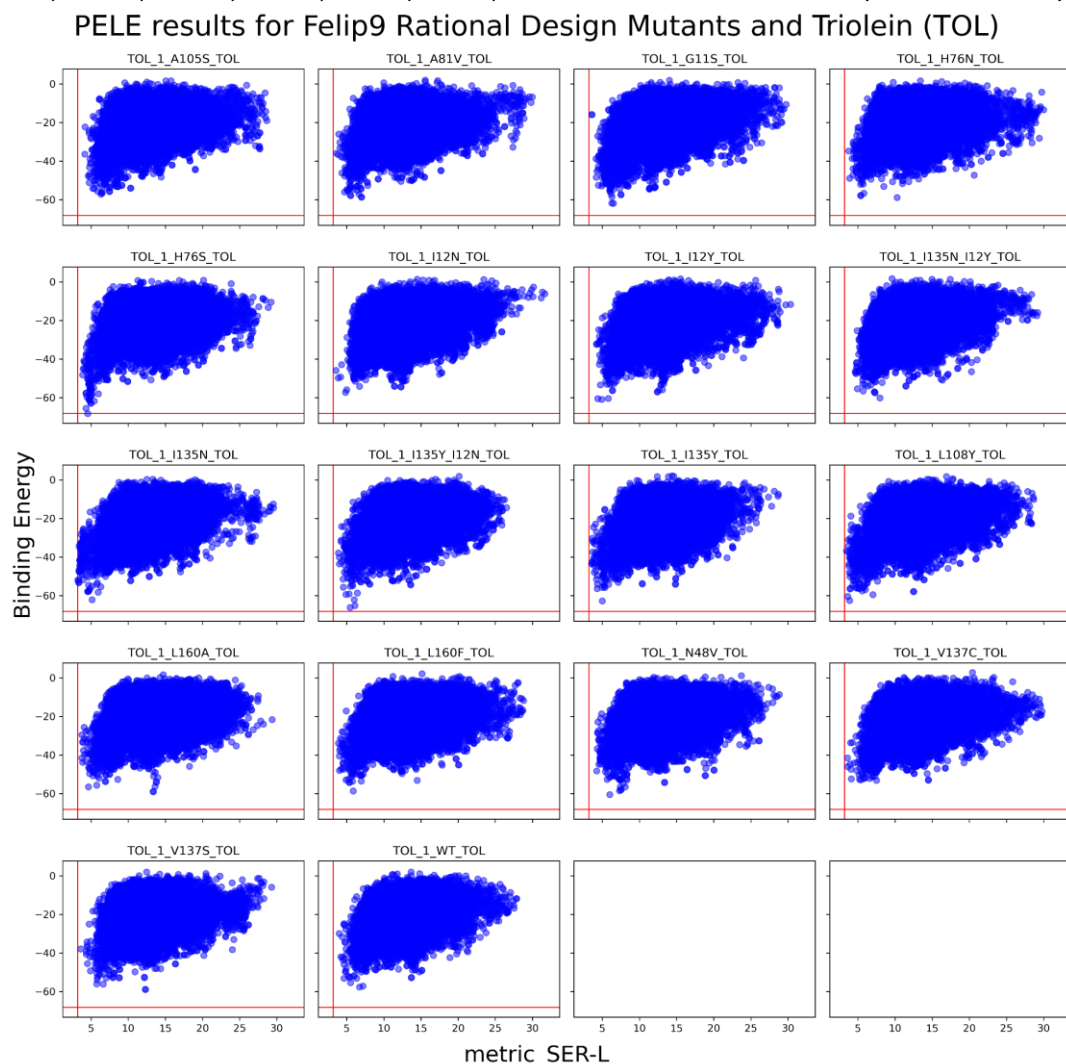
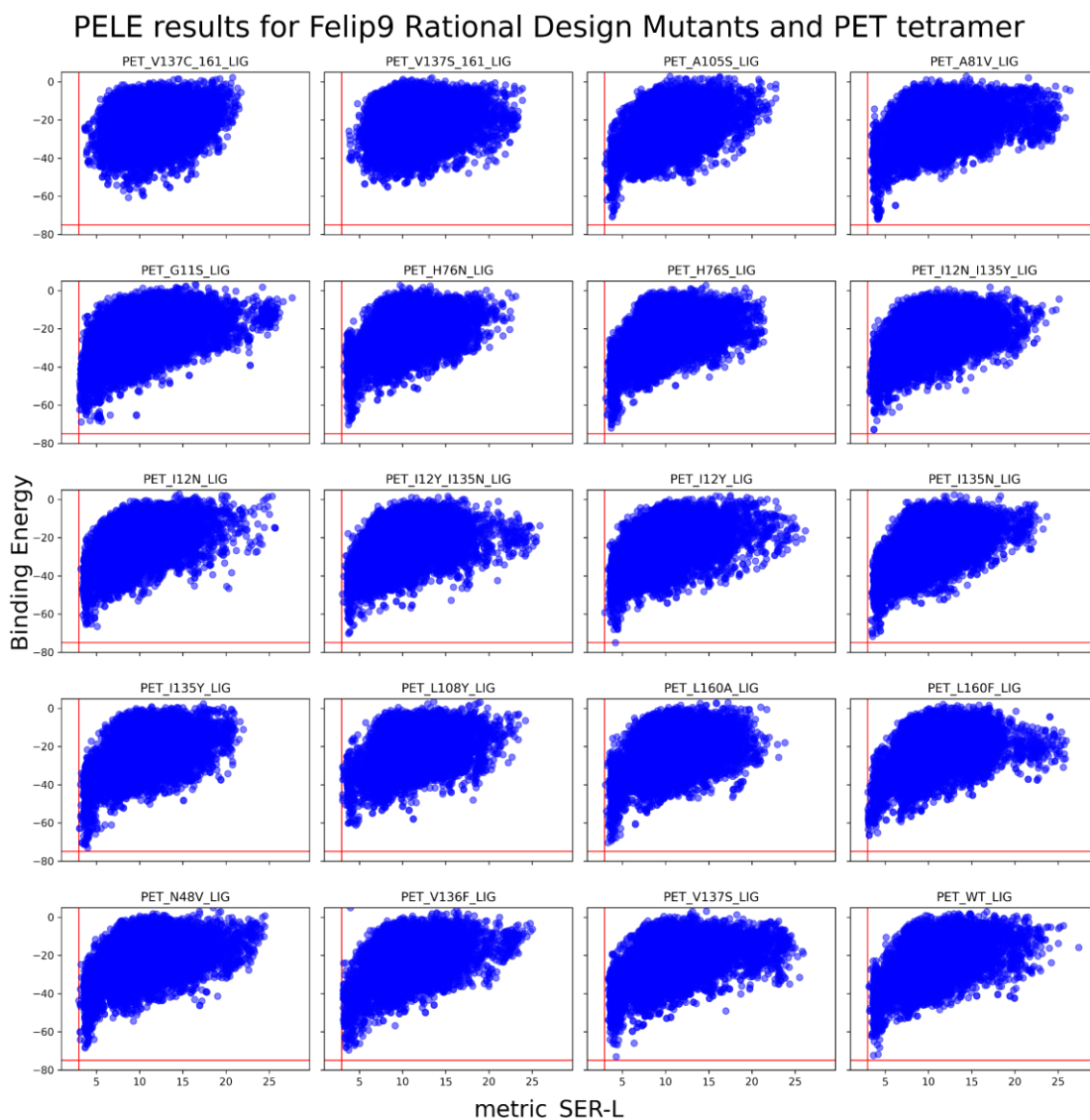
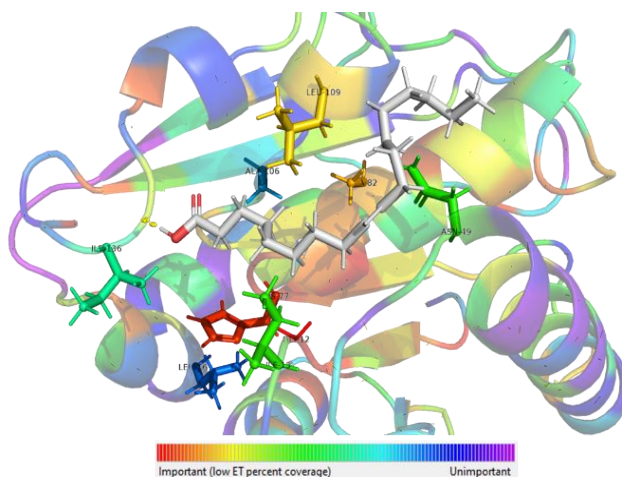


Fig. 16. Multiplot of the energy profiles of the active site local exploration with PELE. It is highlighted with a red line the minimum catalytic distance serine-ligand (A) from all the simulations and the minimum binding energy or interaction energy (kcal/mol).

In order to minimise the number of mutations to be experimentally validated, the residues and mutations selected by PELE, were subjected to HotSpot wizard calculations to screen the beneficial mutation points in the context of the evolutionary trace of Lip9. Combining all calculations, a number of residues, from those selected by PELE calculations, were selected as best candidate to focus on (Fig. 18; Table 3).



**Fig. 17.** Multiplot of the energy profiles of the active site local exploration with PELE. It is highlighted with a red line the minimum catalytic distance serine-ligand (A) from all the simulations and the minimum binding energy or interaction energy (kcal/mol).



**Fig. 18.** Lip9 3D model colored by evolutionary trace coverage value (red-important, violet-less important), oleic acid (white) is positioned by swissdock, the positions suggested are shown as sticks.

**Table 3.** Selected positions in FE\_Lip9 by HotSpot wizard calculations, with the coverage value obtained by evolutionary trace and the aminoacids present in the MSA of trace.

Residue	AA type	Coverage	Variability
106	A	0.69444	.TMNSQLGDCIYAVP
136	I	0.54444	TEVILK.MAFQ
13	I	0.38333	VLINQTFYMW
109	L	0.17778	MLNF.REQA
82	A	0.15000	LPTNSVIAM
12	G	0.01667	GA
77	H	0.04444	HYNFLW
161	L	0.75000	VGIERPKMAT.LCNDS
49	N	0.40000	AINSTVHLQRKM

Finally, in order to obtain thermostable mutants of FE\_Lip9 we performed a stability hot spot assay (hotspot wizard webserver) by sequence consensus. **Fig. 19** shows the residues the modification of which may have an effect on thermal stability. In brief, these residues include I120, I126, S134, V152 and Y192 (**Table 4**).

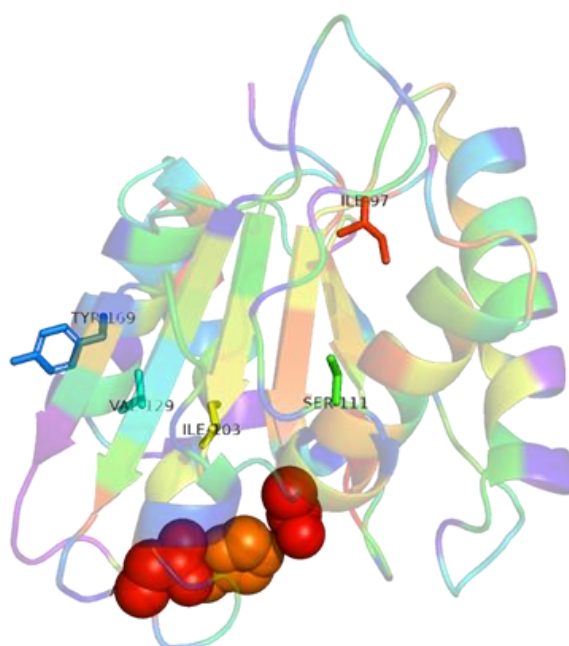


**Fig. 19.** Lip9 3D model colored by evolutionary trace coverage value (red-important, violet-less important), oleic acid (white) is positioned by swissdock, the positions suggested are shown as sticks.

**Table 4.** Selected positions in the MSA of trace by HotSpot wizard calculations, that may have effects on thermal stability of FE\_Lip9. Suggested mutations are highlighted.

Position	Mutant suggested	Variability
152 Val	Trp/Asp	VLEIMFYW
134 Ser	His/Ala	VIACPG.LRTSYQ
126 Ile	Phe	VLIGTFM
120 Ile	Val	VIA
192 Tyr	Gln	GNYK.HAVTSILERQDM

From all the mutations selected to increase the lipase character, the PETase character and the thermostability, 13 were selected for experimental validations, besides the 2 mutations (Val161Ser and Val161Cys) discussed above. They are listed in [Table 5](#).

**Table 5.** Selected mutations to increase the PETase and lipase character and thermostability of FE\_Lip9.

Enzyme	Target	Solubility	Expression (mg/L)	Relative activity (%)							Degradation products (μM)	
				Tri-C <sub>8</sub>	Tri-C <sub>10</sub>	Tri-C <sub>12</sub>	Tri-C <sub>14</sub>	Olive oil	Palm oil	Coconut oil	BHET	nPETc
Lip9 WT		Yes	1.0	100	100	100	100	100	100	100	2971±24	2238±40
Lip9 Val161Cys	Engineering PETase character	Yes	2.0	118.9	115.1	84.1	111.4	80.0	192.8	150.7	2880±13	1581±41
Lip9 Val161Ser	Engineering PETase character	Yes	3.0	123.9	98.1	91.7	102.3	168.9	204.8	179.2	3003±29	3342±63
Lip9 I36N-I159Y	Engineering lipase character	Yes	0.4	2.2	5.3	8.8	0.0	0.0	8.5	2.0	77±22	0
Lip9 H100S	Engineering lipase character	Yes	0.3	0.0	0.0	0.0	0.0	0.0	0.0	0.0	0	0
Lip9 A105F	Engineering lipase character	Yes	1.0	0.0	0.0	0.0	0.0	0.0	0.0	0.0	0	0
Lip9 I36Y	Engineering lipase character	Yes	1.5	7.9	30.4	21.2	14.4	0.0	30.7	21.8	0	0
Lip9 N72Y	Engineering lipase character	Yes	2,1	117.6	95.8	183.6	57.6	35.6	236.4	140.0	251±10	110±10
Lip9 A105V	Engineering lipase character	Yes	4.8	3.9	0.4	0.3	0.0	0.0	0.0	0.6	0	0
Lip9V152W	Thermostability	n.d.	n.d.	n.d.	n.d.	n.d.	n.d.	n.d.	n.d.	n.d.	n.d.	n.d.
Lip9 V152E	Thermostability	n.d.	n.d.	n.d.	n.d.	n.d.	n.d.	n.d.	n.d.	n.d.	n.d.	n.d.
Lip9 S134H	Thermostability	n.d.	n.d.	n.d.	n.d.	n.d.	n.d.	n.d.	n.d.	n.d.	n.d.	n.d.
Lip9 S134A	Thermostability	n.d.	n.d.	n.d.	n.d.	n.d.	n.d.	n.d.	n.d.	n.d.	n.d.	n.d.
Lip9 I126F	Thermostability	n.d.	n.d.	n.d.	n.d.	n.d.	n.d.	n.d.	n.d.	n.d.	n.d.	n.d.
Lip9 I120V	Thermostability	n.d.	n.d.	n.d.	n.d.	n.d.	n.d.	n.d.	n.d.	n.d.	n.d.	n.d.
Lip9 Y192Q	Thermostability	n.d.	n.d.	n.d.	n.d.	n.d.	n.d.	n.d.	n.d.	n.d.	n.d.	n.d.

The mutant genes were synthesized, and the mutants expressed and characterized, as for the wild type variant. In addition to the two mutants described above (Val161Ser and Val161Cys), the expression and characterisation of other 6 mutants have been completed. As shown in Table 5, all eight mutants were found to be produced in soluble form, albeit at different yields, with only 6 being active. Only V161S, V161C, and N72Y did show activities higher than the wild type. Interestingly, whereas mutations all three mutations increased the lipase character by 1.4-2.3-fold by meaning of higher activity toward long triglycerides such as palm and coconut oil, V161S was the only one increasing the PETase character, by meaning of the degradation of nano-sized PET particles.

The data shown in Table 6 demonstrated that the mutant was about 6-fold more active than the wild type enzyme, as well as from 3 to 14-fold more stable at temperatures from 30 to 50°C. Once confirmed, the washing capacity for stained clothes was further evaluated at 30°C. As shown in Fig. 20, Lip9 Val161Ser CSIC released more fatty acids from all the stained clothes of HENKEL than Lip9 WT (wild type). After all these experiments we conclude that this mutant might be more appropriate for washing tests by industry partner Henkel compared to the wild type Lip9.

**Table 6.** Relative activity and thermostability, by meaning of half-life time, of Lip9 Val161Ser, compared to Lip9.

Temperature (°C)	Specific activity (U/mg) <sup>1</sup>		Half life time, T <sub>50</sub> (h)	
			Lip9 WT	Lip9 Val161Ser
30	0.21	1.3	27.22 ± 0.61 h	77.57 ± 0.15 h
40	-	-	1.33 ± 0.01 h	18.18 ± 0.04 h
50	-	-	1.35 ± 0.001 min	17.95 ± 0.02 min

<sup>1</sup>Calculated with Phenol Red assay using tributyrin as substrate at 30°C and pH 8.0.

<sup>2</sup>Calculated as follows: [Enzyme], 0.8 µg/ml; [p-nitrophenyl butyrate, p-NPB], 2 mM; reaction volume, 100 µl HEPES, buffer, 40 mM, pH 7.0; T, 30°C, 40°C or 50°C; assay format, 96-well plates (ref. 655101, Greiner Bio-One GmbH, Kremsmünster, Austria); assay wavelength, 348 nm. Datasets were collected with a Synergy HT Multi-Mode Microplate reader (with Gen5 2.00 software Biotek Instruments), with values obtained from the best linear fit using Excel 2019. All reactions and analyses were performed in triplicate (n = 3).

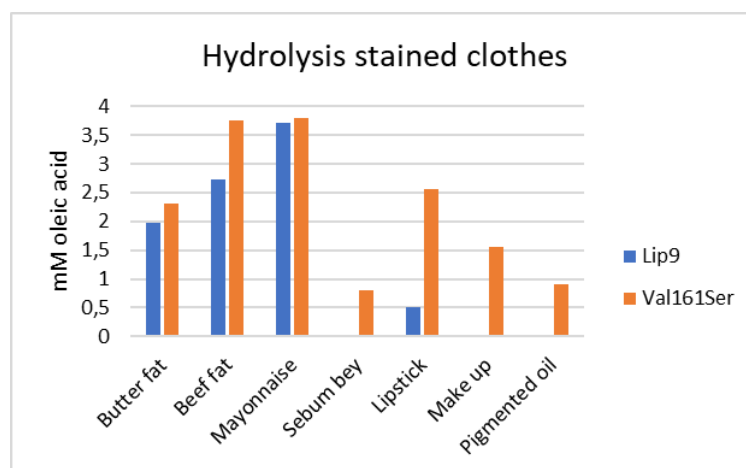


**Fig. 20.** Concentration (mM) of free fatty acids released from stained clothes. The results show the comparison of fatty acid release between Lip9 and Lip9 Val161Ser from CSIC. Reaction conditions: 4 mg of stained cloth; 0.05 mg of enzyme in 100 µl of Washing liquor buffer (2.5 g/l) at 30°C, pH 8.0, 2 hours.

Results demonstrate that the mutant Lip9 Val161Ser is a promising candidate for detergent applications given its higher activity performance and stability compared to wild type Lip9. For datasets see Table S1 in the [www.futureenzyme.eu](http://www.futureenzyme.eu) intranet.

#### 4.2. Engineering FE\_Lip5 by lid domain remodeling: for detergent applications

The hydrolytic activity of purified protein (Lip5) was initially evaluated against a series of triglycerides with different carbon chain lengths, namely, glyceryl tripropionate (TriC<sub>3:0</sub>), tributyrate (TriC<sub>4:0</sub>), trioctanoate (TriC<sub>8:0</sub>), and tridecanoate (TriC<sub>10:0</sub>), as well as coconut oil, which is typically dominated by medium-carbon chain triglycerides of lauric acid (TriC<sub>12:0</sub>), myristic acid (TriC<sub>14:0</sub>), palmitic acid (TriC<sub>16:0</sub>), olive oil (or triolein), which is mostly composed of long-carbon chain triglycerides of oleic acid (TriC<sub>18:1</sub>), and palm oil, which is dominated by long-carbon chain triglycerides of palmitic acid (TriC<sub>16:0</sub>) and stearic acid (TriC<sub>18:0</sub>). The protein was found to be active against short-carbon chain (TriC<sub>3:0</sub> and TriC<sub>4:0</sub>) to medium-carbon chain (TriC<sub>10:0</sub> and coconut oil) triglycerides, with specific activities ranging from 50 to 3230 units/g protein, measured at pH 8.0 and 30 °C (Table 7).

**Table 7.** Substrate specificity of enzyme variants investigated.

Triglyceride	Spec. Act. (Units/g) <sup>1,2</sup>	Spec. Act. (Units/g) <sup>1</sup>	Spec. Act. (Units/g) <sup>1,2</sup>	Spec. Act. (Units/g) <sup>1,2</sup>
	Lip5	Addzyme RD	Lip5 <sub>lid</sub>	Lip5 <sub>W89M/L60F</sub>
TriC <sub>3:0</sub>	960 ± 20	590 ± 80	630 ± 20	550 ± 70
TriC <sub>4:0</sub>	1080 ± 10	1080 ± 90	780 ± 70	640 ± 10
TriC <sub>8:0</sub>	3230 ± 10	13,440 ± 60	2330 ± 90	13,800 ± 290
TriC <sub>10:0</sub>	580 ± 10	9850 ± 350	2220 ± 60	9220 ± 320
Coconut oil	50 ± 10	6630 ± 180	1460 ± 170	1860 ± 370
Palm oil	n.d. <sup>3</sup>	1300 ± 250	1290 ± 210	1050 ± 20
Olive oil	n.d. <sup>3</sup>	3680 ± 270	1210 ± 20	1760 ± 210

<sup>1</sup> Specific activity (unit/g; mean ± SD of triplicates calculated using Excel 2019 STDEV.S function) for 7 model substrates. Activity was determined at 30 °C and pH 8.0. In brief, the activity towards TriC<sub>3:0</sub> and TriC<sub>4:0</sub> was determined using a pH indicator (Phenol Red<sup>®</sup>) assay; for the other substrates, activity was evaluated by the NEFA-Kit. <sup>2</sup> The fact that Lip5 has an initial  $T_d$  of 46.3 ± 1.8 °C suggests that the enzyme does not denature at the optimal temperature (45 °C) under our assay conditions (using *p*-NP butyrate and 1–7 min reaction time), although under other assay conditions (e.g., assay time) where stability may play a role, the optimal temperature plot may differ. This is why, for the determination of specific activity towards triglycerides, where a 30 min reaction assay was used, a temperature of 30 °C was set up to ensure protein stability during the assay. <sup>3</sup> No activity was detected (n.d.) under our assay conditions (30 min reaction time, 30 °C and pH 8.0) or after 24 h of incubation. It is possible that under other reaction conditions, including higher temperature and incubation times, some conversion may be observed.

The enzyme showed maximal activity at 45 °C, retaining more than 35% of the maximum activity at 30–55 °C (Fig. 21A). Analysis by circular dichroism (CD) spectroscopy revealed that the enzyme showed a sigmoidal curve with two transitions, one with a denaturation temperature ( $T_d$ ) of 46.3 ± 1.8 °C and a second at 82.4 ± 0.2 °C (Fig. 21B). We checked whether Lip5 could have a multimeric structure with GalaxyHomomer [40], a protein homo-oligomer structure prediction method, and a plausible dimeric structure was obtained using the sequence-based method. Thus, the presence of these two phases might be due to a multimeric enzyme structure that is disturbed by the thermal conditions. Thermal denaturation of the protein is a condition in which the unique 3D structure of a protein is disturbed, and it is possible that due to changes in temperature, pH, or other chemical conditions, the hydrogen bonds present in the proteins may also be disturbed. Therefore, we cannot rule out that the two phases could also exist under our assay conditions (no salt added and pH 7.0) due to a rapid change in protein conformation, yet to be determined, that impairs but does not inactivate the enzyme, followed by a slow change in protein multimeric structure that results in complete inactivation. Finally, its optimal pH for activity is 9.0, and it retains more than 50% of the maximum activity at pH values from 7.0 to 10.0 (Fig. 22).

The hydrolase did show maximal activity at a pH of 8.5 and a temperature of 30 °C, values similar to those of the lipase from *R. delemar* used as a target for bioprospecting. The substrate specificity of the lipase from *R. delemar* was further evaluated under the same assay conditions used to test Lip5. For that, we used the commercial preparation Addzyme RD (Evoxx Technologies GmbH). As shown in Table 6, under our assay conditions, this preparation was most effective for hydrolysing TriC<sub>8:0</sub> but also converted larger triglycerides such as triolein (specific activities ranging from 590 to 13,440 units/g protein); this is in agreement with the results of previous studies in which this enzyme was tested with triglycerides from tributyrin to triolein [34,35,41]. Note that the hydrolase Lip5 and the lipase Addzyme RD have entirely different specificities with regard to their preference for shorter or larger triglycerides, respectively. This may be due to the low similarity between their sequences (approximately 33%) and the differences in the architecture of their active sites and the structure of their lid domains; the latter point will be discussed below.

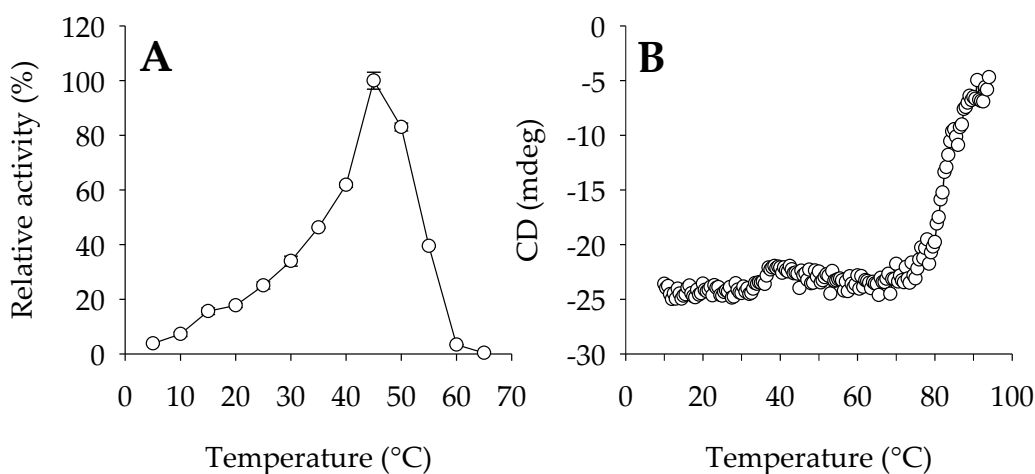


**Fig. 21.** Thermal characteristics of Lip5. **(A)** Temperature profile. The effect of temperature was determined following the hydrolysis of the model ester *p*-NP butyrate at 348 nm in 40 mM 4-(2-hydroxyethyl)-1-piperazineethanesulfonic acid (HEPES) buffer at pH 7.0. Values are plotted as the mean of triplicate results ( $n = 3$ ) with the reported standard deviation (SD) calculated using the STDEV.S function in Excel 2019, with control reactions (no enzyme added) considered. **(B)** The thermal denaturation curve at pH 7.0, as determined by CD spectroscopy measuring the ellipticity changes at 220 nm obtained at different temperatures at a rate of 0.5 °C per min. In A, the maximal activity was defined as 100% ( $597.4 \pm 1.8$  units/mg), and relative activity is shown as the percentage of maximal activity (mean  $\pm$  SD of triplicates). The figure was created using SigmaPlot 14.5.

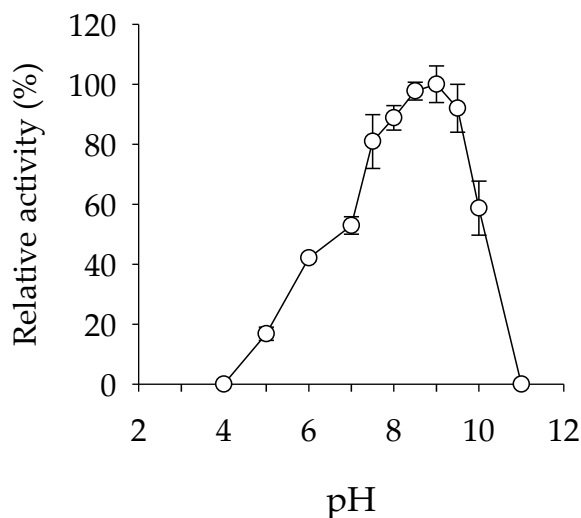


**Fig. 22.** Optimal pH for Lip5 lipase activity. The effect of pH was determined at 30 °C following the hydrolysis of the model ester *p*-NP butyrate at 348 nm in 50 mM Britton-Robinson (BR) buffer at pH 4.0–11. Values are plotted as the mean of triplicate results ( $n = 3$ ) with the reported SD calculated using the STDEV.S function in Excel 2019, with control reactions (no enzyme added) considered. The

maximal activity was defined as 100% ( $384.0 \pm 23.4$  units/mg), and relative activity is shown as the percentage of maximal activity (mean  $\pm$  SD of triplicates). The figure was created using SigmaPlot 14.5.

As shown in Table 6, the enzyme Lip5 was active towards small-carbon chain triglycerides (glyceryl tributyrates) but had no activity against bulkier triglycerides under our assay conditions. Since engineering of the lid domain can lead to drastic changes in the activity and specificity of lipases [19], we visually inspected this structural motif in Lip5 (Fig. 23) to introduce mutations that may allow the hydrolysis of bulkier triglycerides. For that purpose, we first computationally studied the lid opening of the wild-type enzyme and that of the *R. delemar* lipase as a control, and we then tried to design a mutant based on that analysis.

In brief, Lip5 was computationally studied by first obtaining its AlphaFold model and then by preparing and protonating it by Protein Preparation Wizard under conditions similar to those used in our experimental setup and by performing Monte Carlo simulations using Protein Energy Landscape Exploration (PELE).

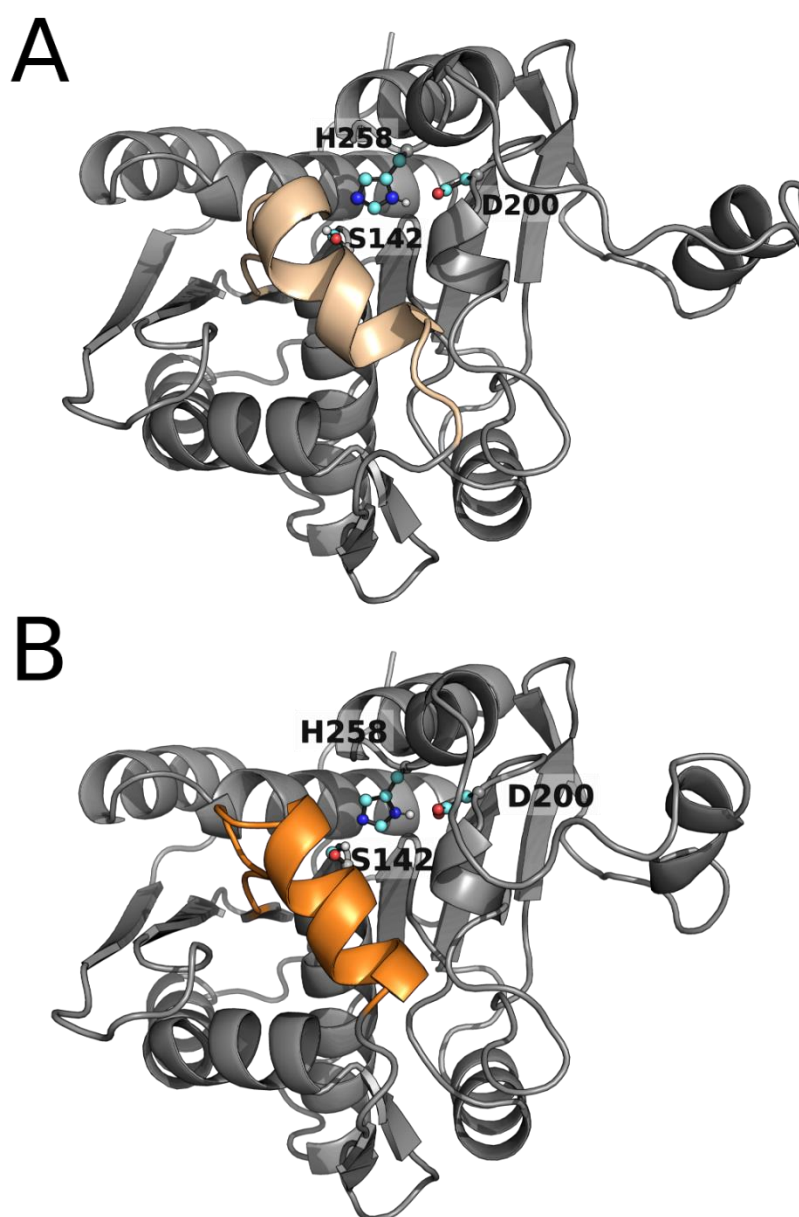


**Fig. 23.** AlphaFold 3D models of Lip5 (A) and Lip5<sub>lid</sub> (B) highlighting the catalytic triad (with C atoms coloured in deep-blue and red) and the lid domain (coloured in wheat and orange).

The original lid domain (FRGTEITQIKDWLTDA) of Lip5 seemed to have a tryptophan residue at the inner side, hindering it from fully opening to bind medium- and long-carbon chain triglycerides (Figures 4 and S3), in agreement with experimental data (Table 6). This amino acid is absent in the lid domain (FRGTNSFRSAITDIVF) of *R. delemar* lipase (Fig. 24). We performed a Monte Carlo simulation with PELE software (version rev12360) to test this hypothesis. The simulation consisted of the lipase being solely perturbed by a vector between the  $\alpha$  carbons of a residue in the lid domain (I83 for the Lip5 enzyme and F209 for the *R. delemar* lipase) and a residue in the loop in front of it (L255 for the Lip5 enzyme and I377 for the *R. delemar* lipase), forcing the opening of the lid domain. After this directed perturbation of the lid domain, the system was minimized, and the step was accepted or rejected based on the Metropolis criterion. Moreover, the sense of the mentioned vector was changed every 100 steps to study the motion related to the opening and closure of the lid domain. This back-and-forth motion allowed us to find the metastable opened and closed states during the calculation. Measuring the difference in a distance that can represent the opening and closure of the lid domain of the opened and closed states between systems can tell us the size of the substrates that each enzyme could bind and hydrolyse. In this study, the distance used was the described vector to move the lid domain (Fig. 25).

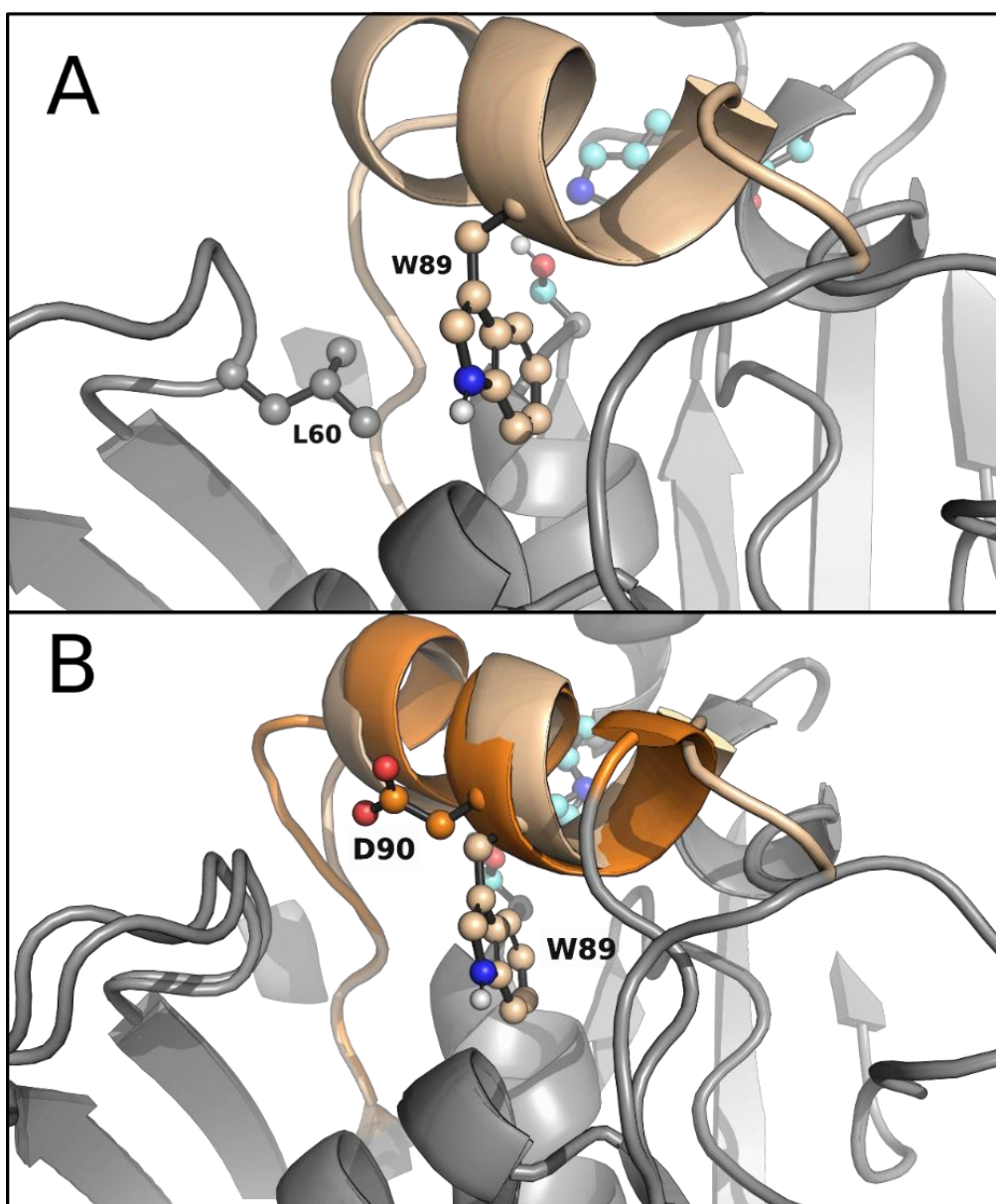


**Fig. 24.** AlphaFold 3D models of Lip5 and Lip5<sub>lid</sub>. **(A)** AlphaFold 3D model of Lip5 highlighting the positions of W89 and L60 in the lid domain (coloured in wheat). **(B)** AlphaFold 3D models of Lip5 and Lip5<sub>lid</sub> depicting the absence of the bulky W89 residue in the lid domain of the mutant (coloured in wheat and orange).

The results of the simulations showed that the wild-type enzyme had a closed metastable state at 8.99 Å and an open metastable state at 14.43 Å, meaning that the lid domain opens up to 5.44 Å (Fig. 25). On the other hand, the *R. delemar* lipase had a closed metastable state at 7.71 Å and an opened state at 15.30 Å, showing a difference in the opening distance of 2.14 Å. Thus, we created a variant aimed at further opening the lid domain of the lipase. The designed mutant replaced W89 with a less bulky residue, methionine, but this was still a reasonable change according to the BLOSUM62 matrix. To compensate for the increase in volume in the closed conformation of the enzyme due to the mentioned mutation and to prevent the access of water molecules to the active site, L60, a residue not placed in the lid domain (Fig. 24) was mutated to phenylalanine. Then, the same type of simulation was performed on the double mutant (W89M/L60F). The results gave a closed metastable conformation (at 8.81 Å) similar to that of the wild-type enzyme but a more open conformation (at 15.78 Å) (Fig. 25). Thus, the difference in the opening distance between the double mutant and the wild-type was approximately 1.5 Å, meaning that the variant appeared to be opening more, potentially allowing it to fit bulkier triglycerides in the active site.

To confirm this hypothesis and evaluate to what extent the mutations and the different lids affect the catalytic binding of bulkier triglycerides, local explorations of the binding of triolein (a long-carbon chain triglyceride) in the active state of the wild-type enzyme (Lip5) and its double mutant (W89M/L60F) as well as the *R. delemar* lipase were performed. The ligand was undockable in the open conformation of the wild-type enzyme (in agreement with the difficulties of the wild-type enzyme in hydrolysing long-carbon chain triglycerides), so we had to migrate a triolein molecule from the solvent to the active site with AdaptivePELE [42–44] with a bias that minimizes the distance between the substrate and the catalytic serine residue. The simulation successfully gave catalytic binding positions of the substrate around the active site. On the other hand, the ligand was easily docked with Glide software (version 95128) on the open conformations of the double mutant and the *R. delemar* lipase. The induced-fit simulations showed that the substrate spent more time bound in a catalytic conformation in the double mutant and the *R. delemar* lipase compared to the wild-type enzyme (Fig. 26). The wild-type enzyme only had ~56% of PELE poses inside the active site (with the serine-substrate distance equal to or lower than 5 Å), while the double mutant and the *R. delemar* lipase had up to ~82% and 99% of poses within the active site, respectively. The number of catalytic events, poses where one of the ester C atoms from the substrate molecule is 4 Å from the nucleophilic O of the catalytic serine residue and the H-bonds of the catalytic triad have appropriate distances, is similar in the double mutant, with 1696 (and 10.412% of all accepted PELE steps), and the wild-type enzyme, with 2023 (and 12.687% of all accepted PELE steps) such events. The *R. delemar* lipase showed more predicted catalytic events than the Lip5 wild-type enzyme with 33,604 (and 91.586% of all accepted PELE steps). The higher number of such catalytic events agrees with the higher catalytic activity of *R. delemar* lipase compared with Lip5, as determined experimentally (see Table 7).

The sequence encoding Lip5 with the two mutations, W89M and L60F (Lip5<sub>W89M/L60F</sub>), was synthesized as for the wild-type. After synthesis, a 294 amino acid-long sequence was obtained encoding an enzyme with a molecular mass of 32,677 Da and an isoelectric point of 5.40. The mutant was expressed, purified, and characterized as the wild-type protein. The protein was found to be active against small- to large-length triglycerides, including trioctanoate (TriC<sub>8:0</sub>), tridecanoate (TriC<sub>10:0</sub>), coconut oil, palm oil, and olive oil (Table 6); note that the last two substrates were not hydrolysed by the wild-type protein. Specific activities ranged from 550 (for TriC<sub>3:0</sub>) to 13,800 (for TriC<sub>8:0</sub>) units/g protein, showing the ability to hydrolyse triglycerides as large as olive oil (1760 units/g) and palm oil (1050 units/g). These results agree with the computational analysis and the role of residue W89, located in the original lid domain, in the substrate specificity and access of bulkier triglycerides to the active site.

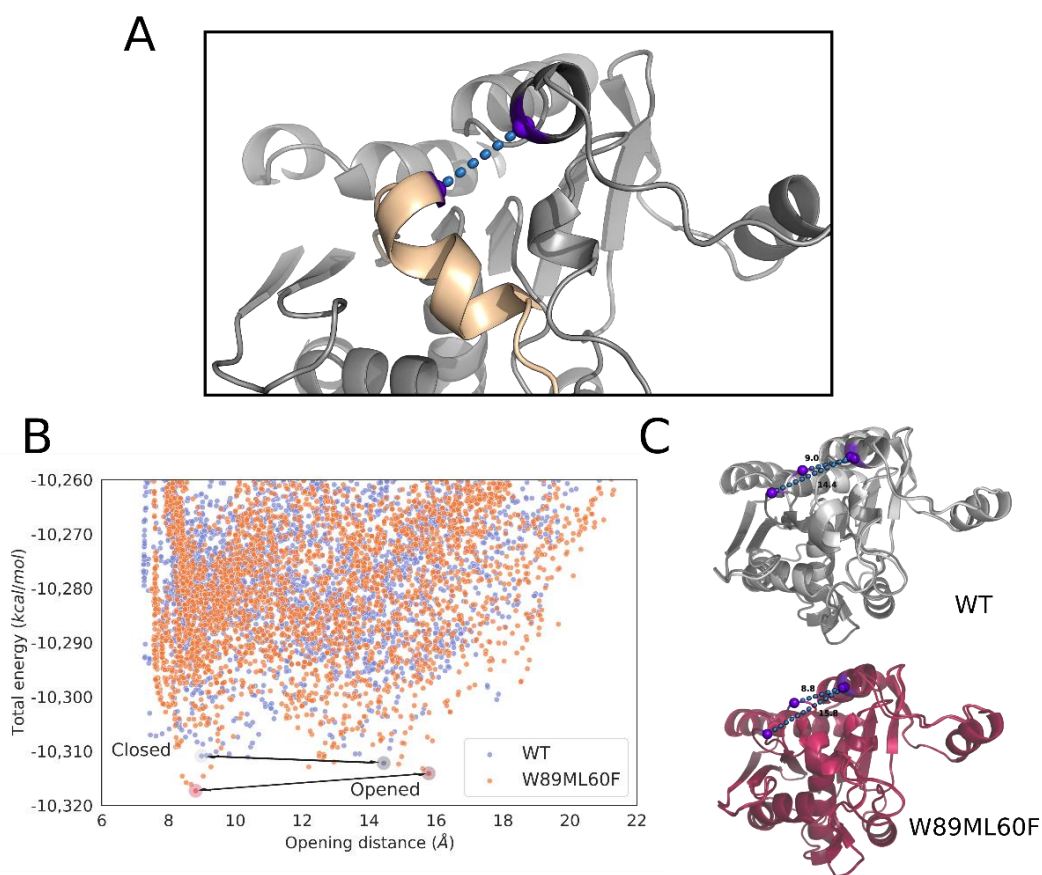


**Fig. 25.** Opening of the lid domain of Lip5 through Monte Carlo simulations. **(A)** 3D representation of the opening distance in the Lip5 system. **(B)** Scatter plots of the opening distance against the total energy of the system. The energy profiles were created with the Matplotlib library. **(C)** 3D displays of the opened and closed metastable states of both the wild-type enzyme and the double mutant.

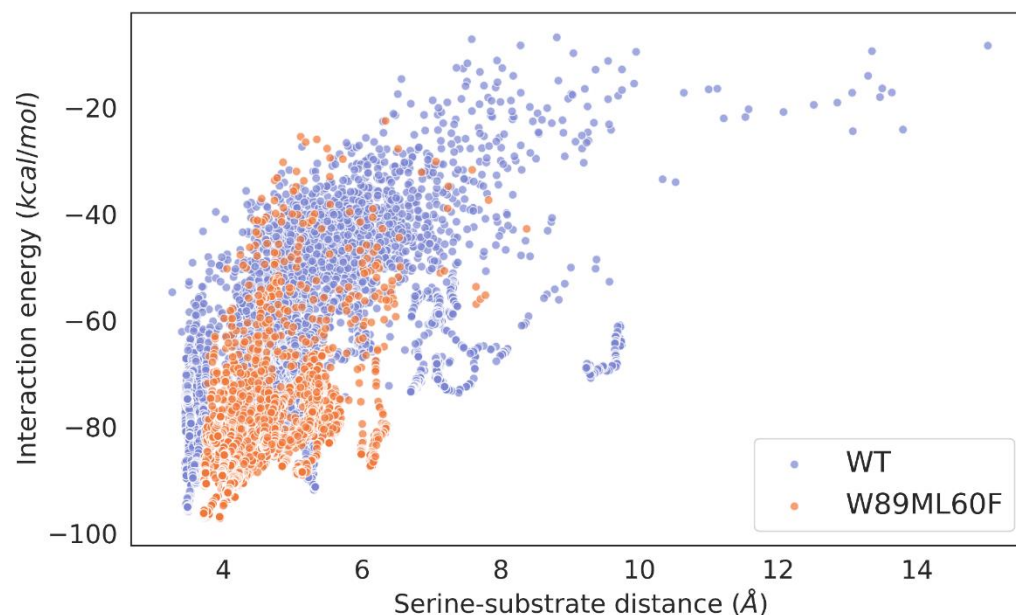


**Fig. 26.** Scatter plots of the serine-substrate (nucleophilic O of the catalytic Ser residue and ester Cs of the substrate) distance against the interaction energy of the wild-type enzyme and the double mutant. The energy profiles were created with the Matplotlib library.

As a complementary strategy to further improve the capacity of the lipase to hydrolyse bulkier triglycerides, and based on the results found by mutating a lid residue, we performed lid swapping. The lid domain (FRGTEITQIKDWLTDA) of Lip5 was replaced by that (FRGTNSFRSAITDIVF) of *R. oryzae* lipase, which was used

as a template for screening Lip5 in the Marine Metagenomics MarRef Database and shares 33.2% sequence identity in a local sequence alignment and an RMSD of  $\sim 3 \text{ \AA}$  with its crystal structure (PDB code: 1TIC, against Lip5's AlphaFold model). This enzyme shows an optimum pH of 8.5 and an optimum temperature of 30 °C and can accept short (TriC<sub>4:0</sub>), medium (TriC<sub>8:0</sub>), and large (triolein) triglycerides (see [Table 7](#)). Such substrate specificity of lipases has been commonly associated with the presence of a lid domain and the residues (e.g., hydrophobic amino acids) that conform to it. The differences in the hydrophobic characteristics of the lid domains of the two enzymes raise the question of whether lid swapping may improve the Lip5 lipase activity.

First, we performed the same computational analysis for the new lid-swapped mutant, named Lip5<sub>lid</sub> (Figures 3 and 4). The lid opening type of simulation for the Lip5<sub>lid</sub> variant showed a closed metastable conformation at 9.40 Å and a more opened conformation at 19.61 Å, meaning that this variant had the highest opening distance of all interrogated species. The induced-fit simulation of the lid-swapped mutant showed that the substrate stayed bound in a catalytic conformation  $\sim 99\%$  of the time. Moreover, the number of catalytic events was 30,392 (and 91.295% of all accepted PELE steps), the highest compared to the wild-type enzyme and the double mutant, and with similar values to the *R. delemar* lipase.

The engineered Lip5<sub>lid</sub> variant was then synthesized as for the wild-type. After synthesis, a 294 amino acid sequence was obtained, encoding an enzyme with a molecular mass of 32,635 Da and an isoelectric point of 5.56. The mutant (N-terminal His<sub>6</sub>-tagged) was expressed, purified, and characterized as for the wild-type protein. The protein was found to be active against all triglycerides tested, with specific activities ranging from 630 (for TriC<sub>3:0</sub>) to 2330 (for TriC<sub>8:0</sub>) units/g protein, being able to hydrolyse triglycerides as large as olive oil (1210 units/g) and palm oil (1290 units/g) to an extent similar to that of the Lip5<sub>W89M/L60F</sub> mutant ([Table 7](#)).

It should be noted that the two mutants designed showed a preference for long triglycerides similar to that of the model *R. delemar* lipase ([Table 6](#)), although the specific activities are not comparable to the latter values derived from a nonpure commercial sample (Addzyme RD).

Results demonstrate that mutants of the lipase Lip5, Lip5<sub>W89M/L60F</sub> and Lip5<sub>lid</sub> showed a preference for long triglycerides similar to that of the model *R. delemar* lipase of industrial use ([Table 7](#)), although the specific activities are not comparable to the latter values derived from a nonpure commercial sample (Addzyme RD). Results suggest that both lipase mutants are promising candidates for detergent applications given its higher activity performance compared to wild type Lip5. For methodological details, detailed results and datasets (open access), see [Fernandez-Lopez et al., 2023](#).

#### 4.3. PEH\_Paes\_PE-H engineering: for textile applications

As detailed in Deliverable D5.1, one of the enzymes was found priority because having characteristics of interest for the detergent and textile sectors, PEH\_Paes\_PE-H: Activity, lipase, PETase; Partner, UDUS; Source, *Halopseudomonas aestusnigri*; Nominated as additive for Henkel detergent and for end-of-life fabric recycling, because high specific activity on fatty standard stains, particularly Lipstick, pink on polyester/cotton (P-S-16), Beef fat on cotton (C-S-61) (see [Fig. 12](#); [Fig. 27A](#)); although, it is not the enzyme with the highest levels of activity against model lipase substrates ([Fig. 27B](#)), the capacity to degrade fatty stains and its full or high percentage of residual activity in the presence of surfactants, i.e. washing liquor, the availability of experimental structural data (structural features of cutinases/PETases), and activity on PES-fabrics (see [Fig. 14](#)) makes an interesting candidate of it. Literature-informed mutagenesis of enzyme Paes\_PE-H yielded a variant that showed increased monomer-release from PET polyester fabrics, outcompeting the benchmark enzyme ISPETase under assay conditions ([Fig. 27B](#)). In addition, the mutation Y250S improved the degradation of a PET-based sample textile 4-b 3X58 (VORB, 100% PES 100g/m<sup>2</sup>) pretreated by alkaline boiling. PET monomer release from Schoeller sample textile increased by Paes \_PE-H mutant ([Fig. 27C](#)). In addition,

we detected for Y250S a 2.5x higher release of fatty acids during the first 2h of incubation than for the wild type. With Lipstick stain, the activity of the mutant for even 4.4x higher.

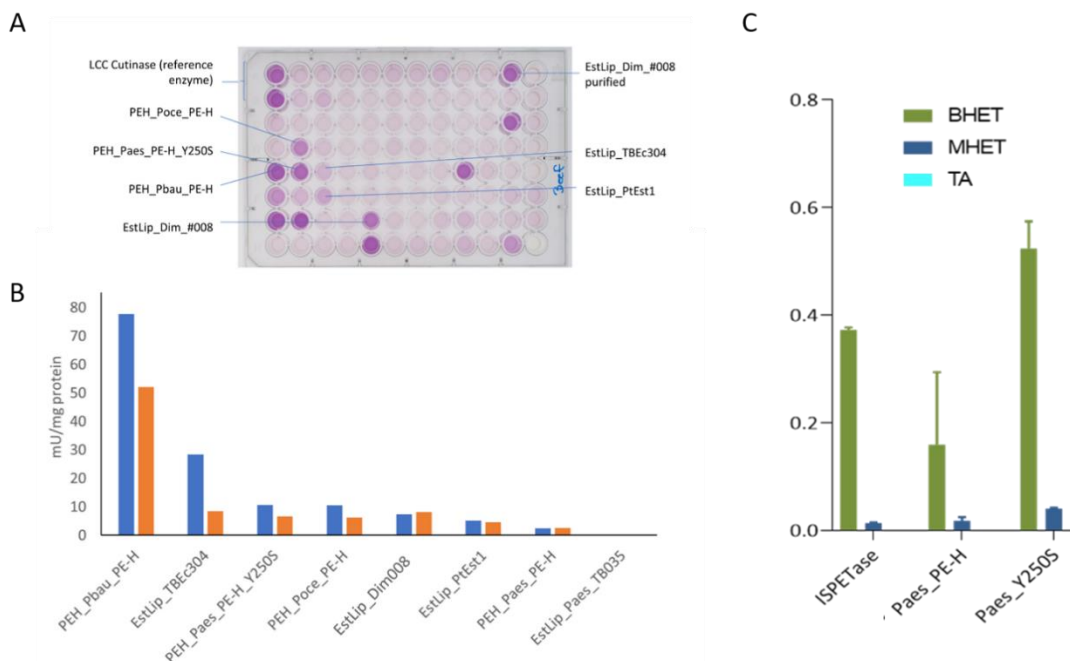


**Fig. 27.** Hydrolases activities on stained swatches. Activity of the selected PEH\_Paes\_PE-H hydrolase compared to other priority hydrolases upon incubation with standard stained fabric material, determined by measuring the released fatty acids. (A) Screening plate assaying the fatty acid concentration after overnight incubation with beef fat-stained fabric. The darker the violet, the higher the fatty acid concentration. (B) Approximated specific activity of purified enzymes [1 U= 1  $\mu$ mol fatty acid released per minute, determined with a serial dilution with oleic acid) after 2 h. (C) Release of building blocks after incubation of pre-treated PET fabrics of wildtype Paes\_PE-H and the engineered variant Y250S in comparison to Is\_PETase (equimolar amounts of enzymes).

Results demonstrate that mutant Y250S of the lipase/PETase PEH\_Paes\_PE-H, is a promising candidate for detergent applications given its higher activity performance compared to wild type PEH\_Paes\_PE-H. For methodological details, detailed results and datasets (open access), see [Bollinger et al., 2020](#), and Protein Data Bank accession numbers [6SCD](#).

#### 4.4. PET46 from *Candidatus Bathyarchaeota* engineering: for textile applications

As detailed in Deliverable D5.1, an additional enzyme was found priority because having characteristics of interest for textile sectors, PET46: Activity, PETase; Partner, UHAM; Source, *Candidatus Bathyarchaeota*; Nominated for end-of-life fabric recycling because availability of experimental structural data and activity on PET polyester fabric (Fig. 14). We designed and characterized PET46 (NCBI accession RLI42440.1), the first enzyme from archaeal origin reported to hydrolyze PET polymer. The enzyme is encoded in the metagenome-assembled genome (MAG) of the *Candidatus Bathyarchaeota* archaeon B1\_G2, a member of the TACK group that was found at the Guaymas Basin. The experimentally established crystal structure of the protein is similar to bacterial PET-degrading enzymes, but reveals several unique features (Fig. 28). PET46 is a promiscuous feruloyl esterase that hydrolyzes MHET, BHET, PET-trimer (3PET) and PET polymers.

Based on the docking results, we identified two amino acids, A46 and A140, nearby both predominant docking poses that might be relevant for the substrate accessibility and binding. Introducing the larger substitutions A46V and A140I should thus impact the catalytic activity. We further identified K147, which possibly interacts with docked poses from the second-largest cluster. Variant K147A abolishes this interaction and widens the binding groove. We then proceeded to incubate PET46 WT and all the constructed variants (including the PET46 $\Delta$ lid) on 3PET at 30, 60 and 70°C. At the two highest temperatures, we observed a very similar activity pattern, where PET46 WT, K147A, and A46V degraded all the 3PET to MHET and TPA within



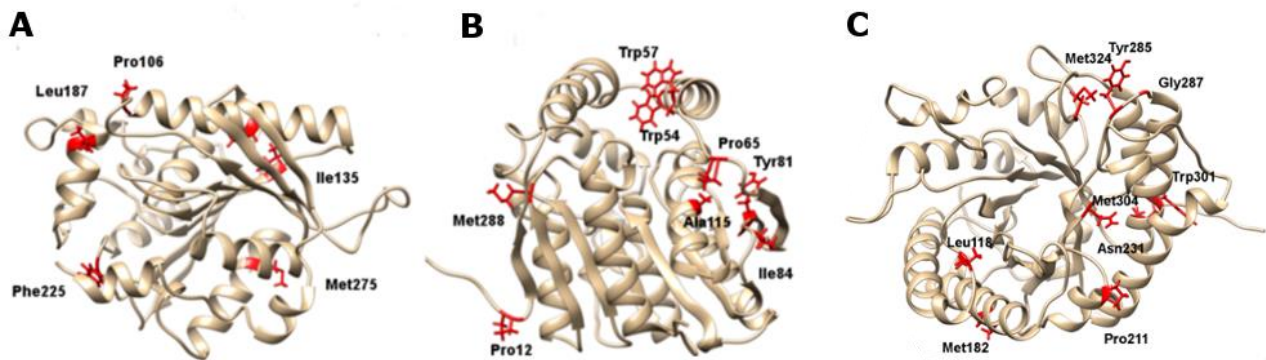


**Fig. 29.** Selection of mutants in Kest3, Gen0105 and Gen0095. **3D** structure of Kest3 (A) and Gen0105 (B) with mutated residues (FireProt) highlighted in red. (C) 3D structure of Gen0095 (see below). The mutated residues (Energy optimization, FireProt) are highlighted in red.

Further, mutated sequences were selected by using the ancestral sequence reconstruction and FireProt energy minimisation approaches. One mutated sequence was synthesized through energy minimisation, while two ancestral reconstructed sequences, were selected and subsequently synthesized for each Kest3 and Gen0105. The ancestral reconstructed sequences for Kest3 (Node58 and Node88; **Fig. 30**) exhibited 63.4% and 40.1% of identity to the Kest3 wild type. As for the ancestral reconstructed sequences for Gen0105 (Node 152 and Node 186; **Fig. 31**) they demonstrated 42% and 51.8% identical to the Gen0105 wild type.

Protein expression in 1 litre medium (Luria-Bertani) identified 2 ancestral Gen0105 sequences (Node152 and Node186) and Kest3 (Kest3\_EMF) energy minimisation mutant being soluble (**Fig. 32A**). However, the activity test revealed that Kest3\_EMF mutant was inactive when screened with *p*-nitrophenyl-substrate (**Fig. 32B**), and no thermostable mutant was identified (**Fig. 33**). The Gen0105 ancestral sequences of Node 152 and Node 186 exhibited activity with *p*-nitrophenyl-substrates ranging from C<sub>6</sub>-C<sub>12</sub>. Node186 displayed a similar activity pattern to Gen0105 wild type, whereas Node152 significantly lost activity with *p*-nitrophenyl-C<sub>6</sub>-C<sub>12</sub> substrates (**Fig. 34**). The thermostability screening of the Gen0105 ancestral sequences demonstrated enhanced properties with model *p*-nitrophenyl-C<sub>8</sub> substrate. After 1h of incubation at 80°C, Node152 retained up to 38% activity, and Node 186 retained 40% of activity during 1h incubation at 60°C (**Fig. 34**). However, tests using the real substrates 3PET, amorphous PET (data not shown) and contaminated textile screens did not confirm higher efficiency of the ancestral reconstructed Gen0105 enzymes (**Fig. 35**). Nevertheless, further investigations are currently being undertaken.

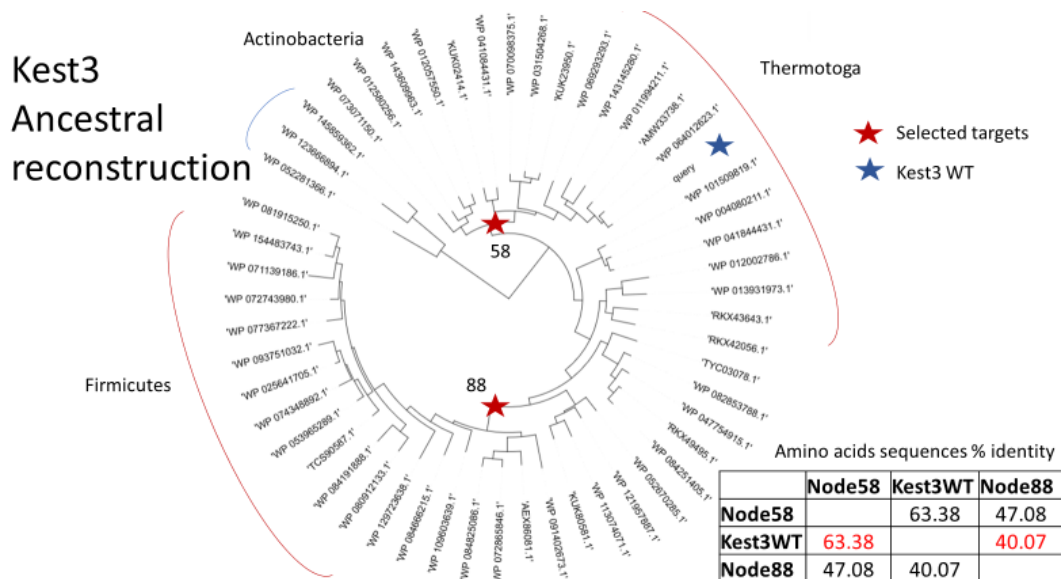


**Fig. 30.** Selection of mutated sequences of Kest3 by the ancestral sequence reconstruction.

# GEN0105: Ancestral reconstruction

- ★ Selected targets
- ★ GEN0105 WT

Amino acids sequences % identity

	Node152	Node186	Gen0105wt
Node152		64.4	42.11
Node186	64.4		51.76
Gen0105wt	42.11	51.76	

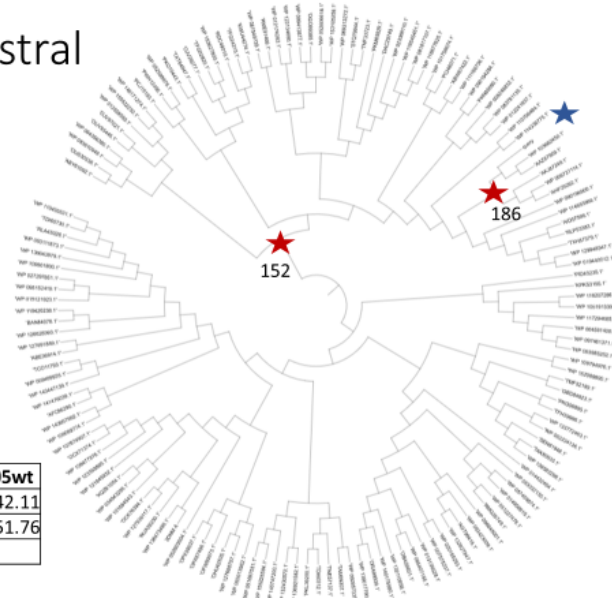


Fig. 31. Selection of mutated sequences of Kest3 by the ancestral sequence reconstruction.

**A**

Protein name	Function	Stabilization method	Solubility
Gen0105_EMF	PETase	Energy minimization	-
Node152	PETase	Ancestral reconstruction	+
Node186	PETase	Ancestral reconstruction	+
Kest3_EMF	Lipase	Energy minimization	+
Node58	Lipase	Ancestral reconstruction	-
Node88	Lipase	Ancestral reconstruction	-

**B**

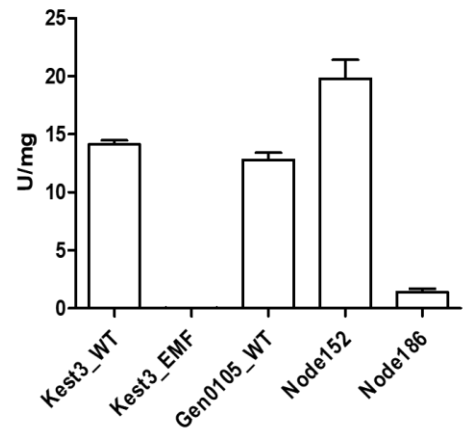


Fig. 32. Protein expression level of the 2 ancestral Gen0105 (Node152 and Node186) and Kest3 (Node58 and Node88) proteins (A). Activity level of the 2 ancestral Gen0105 (Node152 and Node186) and Kest3 (Node58 and Node88) proteins, once expressed in *E. coli* (B).

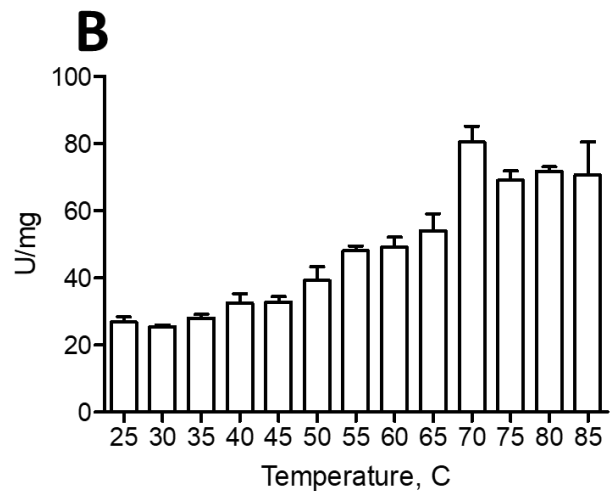
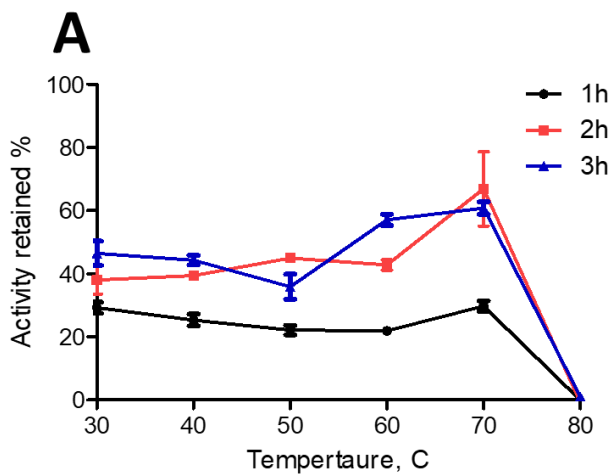
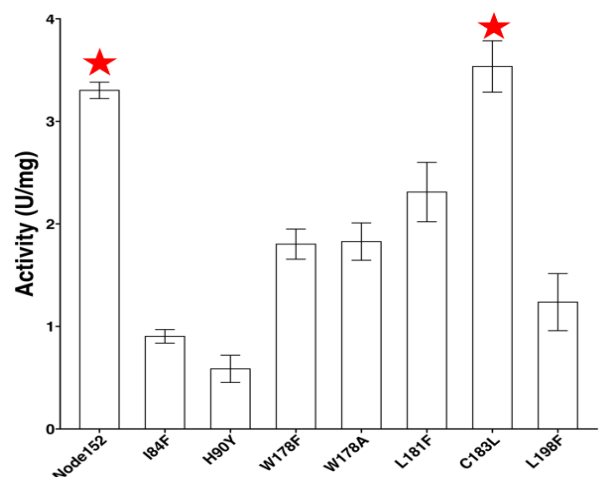


Fig. 33. Thermostability (A) and optimal temperature (B) for activity of Kest3 protein. None of the mutants (Node58 and Node88) turned thermostable, and data are not shown.





**Fig. 37.** SDM mutants screen with pNP-octanoate substrate at 30C, 1 µg enzyme/200 µl reaction mixture.

**Table 8.** Biochemical characteristics of the target GEN0105 esterase, ancestral reconstructed Node152 and Node186 and rationally designed mutant C183L.

Sample	Substrate	Km (mM)	Vmax	Kcat (s-1)	Kcat/Km (s-1 mM-1)
Gen0105	pNP-octanoate	0.8±0.1	11.3	6.6±0.4	8.3
Node186	pNP-octanoate	0.64±0.2	12.7	7.4±0.4	11.6
Node152	pNP-octanoate	0.15±0.05	1.4	0.8±0.2	5.5
C183L	pNP-octanoate	0.11±0.03	4.1	2.4±0.3	21.8

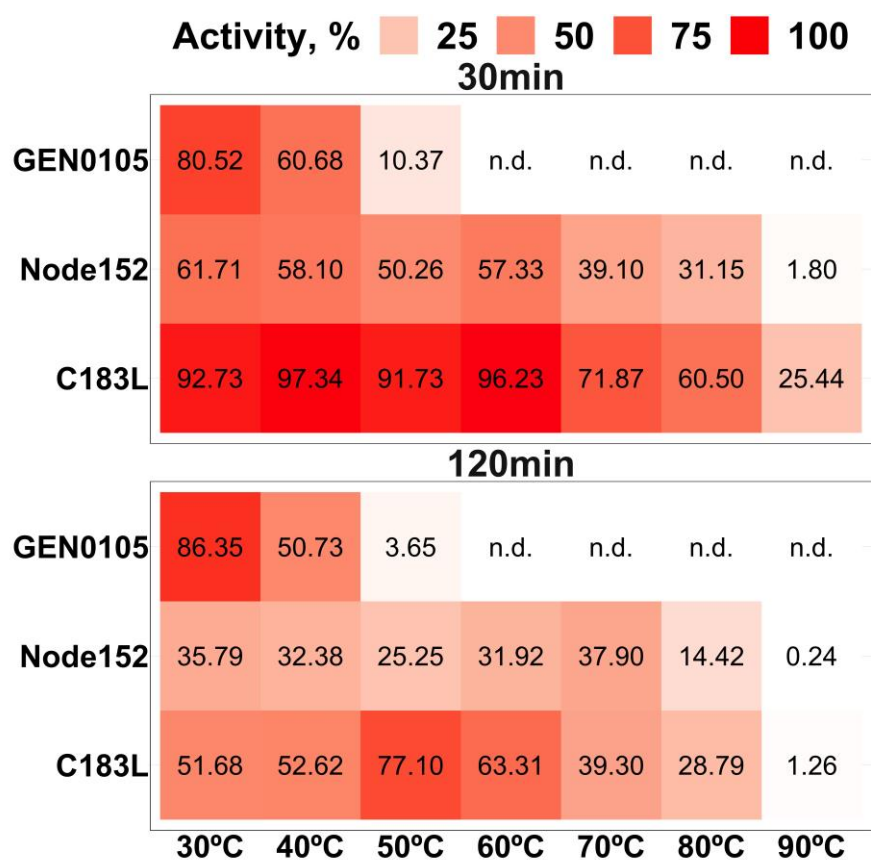


**Fig. 38.** Thermostability of GEN0105, Node152 and C183L mutant. Enzymes were incubated for 30 min and 2h at varying temperature 30-90C. Activity was measured in presence of 1mM pNP-octanoate at 30 °C.

Results demonstrate that mutant of GEN0105, Node152 and C183L, are promising candidates for detergent applications, given its higher activity performance and stability compared to wild type GEN0105. For datasets see Table S2 in the [www.futureenzyme.eu](http://www.futureenzyme.eu) intranet.

#### 4.6. Gen0095 engineering for textile applications

As detailed in D5.1, an additional enzyme was found priority because having characteristics for the detergent sector, Gen0095: Activity, cellulase with activity comparable with benchmark from *Trichoderma* (Sigma 912-54-8); Partner, Bangor; Source, metagenome of a mesophilic anaerobic digester, Evry, France; Nominated based on the screens with stained swatches, and capacity to degrade butterfat on cotton (Fig. 12). Based on energy optimization approach (<https://loschmidt.chemi.muni.cz/fireprotweb/>) 9 mutations were selected: N118L, S182M, Q211P, S231N, N285Y, N287G, S301W, T304M, N324M (Fig. 29C), with all mutations resulting in  $\Delta G$  20.2kcal/mol lower than the wild type protein. No significant improvement in Node 276 thermostability or activity was observed (Fig. 39).

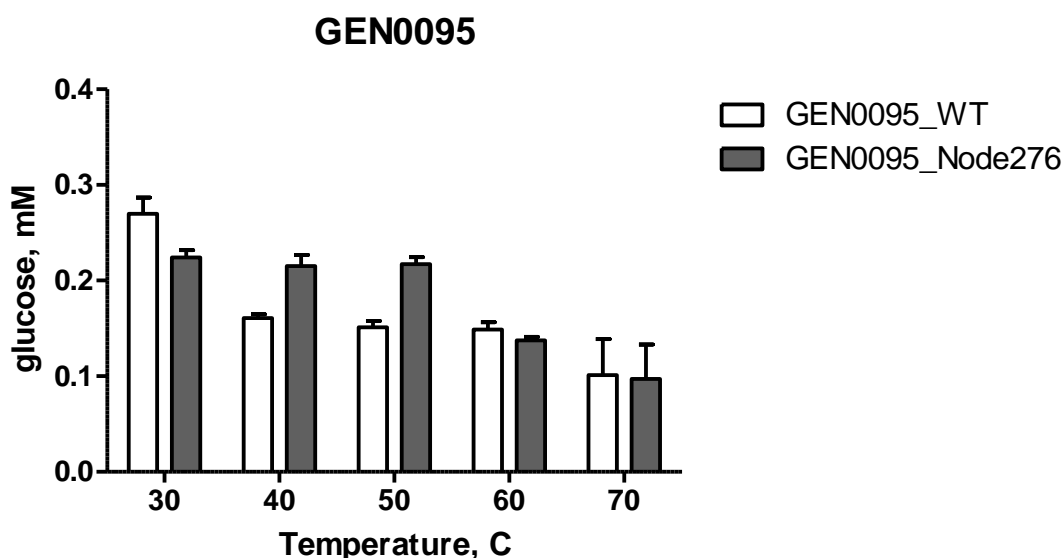


Fig. 39. Temperature stability of GEN0095 (white bars) and Node276 (grey bars). 4  $\mu$ g of each enzyme was incubated at the range of temperatures 30-70  $^{\circ}$ C overnight in presence of 0.01% cellulose in 50mM Tris-Cl buffer pH 8.0.

Results demonstrate that mutant of GEN0095, Node276, is a promising candidate for detergent applications, given its higher activity performance and stability compared to wild type GEN0095. For datasets see Table S2 in the [www.futureenzyme.eu](http://www.futureenzyme.eu) intranet.

#### 4.7. TB035 engineering for textile applications

EstLip\_TB035 was suggested for further exploration in the first place because of its remarkable resistance towards denaturing agents, including surfactants. Further, it shows a rather high structural melting point, although unfolding already starts at a temperature below 40 $^{\circ}$ C. Despite being highly substrate-promiscuous, this enzyme, unfortunately, is not able to hydrolyze long-chain triglycerides. The yet unpublished structure reveals an uncommon topology with two cap domains that may be targeted for engineering. The enzyme originates from *Halopseudomonas aestusnigri*. It is membrane-bound in its original form, linked to membrane lipids by the Sec Typell Lipoprotein secretion machinery which leads to low yields in recombinant expression and hampers purification. To improve expression and purification, a variant was constructed by PCR and restriction/ligation in which the Typell-Sec signal peptide predicted by SignalP5.0 was exchanged for a SecI signal peptide sequence from the *Escherichia coli* protein PelB. The fusion protein could be obtained in a mg /L culture scale.

Results demonstrate that mutant of EstLip\_TB035 in which Typell-Sec signal peptide was substituted by a SecI signal peptide sequence is produce at much higher level than the original enzyme, and thus this mutant

may be prioritized compared to wild type. Note that this mutant has been point in the frame of Deliverable D7.1 as a priority target for full scale wash pre-industrial validation test.

**Conclusions Section 4.** The results demonstrate that the Lip9 Val161Ser mutant is a promising candidate for detergent applications due to its higher performance and stability compared to wild-type Lip9. Mutants of the lipase Lip5, Lip5W89M/L60F, and Lip5lid showed a preference for long triglycerides similar to that of the industrially used R. delemar lipase, although their specific activities are not comparable to those of a non-pure commercial sample (Addzyme RD). Both lipase mutants are promising candidates for detergent applications due to their higher performance compared to wild-type Lip5. The Y250S mutant of the lipase/PETase PEH\_Paes\_PE-H is a promising candidate for detergent applications due to its higher performance compared to wild-type PEH\_Paes\_PE-H. The A46V mutant of the lipase/PETase PET46 is a promising candidate for textile applications, particularly for recycling polyester (PES) fabrics and their macro-, micro-, and nanosized particles, for example, in waste streams during textile processing, due to its higher performance compared to wild-type PET46. Mutants of GEN0105, Node152, and C183L are promising candidates for detergent applications due to their higher performance and stability compared to wild-type GEN0105. The GEN0095 Node276 mutant is a promising candidate for detergent applications due to its higher performance and stability compared to wild-type GEN0095. The mutant of EstLip\_TB035 in which the Type II-Sec signal peptide was substituted by a SecI signal peptide sequence is produced at a much higher level than the original enzyme, and thus this mutant may be prioritized compared to wild-type.

## 5. New mutants designed by genetic engineering and characterized

### 5.1. PE-H from Halopseudomonas formosensis (Pform\_PE-H)

Many groups researching PETases have already identified the amino acid position between the active site histidine and disulfide bridge forming cysteine as being important for stabilizing the active site, as well as being important for opening the active site cleft. Likewise, [Bollinger et al. \(2020\)](#) found in the structure of Haes\_PE-H, that the amino acid position between the active site histidine and the disulfide bridge forming cysteine as a very important position for polyester hydrolase activity. Since this position has already proven to enhance the PET hydrolysis capabilities of Haes\_PE-H, IsPETase and many other enzymes, I aimed to assess the transferability of this approach to the most active enzymes in my enzyme set, namely Poce\_PE-H and Pfor\_PE-H, which already show the most promising activities on aliphatic polyesters. For Pfor\_PE-H from the novel organism *H. formosensis* FZJ ([de Witt et al., 2023](#)), selected amino acid exchanges were introduced to increase the activity. The selected amino acid substitutions were serine, alanine, valine, and phenylalanine. Serine was chosen since it is described by [Bollinger et al. \(2020\)](#) and others as activity increasing. Alanine and valine were chosen as they are more hydrophobic and small residues, that might help in opening the active site cleft for the hydrophobic substrates. Phenylalanine was chosen, since it is like the wild type tyrosine however, but hydrophobic.

The amino acid substitutions of Pfor\_PE-H did not change the melting temperature of the enzymes ([Table 9](#)), however, the amino acid changes against serine and alanine lead to enzymes having significantly higher activities with the esterase substrate pNP-hexanoate at lower temperatures. The activities at 30°C or higher on esterase substrates as well as the activities on polyester substrates did not significantly change ([Table 9](#)).

**Table 9.** Biochemical characteristics of the target mutants of Pform\_PE-H.

Mutation	Melting temperature °C		Polyester substrates	
Name	Melting temperature °C	SD	Activity with Impranil DLN-SD (ΔOD580/mg enzyme)	SD of Activity

Pfor_PE-H_Y250S	53,9	0,047	1,943	0,033
Pfor_PE-H_Y250A	53,8	0,008	1,585	0,210
Pfor_PE-H_Y250V	53,7	0,003	1,222	0,290
Pfor_PE-H_Y250F	54,1	0,045	0,870	0,196

Results demonstrate that mutant of Haes\_PE-H in which amino acid 265 changes against serine and alanine lead to enzymes having significantly higher activities at lower temperatures, and thus are more suitable for detergent and textile applications compared to wild type.

## 5.2. PE-H from *Halopseudomonas oceanis* (Poce\_PE-H)

The enzyme Poce\_PE-H from the organism *H. oceanis* has shown itself as one of the most active and promising enzymes in my enzyme set. It shows high activities towards some polyester substrates, even surpassing the activities of already established enzymes like the IsPETase as well as Haes\_PE-H. Especially the activity on polyester-polyurethane seems very promising since not a lot of enzymes are yet known to degrade such material. As mentioned in the explanation for Pfor\_PE-H, the position right next to the active site histidine in the enzyme IsPETase has been described as crucial for elevated polyester degradation activity. Tournier et al. (2020) found this position by performing a saturation mutagenesis at the predicted MHET binding site of the LCC. They found by molecular dynamics simulations, that the mutated variant has a higher affinity to MHET compared to the wild type. According to [Bollinger et al. \(2020\)](#) this position seems to enlarge the active site cleft of the Haes\_PE-H. Since Poce\_PE-H is a close homologue of Haes\_PE-H with a sequence identity of 71.19 % changing this position seems promising to elevate the polyester or polyester-polyurethane degradation even further than what the Haes\_PE-H can do now. Notably, it was the only *Halopseudomonas* enzyme with a phenylalanine residue instead of tyrosine at the position of interest in my enzyme set.

The saturation mutagenesis lead to the identification of a significant rise in melting temperature for the substitutions N, T, D, C, and E of up to 8°C (Table 10). This could not yet be explained. For the mutation against methionine, an increase in activity at 50°C of about 150% of wild type activity was observed. The change in melting temperature compared to the wild type was in this case around 4°C. Some mutations like the substitutions with aromatic residues (W, Y) and negatively charged residues (E, D) showed a change in optimal pH towards more acidic values compared to the wild type. A connection of the charge of the amino acid residue at this position with activity towards Impranil-DLN could be observed (Table 10). A neutral charge seems to increase activity. The activity on polyester substrates did not significantly change.

**Table 10.** Biochemical characteristics of the target mutants of Poce\_PE-H.

Mutation	Melting temperature °C		Polyester substrates		
	Name	Melting temperature °C	SD	Activity with Impranil DLN-SD (ΔOD580/mg enzyme)	SD of Activity
Poce_PE-H_F265A		49,1	0,16	1,487	0,740
Poce_PE-H_F265C		52,9	0,25	0,493	0,007
Poce_PE-H_F265D		52,4	0,04	0,909	0,008
Poce_PE-H_F265E		53,6	0,06	2,087	0,034
Poce_PE-H_F265G		49,8	0,19	1,770	0,049
Poce_PE-H_F265H		51,6	0,13	0,842	0,016
Poce_PE-H_F265I		49,7	0,28	0,428	0,049
Poce_PE-H_F265K		48,7	0,23	1,869	0,012
Poce_PE-H_F265L		49,3	0,50	0,908	0,143
Poce_PE-H_F265M		51,4	0,24	0,748	0,006

Poce_PE-H_F265N	53,0	0,01	1,367	0,503
Poce_PE-H_F265P	49,2	0,40	0,631	0,009
Poce_PE-H_F265Q	50,0	0,09	2,067	0,035
Poce_PE-H_F265R	47,8	0,01	0,789	0,005
Poce_PE-H_F265S	50,9	0,02	1,055	0,002
Poce_PE-H_F265T	53,8	0,21	1,767	0,033
Poce_PE-H_F265V	50,1	0,05	1,040	0,009
Poce_PE-H_F265W	50,9	0,20	1,018	0,006
Poce_PE-H_F265Y	52,1	0,66	1,000	0,046

Results demonstrate that mutant of Pfor\_PE-H in which amino acid 250 changes against N, T, D, C, and E are more stable, those changes by A about 150% more active, and those changes by aromatic residues (W, Y) and negatively charged residues (E, D) showed a change in optimal pH towards more acidic values. These mutants are thus more suitable for detergent and textile applications compared to wild type. For datasets see Table S3 in the [www.futureenzyme.eu](http://www.futureenzyme.eu) intranet

### 5.3. Engineering of new PET44 variants

In our global metagenomic mining project using the Hidden Markov model (HMM), which aims to obtain new biocatalists, that efficiently degrade PET, the best candidates were further characterized and tested on different substrates. One promising construct with a high score is PET44 (NCBI: WP\_116302305.1), which is annotated as a diene lactone hydrolase. The mesophilic enzyme originates from *Alkalilimnicola ehrlichii* AK92/AK93 (NCBI accession: PRJNA385252) and was isolated from the hypersaline and alkaline Sambhar Salt Lake in India. The alpha-beta hydrolase PET44 displays high sequence similarity of 53,28 % to the IsPETase and contains the same catalytic triad (Ser172, Asp218, His250) and binding triad (Tyr99, Met173, Trp196). With comparable PET degradation rates, it is a good candidate for mutation strategies.

To further investigate and understand the overall structural features of an efficient PETase, mutants of PET44 were generated, analogous to those mutations introduced in the popular and industrially relevant PET-degrading enzymes LCC and IsPETase. A common strategy for achieving higher end-product yield is to increase enzymatic thermostability by introducing cysteine- or salt-bridges, allowing for greater accessibility to the more flexible PET-substrate at higher incubation temperatures. Other targets include increasing the mobility of relevant PET-binding loops or simply enlarging of the active site to enhance PET-hydrolysis. Popular modifications (ThermoPETase, DuraPETase, HotPETase, Y251S, H226S/F230I) are introduced to investigate similar trends on overall enzymatic performance. Additionally, the introduction of ICCG amino acids, comparable to the LCC-ICCG mutant, were implemented. The mutation Y251C was randomly obtained during mutagenesis experiments and included for degradation experiments. Table 11 displays all relevant changes of amino acid composition within the selected PET44 mutants.

**Table 11.** Amino acid substitutions of PET44 mutants. The mutations for the TS-PETase are: 44-Thermo + S246C/S297C, but this mutant was not separately generated.

Mutation	Amino acid substitution
44-Thermo	P133E/N197H/Q295A
44-ICCG	Y251I/S246C/S297C/Q131G
44-DuraPETase	A227H/W171H/S199Q/Q295A/G177A/Q131Y/S129F/S152D
44-HotPETase	TS-PETase+G192V/S219R/H226Y/Q131K/S225E/Y102T/L193M/R224K/S237L/S69A/R73V/S107N/L166G/N254C/K265M/P283Q
44-Y251C	Y251C
44-H226S/F230I	H226S/F230I
44-Y251S	Y251S

Shown in **Tables 12-15** are heatmaps displaying the total product yield of PET-degradation with PET44, LCC, IsPETase and all PET44 mutants at temperatures ranging from 30°C to 80°C. PET44, LCC and IsPETase were incubated with 7 mg PET powder (product no. ES306000; >40% crystallinity, d≈300 μm; 9.6 μmol or 48 mM TPA eq.; GoodFellow GmbH, Hamburg, Germany) and 7 mg amorphous PET foil platelet (product no. ES301445; a=5 mm<sup>2</sup>, 33.6 μmol or 168 mM TPA eq.; GoodFellow GmbH, Hamburg, Germany). PET44 mutants were incubated with 7 mg PET powder (product no. ES306000/1, >50% crystallinity, d≈300 μm; 9.6 μmol or 48 mM TPA eq.; GoodFellow GmbH, Hamburg, Germany) and the same PET foil as the wildtype-enzymes.

On PET powder, the optimal temperature of many variants has increased, which is visible especially in the 2-hour values. While the PET44 wildtype has an optimum at 40°C, some mutants (e.g. 44-ICCG and Y251C) show high activity at 50°C or 60°C. However, it is yet unclear if the overall efficiency of PET hydrolysis is increased as well. Further testing and new data for the wildtype enzymes is required.

**Table 12.** Degradation after 2 hours on PET powder (50% crystallinity). Values are displayed in μM.

	30°C	40°C	50°C	60°C	70°C	80°C
44-Thermo	19.18	114.74	47.54	9.64	4.23	2.27
44-ICCG	2.66	30.35	145.17	6.57	3.74	3.44
44-DuraPETase	N.A.	N.A.	N.A.	N.A.	N.A.	N.A.
44-HotPETase	N.A.	N.A.	N.A.	N.A.	N.A.	N.A.
44-Y251C	N.A.	N.A.	N.A.	N.A.	N.A.	N.A.
44-H226S/F230I	7.12	66.36	5.34	8.31	7.47	5.16
44-Y251S	4.91	37.20	3.26	2.85	0.54	0

**Table 13.** Degradation after 2 hours on PET powder (40% crystallinity). Values are displayed in μM.

	30°C	40°C	50°C	60°C	70°C	80°C
PET44	38.42	232.50	72.84	N.A.	N.A.	N.A.
IsPETase	211.69	857.41	251.44	N.A.	N.A.	N.A.
LCC	93.49	519.37	3657.08	N.A.	N.A.	N.A.

**Table 14.** Degradation after 24 hours on PET powder (50% crystallinity). Values are displayed in μM.

	30°C	40°C	50°C	60°C	70°C	80°C
44-Thermo	214.09	3337.59	100.90	12.10	10.00	0
44-ICCG	75.33	2519.83	2882.75	0	0.49	0
44-DuraPETase	1.65	1.92	1.47	2.67	4.82	0
44-HotPETase	0,08	0	4.01	21.70	14.18	0
44-Y251C	11.34	111.87	291.24	2147.99	296.36	69,05
44-H226S/F230I	80.71	848.34	24.72	601.15	40.98	0
44-Y251S	60.40	1023.82	8.65	8.60	8.44	0

**Table 15.** Degradation after 24 hours on PET powder (40% crystallinity). Values are displayed in μM.

	30°C	40°C	50°C	60°C	70°C	80°C
PET44	201.69	2840.69	123.38	N.A.	N.A.	N.A.
IsPETase	1639.42	2275.23	261.69	N.A.	N.A.	N.A.

LCC	814.47	2861.38	3292.49	N.A.	N.A.	N.A.
-----	--------	---------	---------	------	------	------

**Table 16.** Degradation after 2 hours on PET foil

	30°C	40°C	50°C	60°C	70°C	80°C
PET44	0,44	3,85	1,64	N.A.	N.A.	N.A.
IsPETase	8,26	10,62	3,76	N.A.	N.A.	N.A.
LCC	1,55	9,91	61,70	N.A.	N.A.	N.A.

**Table 17.** Degradation after 24 hours on PET foil.

	30°C	40°C	50°C	60°C	70°C	80°C
PET44	1,58	54,99	3,28	N.A.	N.A.	N.A.
IsPETase	60,43	13,71	4,34	N.A.	N.A.	N.A.
LCC	9,78	196,86	2421,85	N.A.	N.A.	N.A.

In general, the total product yield was higher on PET powder than on PET foil. On PET foil, only the LCC showed significant activity at the optimal temperature of 50°C (Table 16 and Table 17). A low amount of degradation products was also detected for PET44 and IsPETase, suggesting that this substrate is too challenging for the wildtype constructs. PET44 mutants showed no significant activity on PET foil.

Results demonstrate that mutant of PET44 with Y251C, or H226S/F230I, or Y251S are more stable and active than wild type, and are thus more suitable for detergent and textile applications compared to wild type.

#### 5.4. Engineering of EH<sub>37</sub> variants

The objective to evaluate the effect of a number of mutations in the thermostability of the esterase EH<sub>37</sub> (Protein data Bank acc. nr. 5JD5). A total of 100 mutations were selected by partner BSC on the basis of DDG values. From those, 11 mutations were introduced into EH<sub>37</sub> and the corresponding mutants produced by gene synthesis and purified as for the wild type. Circular dichroism (CD) spectra were acquired between 190 and 270 nm with a Jasco J-720 spectropolarimeter equipped with a Peltier temperature controller, employing a 0.1 mm cell at 25°C. Spectra were analyzed, and denaturation temperatures were determined at 220 nm between 10 and 85°C at a rate of 30°C per hour, in 40 mM (4-(2-hydroxyethyl)-1-piperazineethanesulfonic acid (HEPES) buffer, pH 7.0. A protein concentration of 1.0 mg ml<sup>-1</sup> was used. Denaturation temperatures were calculated by fitting the ellipticity (mdeg) at 220 nm at each of the different temperatures using a 5-parameters sigmoid fit with Sigma Plot 14.0.. Their denaturation temperature (Td) ranged from 31,7734 ± 1,1269°C to 39.36±0.33°C (Table 18). We further observed that although activity was not improved by the mutations, three of them promote the stability in the presence of washing detergent liquor.

**Table 18.** Characteristics of EH<sub>37</sub> mutants.

	Predictor	Mutation	DDG value	Td (°C)	Units/mg <sup>1</sup>	Units/mg <sup>2</sup>
1	5JD5	None	None	35,9916 ± 0.1981	2970 ± 22	0
2	AL	36F	-1,593600001	39,3643 ± 0,3303	2830 ± 70	0
4	AL	36H	-0,902499993	37,9995 ± 0,2993	670 ± 10	0
5	AL	62I	-0,844500003	31,7734 ± 1,1269	350 ± 10	0
6	AL	87G	-0,791399995	35,9748 ± 0,4417	2550 ± 60	165.6
7	AL	242G	-0,769099992	32,1130 ± 0,8538	380 ± 7	1242.6
9	AL	41W	-0,8463	34,5942 ± 0,2387	620 ± 9	0

10	AL	214I	-0,885600004	34,4547 ± 0,3126	1000 ± 10	0
15	AL	36M	-0,680699998	38,1635 ± 0,4528	620 ± 8	0
16	AL	294S	-0,426099996	37,3991 ± 0,3948	1140 ± 16	0
17	AL	36E	-0,378099997	38,2672 ± 0,5226	2570 ± 56	1088.7

Results demonstrate that mutants of EH<sub>37</sub> with 87G, or 242G or 36E are more suitable than wild type EH<sub>37</sub> as they promote stability in the presence of detergent washing liquor. Other mutations such as 36H, 36H, 36M, 36E or 294S improved the thermostability, so that 87G, or 242G or 36E can be combined with any of the previous ones to generate more stable mutants for detergent applications compared to wild type. For datasets see Table S4 in the [www.futureenzyme.eu](http://www.futureenzyme.eu) intranet.

### 5.5. Engineering of non-catalytic proteins into enzymes

The fact that we have a computational tool that allows us to add active sites to non-catalytic enzymes and proteins (see Section 3), we subsequently used it to genomically edit *Escherichia coli*, engineering its own proteins so that they degrade plastic by incorporating artificial active sites supporting activities relevant to the project, namely, for degrading PET polyester (PES) fabrics and their macro-, micro- and nano-sized particles, e.g., in waste streams during textile processing.

In details, by analyzing *E. coli* proteins by PELE software (see Section 3), we identified 100 candidates binding to PET substrates (a PET trimer, a PET dimer, and an MHET molecule) and we were able to transform the binding site of 24 of these proteins into Ser-Asp-His hydrolytic catalytic sites. They include the following *E. coli* proteins: AF\_AOA140N1V2 (BM1), AF\_AOA140N8N6 (BM2), AF\_AOA140ND91 (BM3 or *lsrB*), AF\_AOA140N4H6 (BM4), AF\_AOA140N8S2 (BM5), AF\_AOA140NDB3 (BM6), AF\_AOA140N5B8 (BM7), AF\_AOA140N9L6 (BM8), AF\_AOA140NE77 (BM9), AF\_AOA140N7H1 (BM10), AF\_AOA140N9U9 (BM11), AF\_AOA140NEP6 (BM12), AF\_AOA140N7K9 (BM13), AF\_AOA140NBR2 (BM14), AF\_AOA140NFM8 (BM15), AF\_AOA140N843 (BM16), AF\_AOA140NCA9 (BM17 or *SsuA*), AF\_AOA140NGB7 (BM18), AF\_AOA140N8B6 (BM19), AF\_AOA140NCF6 (BM20), AF\_AOA140NHK0 (BM21), AF\_AOA140N8D2 (BM22), AF\_AOA140NCW7 (BM23), AF\_AOA140NHP9 (BM24).

After gene synthesis and protein production, out of 23 mutants two (mutants of the *E. coli* *lsrB* and *SsuA* proteins) were found to effectively degraded raw and nano-sized polyester material (4-b 3X58: VORB, 100% PES 100g/m<sup>2</sup>) in vitro at 37°C (Fig. 40). By using nano-sized polyester material at a concentration of 1.71 mg/ml, 20 mM HEPES pH 7, 37°C, and 950 rpm, yielding total degradation product concentrations of 4900 μM for BM3 mut giving a activity of 377.3 mM/mg (mM of degradation products per mg of enzyme) and 7136 μM giving a activity of 548.92 mM/mg for BM17. These enzymes were further tested with 5.7 mg of raw polyester material for 96 hours, resulting in total degradation product concentrations of 119 μM for BM3 mut and 168 μM for BM17 mut (Fig. 40).

Using CRISPR-editing, we replaced *lsrB* in *E. coli* with the mutant. Additional genes (*Fuc0* and *AldA*) were added to enable using ethyleneglycol as carbon source. Results demonstrate the strain's ability to degrade 10-nm particles from textile 4-b 3X58 (VORB, 100% PES 100g/m<sup>2</sup>), provided by partner Schoeller, within 5 hours during cultivation at 37°C (15682 μM degradation products) and grow using resulting ethylene glycol (growth rate: 0.05 h<sup>-1</sup>) (Fig. 41). This research, showcases the potential of genomically editing *E. coli* for sustainable PET or polyester recycling.

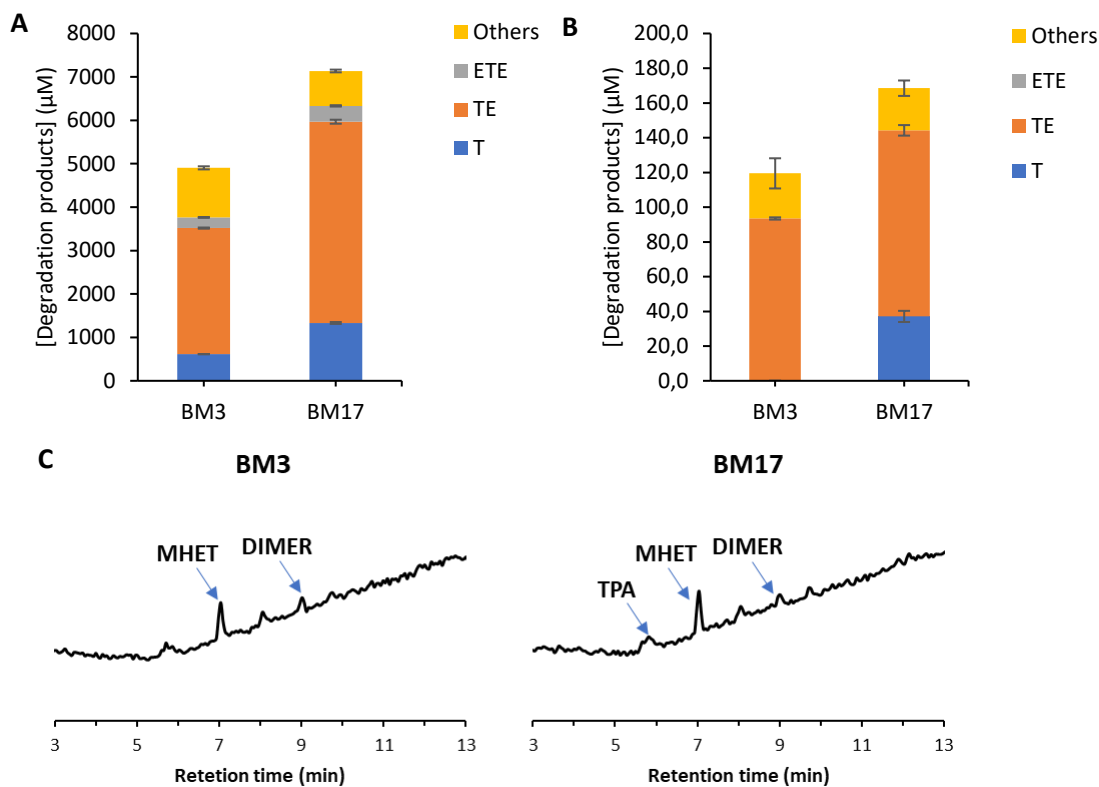


**Fig. 40.** **A.** BM3 and BM17 raw and nano-sized polyester material (4-b 3X58: VORB, 100% PES 100g/m<sup>2</sup>). Reaction conditions: 1.71 mg/ml of nano-sized polyester material in HEPES buffer 40 mM, pH 7.0 with 0.13 mg/ml of pure enzyme (BM3mut and BM17mut). All experiments were carried out in triplicate, with nano-sized polyester material without enzyme as a negative control. Tubes were incubated at 37 °C with 950 rpm agitation for 24 hours. **B.** BM3 and BM17 raw polyester material hydrolysis. Reaction conditions: 5.7 mg of raw polyester material hydrolysis were added to sterile 2-ml safe-lock Eppendorf® polypropylene tubes (ref. 0030120094) with HEPES buffer 40 mM, pH 7.0 and 0.43 mg/ml of pure enzyme (BM3mut and BM17mut). The experiment was carried out in triplicate, with raw polyester material hydrolysis without enzyme as a negative control. Tubes were incubated at 37 °C with 1000 rpm agitation for 96 hours. **C.** Chromatograms of BM3 and BM17 PET hydrolysis.

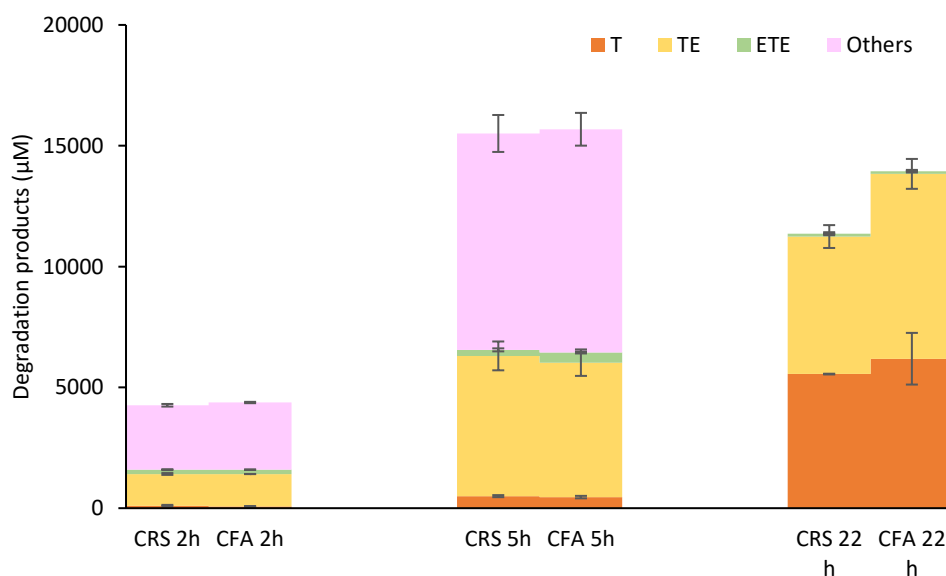


**Fig. 40.** Degradation of 10-nm particles from textile 4-b 3X58 (VORB, 100% PES 100g/m<sup>2</sup>), provided by partner Schoeller, by *E. coli* BL21(D3) with CRISPR-introduced PETase BM17mut and pET45b(+) plasmid containing FuC0 and AldA genes. Degradation products measured at 2, 5 and 22 hours. Abbreviations as follows: CRS, CRISPR BM17 mut (CRS): *E. coli* BL21(D3) with CRISPR-introduced PETase BM17mut; CFA, CRISPR BM17 mut – FuC0, AldA (CFA): *E. coli* BL21(D3) with CRISPR-introduced PETase BM17mut and FuC0, AldA.

pET45b(+) plasmid containing FuCO and AldA genes. All these cultures were supplemented with 50 µg/mL ampicillin (Amp), except CRS, which did not carry any antibiotic resistance plasmid. Cultures were allowed to grow overnight at 37 °C and 100 rpm. The following day, cultures were centrifuged. Cells were washed three times with M9 2X minimal media, and finally resuspended in 2 mL of M9 2X. Dilutions of 2 mL for each cell type with M9 2X media were prepared at OD600nm 0.2, with 100 µg/mL Amp and 2 mM IPTG, excluding CRS, and glycerol 0.2 mg/ml. 250 µL of these dilutions were added to sterile 2-ml safe-lock Eppendorf® polypropylene tubes (ref. 0030120094). 250 µL of a nano-sized polyester material (4-b 3X58: VORB, 100% PES 100g/m<sup>2</sup>) small stock in water, were added to samples in order to obtain final cultures with M9 1X, OD600nm 0.1, 50 µg/mL Amp, 1 mM IPTG (except CRS), glycerol 0.1 mg/ml and nano-sized polyester material (4-b 3X58: VORB, 100% PES 100g/m<sup>2</sup>) small 1.71 mg/ml. Cultivation in M9 1X media contains Na<sub>2</sub>HPO<sub>4</sub>, KH<sub>2</sub>PO<sub>4</sub>, NaCl, NH<sub>4</sub>Cl, and 2 mM MgSO<sub>4</sub>. Products abbreviations: T, Terephthalic acid; TE, MHET; ETE, BHET.

Results demonstrate that it is possible to engineer non-catalytic proteins from Escherichia coli into PET degrading enzymes, and further genomically edit an E. coli strain by CRISP techniques, to degrade TEP nanoparticles. By doing so we have generated two mutants, named BM3 mut (or IsrB mut) and BM17 mut (or SsuA mut) suitable for textile applications, namely, for recycling of polyester (PES) fabrics and their macro, micro- and nanosized particles, e.g., in waste streams during textile processing. For datasets see Table S1 in the [www.futureenzyme.eu](http://www.futureenzyme.eu) intranet.

**Conclusions for Section 5. To date, a total of 98 mutants from 35 different proteins have been generated and their datasets are available. These proteins are relevant to detergent and textile applications. The complete list of mutants per proteins is detailed: 23 mutants E. coli proteins PETase, 19 mutants Pform\_PE-H PETase, 15 mutants Lip9 lipase, 11 mutants EH37 esterase, 10 mutants Gen0105, 4 mutants PET46 lipase/PETase, 4 mutants Poce\_PE-H PETase, 3 mutant Kest3, 3 mutants PET44 PETase, 2 mutants Lip5 lipase, 2 mutant Gen0095, 1 mutant PEH\_Paes\_PE-H lipase/PETase and 1 mutant EstLip\_TB035 lipase. Results demonstrate that the mutant of Haes\_PE-H, with amino acid 265 changed to serine and alanine, leads to enzymes with significantly higher activities at lower temperatures, making them more suitable for detergent and textile applications compared to the wild type. Mutants of Pfor\_PE-H, in which amino acid 250 changes to N, T, D, C, and E, exhibit enhanced stability. Changes by A result in approximately 150% higher activity, while changes by aromatic residues (W, Y) and negatively charged residues (E, D) shift the optimal pH towards more acidic values. These mutants are thus more suitable for detergent and textile applications compared to the wild type. Mutants of PET44 with Y251C, or H226S/F230I, or Y251S show improved stability and activity compared to the wild type, making them more suitable for detergent and textile applications. Mutants of EH37 with 87G, 242G, or 36E are more suitable than the wild type EH37, promoting stability in the presence of detergent washing liquor. Additional mutations such as 36H, 36M, or 294S improve thermostability. These mutations can be combined with 87G, 242G, or 36E to generate more stable mutants for detergent applications compared to the wild type. The results demonstrate the possibility of engineering non-catalytic proteins from Escherichia coli into PET-degrading enzymes. Further genomic editing of an E. coli strain using CRISPR techniques allows degradation of TEP nanoparticles. This approach has generated two mutants, named BM3 mut (or IsrB mut) and BM17 mut (or SsuA mut), suitable for textile applications, particularly for recycling polyester (PES) fabrics and their macro, micro, and nanosized particles, such as those found in waste streams during textile processing.**

## 6. Supramolecular engineered enzymes reported in Deliverable D5.5, updated

The technology of enzyme immobilization and shielding was applied on a number of selected enzymes , summarized in Table 19. These enzymes find applications in detergent and textiles processing industries. Below the work done and datasets and results obtained are detailed.

**Table 18.** Description of the 18 enzymes produced by supramolecular engineering.

	Name	Supramolecular engineering strategy	Industrial application
1	Fe_Lip <sub>MIRD9</sub>	Enzyme immobilization and shielding including cyclodextrin as building blocks.	Textile (spinning oil removal). Detergent (formulation). PET hydrolysis.

2	PEH_Paes_PE-H-Y250S	Enzyme immobilization by homobifunctional crosslinker and shielding.	Textile (spinning oil removal). Detergent (formulation).
3	EstLip_TB035	Enzyme immobilization by homobifunctional crosslinker and shielding	Textile (spinning oil removal). Detergent (formulation).
4	EstLip_Dim (AT)	Enzyme immobilization by homobifunctional crosslinker and shielding.	Textile (spinning oil removal). Detergent (formulation)
5	EstLip_Dim (ATH)	Enzyme immobilization by homobifunctional crosslinker and shielding.	Textile (spinning oil removal). Detergent (formulation).
6	EstLip_Dim (ATP)	Enzyme immobilization by homobifunctional crosslinker and shielding.	Textile (spinning oil removal). Detergent (formulation).
7	EstLip_Dim (ATB)	Enzyme immobilization by homobifunctional crosslinker and shielding.	Textile (spinning oil removal). Detergent (formulation).
8	FE-Polur1 (AT)	Enzyme immobilization by homobifunctional crosslinker and shielding.	Textile (spinning oil removal). Detergent (formulation)
9	FE-Polur1 (ATH)	Enzyme immobilization by homobifunctional crosslinker and shielding.	Textile (spinning oil removal). Detergent (formulation).
10	FE-Polur1 (ATP)	Enzyme immobilization by homobifunctional crosslinker and shielding.	Textile (spinning oil removal). Detergent (formulation)
11	FE-Polur1 (ATB)	Enzyme immobilization by homobifunctional crosslinker and shielding.	Textile (spinning oil removal). Detergent (formulation).
12	EstLip_PTEST 1 (AT)	Enzyme immobilization by homobifunctional crosslinker and shielding.	Textile (spinning oil removal). Detergent (formulation).
13	EstLip_PTEST 1 (ATH)	Enzyme immobilization by homobifunctional crosslinker and shielding.	Textile (spinning oil removal). Detergent (formulation).
14	EstLip_PTEST 1 (ATP)	Enzyme immobilization by homobifunctional crosslinker and shielding.	Textile (spinning oil removal). Detergent (formulation)
15	EstLip_PTEST 1 (ATB)	Enzyme immobilization by homobifunctional crosslinker and shielding.	Textile (spinning oil removal). Detergent (formulation).
16	<i>Candida antarctica</i> lipase A (CaLA)	Oriented enzyme immobilization through the His-Tag of the enzyme. Shielding with a regular layer.	Textile (spinning oil removal). Detergent (formulation).
17	Laccase ( <i>Trametes versicolor</i> )	Enzyme immobilization through the glycans present in the protein and shielding.	Textile (dye degradation).
18	EH <sub>3</sub>	Enzyme immobilization and shielding.	Textile (spinning oil removal).

### 6.1. Fe\_LipMRD9 (or Lip9)

A lipase from *Bacillus subtilis* (Lip<sub>MRD9</sub>) was used as a model enzyme to develop a method of enzyme shielding to enhance not only the stability in harsh condition (*e.g.*, presence of solvents) but also the thermostability of enzymes used in industrial processes. Lip<sub>MRD9</sub> was immobilized onto silica particles and shielded with an organosilica layer containing cyclodextrin (CDs) as artificial chaperones. To incorporate CDs in the protective shield, a new building block was synthesized by reacting  $\beta$ -cyclodextrin ( $\beta$ -CD) with 3-isocyanatopropyl-trimethoxysilane to produce CD-TES. After crosslinking of Lip<sub>MRD9</sub> onto the surface of the silica particles through glutaraldehyde coupling, the enzyme was shielded with an organosilica layer containing CD-TES and (3-aminopropyl)-triethoxysilane (APTES). The complete shielding of the enzyme was obtained with a layer of 7 nm (Fig. 41A). A solution containing 1% vol sodium dodecyl sulfate (SDS) was used to study the stability of the shielded enzyme under denaturing conditions. In particular, the catalytic activities of soluble Lip<sub>MRD9</sub>, Lip<sub>MRD9</sub> shielded in a layer not containing CD-TES and Lip<sub>MRD9</sub> shielded in a layer containing CD-TES were measured right after the incubation with SDS or after a step of dialysis (to remove the denaturing agent SDS) to allow the refolding of the protein. It was found that, after incubation in SDS, the soluble Lip<sub>MRD9</sub> lost more than the 80% of the initial activity, the Lip<sub>MRD9</sub> shielded in a layer not containing CD-ES (SP-Lip<sub>MRD9</sub>-OS) preserves the 18% of activity and the Lip<sub>MRD9</sub> shielded in a layer containing CD-TES (SP-Lip<sub>MRD9</sub>-OSCD)

preserves the 25% of activity. When the activity was tested after the dialysis step, the Lip<sub>MRD9</sub> retained only the 15% of its initial activity, the SP-Lip<sub>MRD9</sub>-OS preserved the 70% of its initial activity and SP-Lip<sub>MRD9</sub>-OSCD preserves more than the 80% of its activity (Fig. 41B). These results indicate that the cyclodextrins present in the shield not only protect the enzyme but also support and assist its re-folding after incubation in denaturing conditions. Moreover, to study the thermal stability, the enzymes were incubated for 30 min at 50 °C. The Lip<sub>MRD9</sub> lost more than the 70% of the catalytic activity already after 20 min and it was not active after 40 min incubation. SP-Lip<sub>MRD9</sub>-OS preserved more than the 50% of the initial activity after 20 min and retained only the 10% of activity after 60 min. SP-Lip<sub>MRD9</sub>-OSCD preserved more than then 50% of activity after 30 min incubation at 50 °C and more than the 20% of activity after 60 min (Fig. 41C).

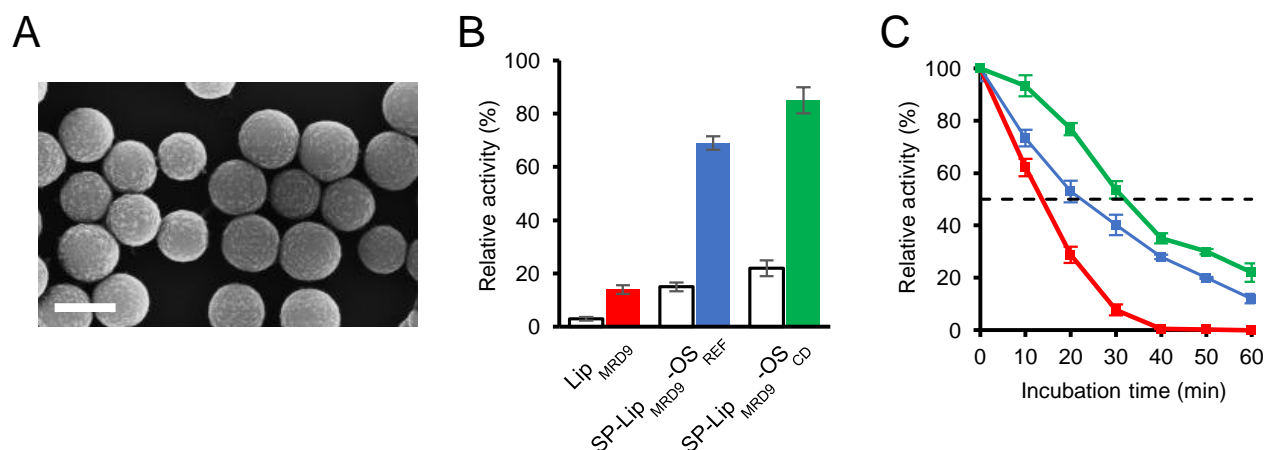


**Fig. 41.** (A) Scanning electron micrograph of shielded SP-Lip<sub>MRD9</sub>-OSCD (scale bar: 200 nm). (B) White bars from left to right: Relative activity of Lip<sub>MRD9</sub>, SP-Lip<sub>MRD9</sub>-OS and SP-Lip<sub>MRD9</sub>-OSCD after incubation in a solution containing 1% vol of SDS. Colored bars: Lip<sub>MRD9</sub> (red bar), the SP-Lip<sub>MRD9</sub>-OS (blue bar) and SP-Lip<sub>MRD9</sub>-OSCD (green bar) after incubation in a solution containing 1% vol of SDS and after refolding time. (C) Normalized enzymatic activity during 60 min incubation at 50 °C of the soluble Lip<sub>MRD9</sub> (red), of SP-Lip<sub>MRD9</sub>-OS (blue), and of SP-Lip<sub>MRD9</sub>-OSCD (green).

The obtained results showed that the presence of CD derivatives into the shield of Lip<sub>MRD9</sub> increased the stability of the enzyme in the presence of solvents and at elevated temperatures. These findings are of huge importance for the implementation of enzymes in industrial processes.

### 6.2. PEH\_Paes\_PE-H\_Y250S

For detergent applications, the lipase PEH\_Paes\_PE-H\_Y250S shows high specific activity on fatty standard stains, particularly on polyester and cotton fabrics. This enzyme was anchored onto silica particles by using glutaraldehyde as homobifunctional crosslinker. After immobilization, it was shielded with an organosilica layer made of APTES and TEOS. The activity of the shielded enzyme was measured using p-nitrophenyl butyrate (pNPB). Fe\_Lip 9, which has high affinity for hydrophobic substrates such as triglycerides, was used as a negative control (Fig. 42). The results obtained showed that the shielding does not hamper the catalytic activity of the enzyme and that particles containing this enzyme may be suitable for industrial applications.

### 6.3. EstLip\_TB035

The lipase EstLip\_TB035 has remarkable resistance towards denaturing agents, including surfactants. The enzyme was immobilized onto silica particles using glutaraldehyde as crosslinker. After immobilization, EstLip\_TB035 was shielded with an organosilica layer made of APTES and TEOS in a similar way as for PEH\_Paes\_PE-H\_Y250S. The activity of the shielded enzyme was measured using pNPB. Fe\_Lip 9 was used as a negative control enzyme (Fig. 42). The obtained results showed that the shielding does not hinder the catalytic activity of the enzyme and that particles containing this enzyme can be implemented in industrial applications.

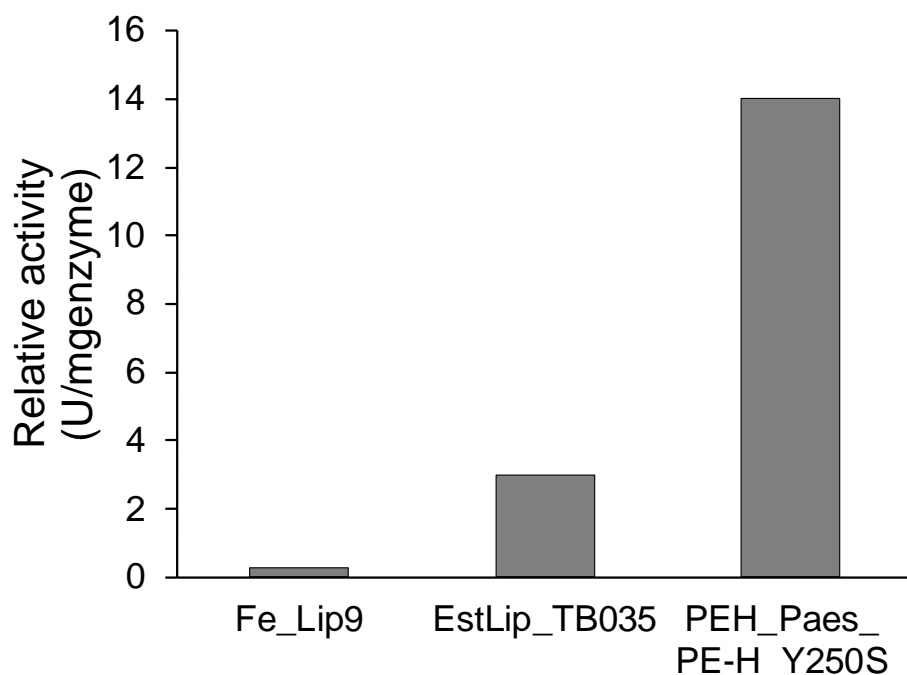


**Fig. 42.** Activity of the immobilized and shielded EstLip\_TB035 and of PEH\_Paes\_PE-H\_Y250S compared to the activity of FeLip-9.

#### 6.4. EstLip\_Dim (AT); 5. EstLip\_Dim (ATH); 6. EstLip\_Dim (ATP); 7. EstLip\_Dim (ATB)

The lipase EstLip\_Dim was anchored through glutaraldehyde coupling onto the surface of amino modified silica particles. The immobilized enzyme was shielded with a complex organosilica layer containing mixtures of different organosilanes building blocks such as: (3-aminopropyl)-triethoxysilane (A), tetraethyl orthosilicate (T), hydroxymethyl-triethoxysilane (H), propyl-triethoxysilane (P) and benzyl-triethoxysilane (B). For all the organosilanes compositions, the thicknesses of the obtained shields (8 nm, 7 nm, 4 nm and 5 nm for AT, ATH, ATP and ATB respectively) allowed the complete covering of the enzyme (Fig. 43A). The catalytic activities of the immobilized and shielded EstLip\_Dim enzymes were measured by using pNPB as a model substrate (Fig. 43B). It was observed that by increasing the hydrophobicity of the layer, as in the case of the composition containing benzyl-triethoxysilane, an improvement of the activity of the shielded Est-Lip-Dim was obtained. Scanning electron micrographs of EstLip\_Dim are shown in Fig. 43C).

#### 6.5. FE-Polur1 (AT); 9. FE-Polur1 (ATH); 10. FE-Polur1 (ATP); 11. FE-Polur1 (ATB)

In a similar manner to the procedure used for the enzyme EstLip\_Dim, the enzyme FE-Polur1 was anchored onto the surface of amino-modified silica particles and protected with organosilica layers of different compositions. For all the tested organosilanes compositions, the thicknesses of the obtained shields (13 nm, 10 nm, 9 nm for AT, ATH, ATP and ATB respectively) allowed the complete shielding of the enzyme (Fig. 44A). For this enzyme, it was observed that the presence of organosilanes with different chemical functionalities did not improve the hydrolysis of the substrates compared to a shield made of AT (Fig. 44B).

#### 6.6. EstLip\_PTEST 1 (AT); 13. EstLip\_PTEST 1 (ATH); 14. EstLip\_PTEST 1 (ATP); 15. EstLip\_PTEST 1 (ATB)

As in the case of the enzymes EstLip\_Dim and FE-Polur1, EstLip\_PTEST 1 was anchored and shielded onto the surface of silica particles. For all the designed organosilanes compositions, the thicknesses of the obtained shields (7 nm, 13 nm, 10 nm and 9 nm for AT, ATH, ATP and ATB respectively) allowed the full protection of the enzyme (Fig. 45A). The catalytic activities were measured by using pNPB (Fig. 45B). It was observed that

by increasing the hydrophilicity of the layer, as in the case of the composition containing hydroxymethyl-triethoxysilane an improvement of the activity of the immobilized and shielded EstLip-PtEst1 was obtained.

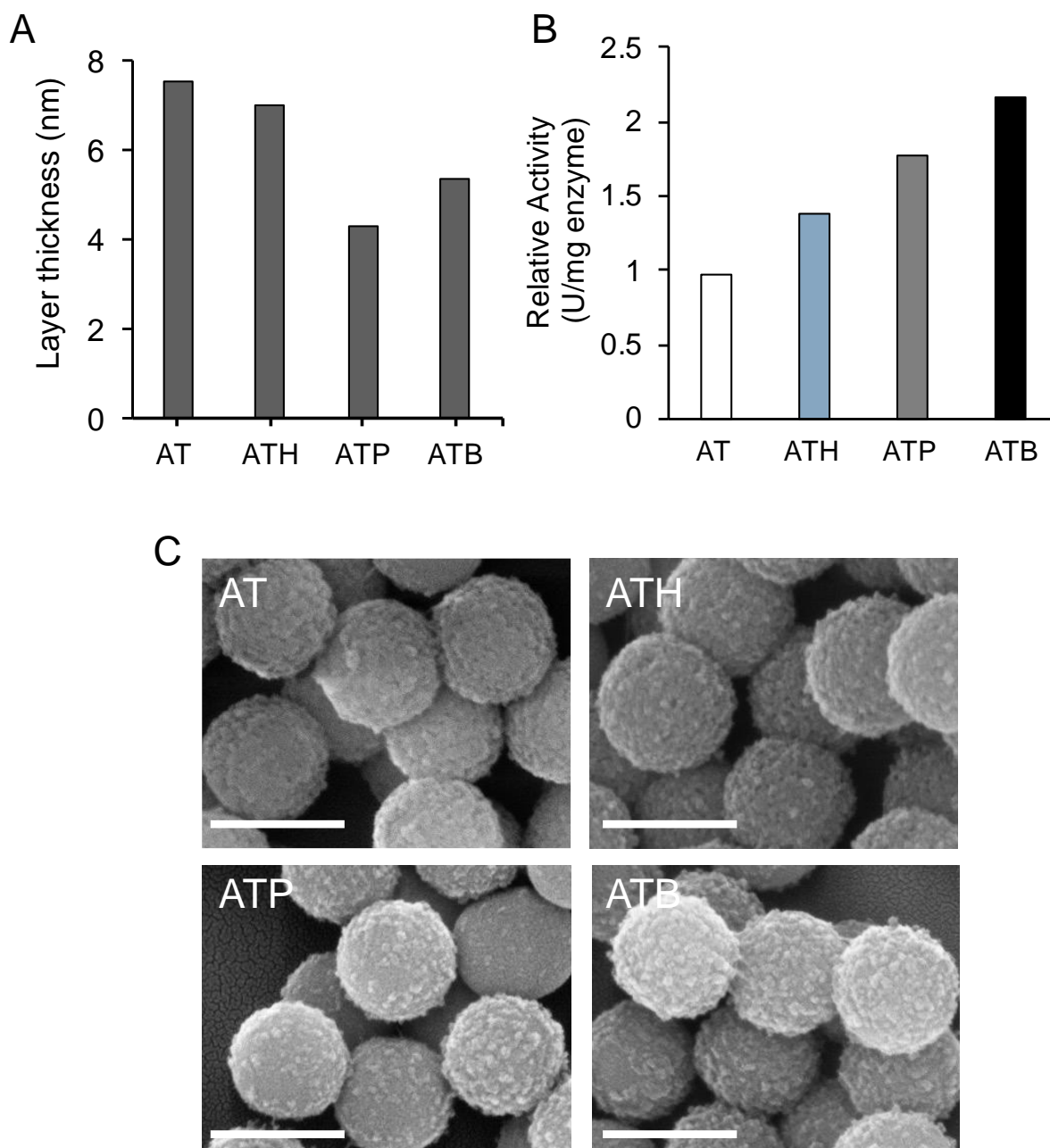


**Fig. 43.** Layer thicknesses (A) and relative activities (B) of EstLip\_Dim shielded with layers of different compositions. (C) Scanning electron micrograph of EstLip\_Dim shielded with aminopropyl-triethoxysilane and tetraethyl orthosilicate (AT), aminopropyl-triethoxysilane, tetraethyl orthosilicate and hydroxymethyl-triethoxysilane (ATH), aminopropyl-triethoxysilane, tetraethyl orthosilicate and propyl-triethoxysilane (ATP), and with aminopropyl-triethoxysilane, tetraethyl orthosilicate and benzyl-triethoxysilane (ATB) (scale bar: 200 nm).

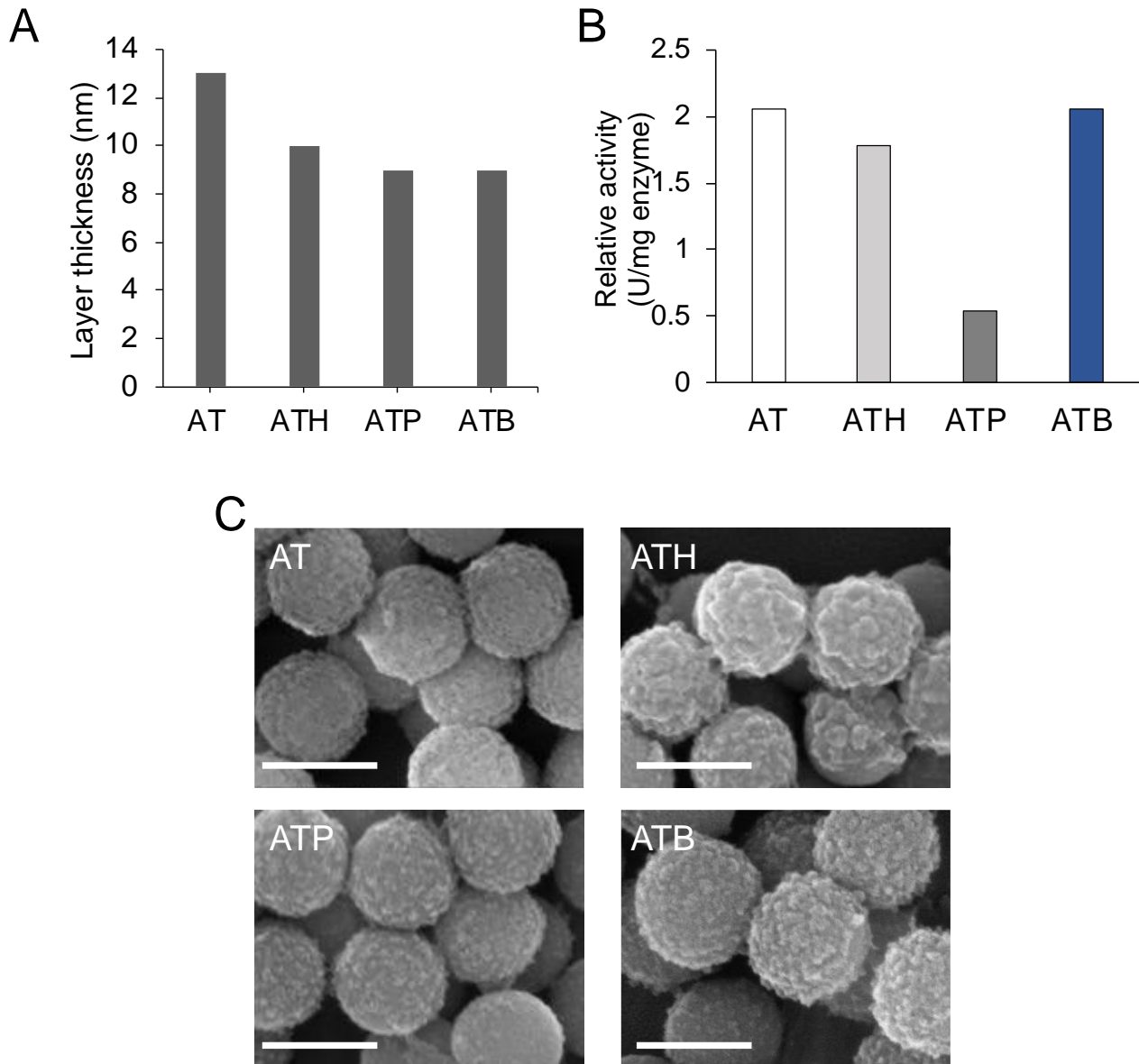


**Fig. 44.** Layer thicknesses (A) and relative activities (B) of FE-Polur1 shielded with layers of different compositions. (C) Scanning electron micrograph of FE-Polur1 shielded with aminopropyl-triethoxysilane and tetraethyl orthosilicate (AT), aminopropyl-triethoxysilane, tetraethyl orthosilicate and hydroxymethyl-triethoxysilane (ATH), aminopropyl-triethoxysilane, tetraethyl orthosilicate and propyl-triethoxysilane (ATP), and with aminopropyl-triethoxysilane, tetraethyl orthosilicate and benzyl-triethoxysilane (ATB) (scale bar: 200 nm).

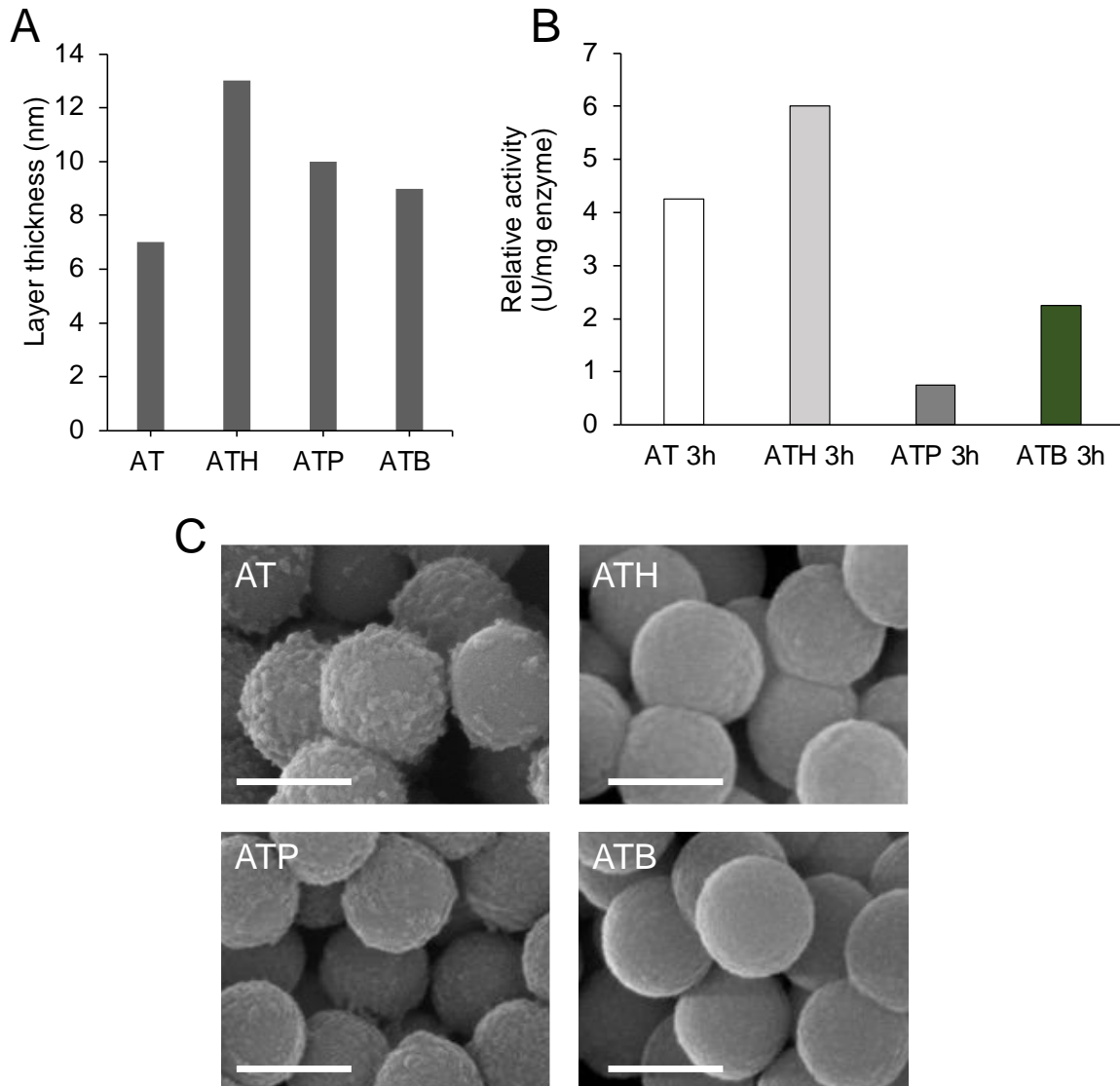


**Fig. 45.** Layer thicknesses (A) and relative activities (B) of EstLip\_PTEST 1 shielded with layers of different compositions. (C) Scanning electron micrograph of EstLip\_PTEST 1 shielded with aminopropyl-triethoxysilane and tetraethyl orthosilicate (AT), aminopropyl-triethoxysilane, tetraethyl orthosilicate and hydroxymethyl-triethoxysilane (ATH), aminopropyl-triethoxysilane, tetraethyl orthosilicate and propyl-triethoxysilane (ATP), and with aminopropyl-triethoxysilane, tetraethyl orthosilicate and benzyl-triethoxysilane (ATB) (scale bar: 200 nm).

### 6.7. CalA lipase

For an easy purification, engineered enzymes are usually produced with a tag (*e.g.*, poly-histidine tag, abbreviated as His-tag). The separation of these proteins is performed through affinity chromatography, using beads that have a nickel [II] ion chelated by a molecule of nitrilotriacetic acid (NTA). On the basis of this model, the surface of silica particles (diameter 300 nm) was modified to allow at the same time the “fishing” of the enzyme of interest for example from a cell extract, and the immobilization on the carrier. In more details, amino modified silica particles were reacted with glutaraldehyde. Afterwards, the modified particles were reacted with lysyl-nitrilotriacetic acid (Lys-NTA). The obtained particles suspension was activated with  $\text{Ni}^{2+}$ , and it was incubated with a commercially available poly-His-lipase (*Candida antarctica* lipase A, CalA). The following control samples were included in the experimental procedure: 1) particles modified with Lys-NTA but without  $\text{Ni}^{2+}$ ; 2) silica particles crosslinked with glutaraldehyde and 3) amino modified silica particles. The catalytic activity of the lipase was measured using pNPB as a substrate. As shown in Fig. 46, the lipase which was immobilized through the His-Tag onto particles carrying not only the Lys-NTA moiety but also the  $\text{Ni}^{2+}$ , had the highest activity (140 U/mg<sub>Cal-A</sub>) compared to the control samples. The lipase

immobilized through the His-tag was further shielded with an organosilica layer containing (3-aminopropyl)-triethoxysilane and tetraethyl orthosilicate. The results showed that after the shielding, the lipase preserved as much as the 57% of activity compared to the immobilized version of the enzyme. These results confirm that the shielding of an enzyme anchored by a non-covalent interaction into the carrier (poly-His-Ni<sup>2+</sup>-NTA) is stable and prevent the leaching of the enzyme from the carrier.

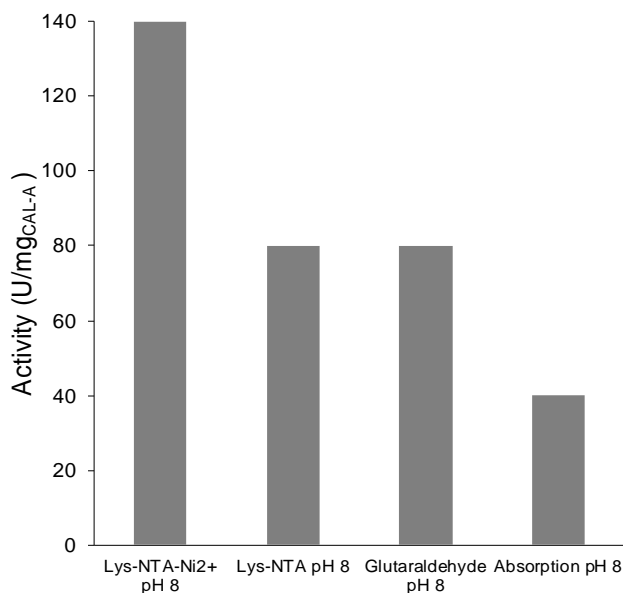


**Fig. 46.** Catalytic activity of a His-tag lipase (CalA) immobilized on silica particles. Different methods of enzyme anchoring are shown.

### 6.8. EH3 esterase

By applying the technology of enzyme supramolecular engineering, a non-enantioselective ester hydrolase, namely EH<sub>3</sub> has been converted into a highly enantioselective yet promiscuous biocatalysts. EH<sub>3</sub> was covalently anchored onto the surface of amino modified silica particles and shielded with layers of different compositions including organosilanes able to enhance hydrophobic effects (H-bonding,  $\pi$ - $\pi$ , and electrostatic interactions), with the surface of the enzyme: (3-aminopropyl)triethoxysilane (A), tetraethyl orthosilicate (T), 1-(3-(trimethoxysilyl)propyl)urea (Ur), benzyltriethoxysilane (Bz), hydroxymethyltriethoxysilane (Hm), and n-butyltriethoxysilane (Bu). The immobilized and shielded H<sub>3</sub> catalysts were tested for the kinetic resolution of different ester substrates. The soluble enzyme, EH<sub>3</sub>, did not display enantioselectivity for any of the esters tested. The absence of enantioselectivity can be attributed to the large volume of the active site of the enzyme. No significant improvement in enantioselectivity was observed after immobilization in the absence of the shield. EH<sub>3</sub> shielded with organosilanes including different ratios of A and T had a relevant enantioselectivity (results reported in the Table 20). The gain in enantioselective properties of EH<sub>3</sub> can be explained in terms of a rearrangement of the residues in the proximity of the catalytic site of the enzyme by means of the enzyme–shield interaction. Such a reorientation might position hydrophilic residues pointing toward the acyl/alcohol binding sites, enabling specific interactions that favour one enantiomer rather than another. Moreover, the beneficial effect of the shielding on the enzyme stability in solvent has been demonstrated. In more details,  $\alpha$ -naphthyl acetate was selected as a model substrate. The hydrolysis of the substrate was followed in solutions containing increasing proportions of acetonitrile (ACN), a solvent extensively used in industrial processes. Samples were measured using high-performance liquid chromatography (HPLC).

**Table 20.** Enantiomeric excess (%) for methyl (R/S)-2-phenylpropanoate as determined by gas chromatography (GC) following hydrolysis of a racemic mixture using soluble EH<sub>3</sub>, EH<sub>3</sub>-immobilized and EH<sub>3</sub> shielded with layers of different composition. (Results correspond to average values of three technical assays using one immobilized preparation per each enzyme).

Sample	Enantiomeric excess (%)
--------	-------------------------

EH <sub>3</sub>	41.70±0.48 %
EH <sub>3</sub> -immobilized	70.80±0.50%
EH <sub>3</sub> -T/A [1/1]	83.50±1.17%
EH <sub>3</sub> -T/A [4/1]	98.40±0.14%
EH <sub>3</sub> -T/A [6/1]	99.80±0.44%
EH <sub>3</sub> -T/A [10/1]	99.90±0.18%
EH <sub>3</sub> -TBz/A [4/1]	99.99±0.23%
EH <sub>3</sub> -TUr/A [4/1]	62.00±0.61%
EH <sub>3</sub> -TBu/A [4/1]	99.90±0.80%
EH <sub>3</sub> -THm/A [4/1]	70.50±0.98%
EH <sub>3</sub> -TBzUrBuHm/A [4/1]	99.90±0.18%

The obtained results show that the specific activity of the soluble EH<sub>3</sub> dramatically decreased to the 20% of its initial activity in the presence of 20% ACN and to a value lower than 10% with 40% ACN. At the opposite, the stability of the shielded EH<sub>3</sub> was tremendously improvement for EH<sub>3</sub>-T/A [4/1], EH<sub>3</sub>-T/A [6/1], and EH<sub>3</sub>-T/A [10/1], which displayed high activity even in the presence of large proportions of acetonitrile (Fig. 47). These results confirm that the shield establishes a stable environment around the enzymes.

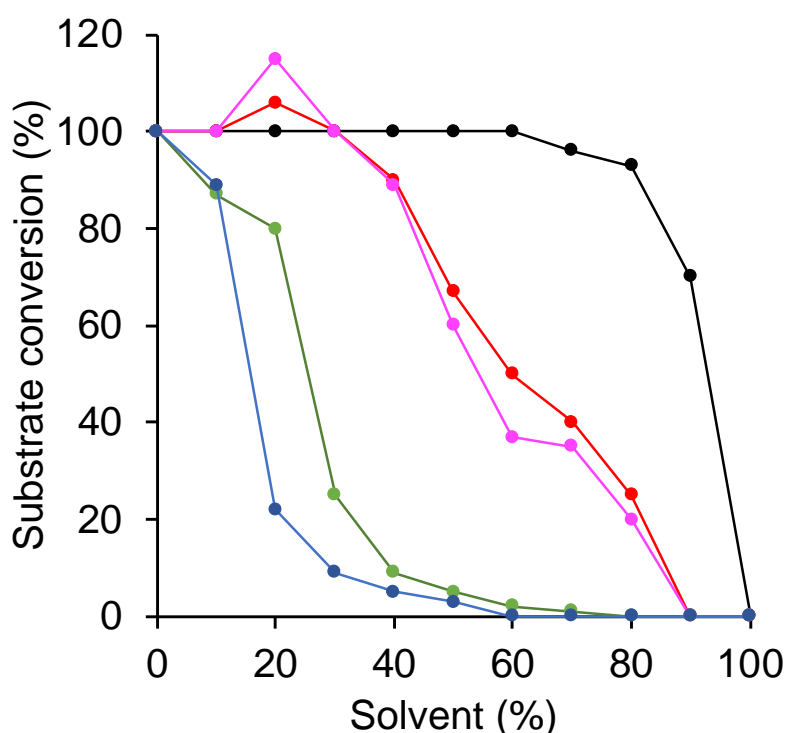


**Fig. 47.** Solvent stability study. Conversion of  $\alpha$ -naphthyl acetate in the presence of increasing proportions of acetonitrile, by soluble EH<sub>3</sub> (blue), EH<sub>3</sub>-T/A[1/1] (green), and EH<sub>3</sub>-T/A[10/1] (purple), EH<sub>3</sub>-T/A[6/1] (red) and EH<sub>3</sub>-T/A[4/1] (black). Reactions were quantified by HPLC.

### 6.9. Laccase from *Trametes versicolor*

Laccases find applications in several industrial processes including textiles manufacturing. In the frame of this deliverable, and as agreed with the consortium's partners, a laccase from *Trametes versicolor* to be applied in the discoloration of dyes used in the textile production, was studied. In more details, the laccase was anchored onto the surface of silica particles via its glycan residues. This immobilization approach is based on the selective boronate ester formation between the glycans of the enzyme and a boronate derivative present on the surface of the carrier. Specifically, amino modified silica particles were reacted with 4-chloromethylphenylboronic acid (CMBA) in basic conditions. After enzyme anchoring, the particles were

shielded with an organosilica layer made of (3-aminopropyl)-triethoxysilane (A) and tetraethyl orthosilicate (T) (Fig. 48A). Particles carrying 2 Units of laccase were resuspended in a solution containing the textile dye Bemaplex Black, and the mediator 2,2,6,6-tetramethylpiperidinyl-1-oxyl (TEMPO). The particles suspension was incubated with the dye for 72 hours at 30 °C under shaking. As shown in Fig. 48B, after 24 and 72 hours, the 48% and the 61% respectively, of dye was discolored.

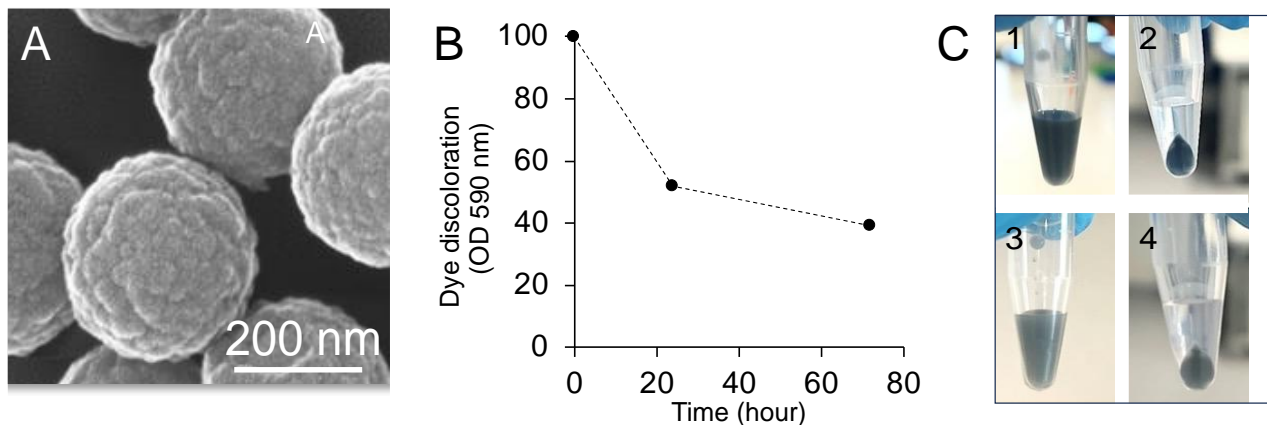


**Fig. 48.** (A) Scanning electron micrographs of shielded silica particles. (B) Bemaplex Black dye discoloration (shown as decrease of the absorbance at 590 nm) catalyzed by the shielded laccase. (C) Suspension of the shielded silica particle at the time zero of the reaction (C1) and after centrifugation (C2). In C3 the suspension of the shielded silica particle after 24 hours of reaction and after centrifugation (C4).

During the experimental procedure, it was observed that the dye was adsorbed into the silica particles (Figure 8C). The obtained results indicated that the absorption of the dye in the particles had a positive impact on the dye discoloration catalyzed by the shielded laccase. Indeed, silica particles act as a concentrator, increasing the efficiency of the enzyme by improving the concentration of dye. To confirm this result, soluble laccase was incubated with Bemaplex Black dye in the presence of enzyme carriers of different type, namely colloidal silica particles, amorphous silica particles and methacrylate resin (Fig. 49). The objective of this experiment was to concentrate the dye in a solid carrier, in order to reduce the volumes during enzymatic reactions. This procedure cannot be accomplished with soluble enzymes, thus limiting their use in industrial applications. In more details, suspensions of different solid carriers (colloidal silica particles, amorphous silica particles and methacrylate resins) were incubated with Bemaplex Black dye in a volume of 10 mL and centrifuged. After centrifugation, the obtained supernatants resulted clear indicating the absence of dye in the suspension, while the particles were stained of dye. The particles were re-suspended in a smaller volume (1 mL) of a buffer solution containing soluble laccase. The dye discoloration mediated by the laccase was run and the measured by UV-VIS at 590 nm (Fig. 50).

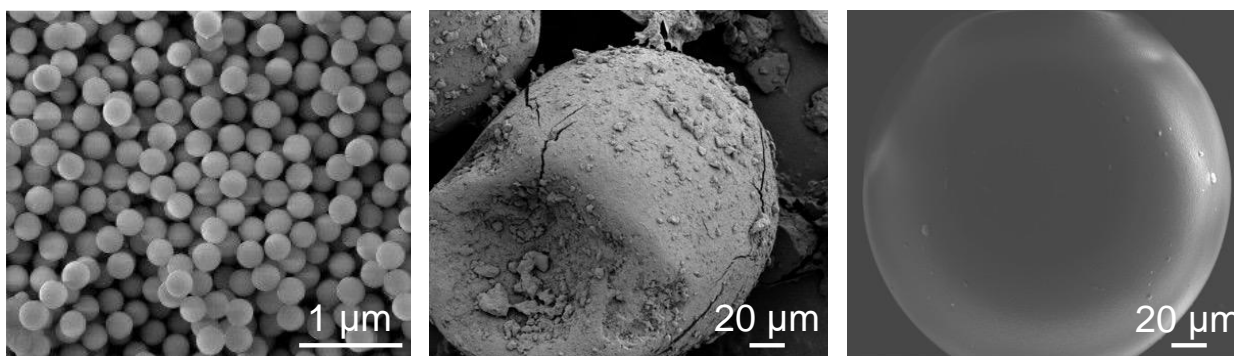


**Fig. 49.** Scanning electron micrographs of particulate carriers used as dye adsorbent. From left to right: colloidal silica particles, (diameter: 300 nm); amorphous silica particles, (average diameter: 250 μm) and methacrylate resin, (average diameter: 300 μm).

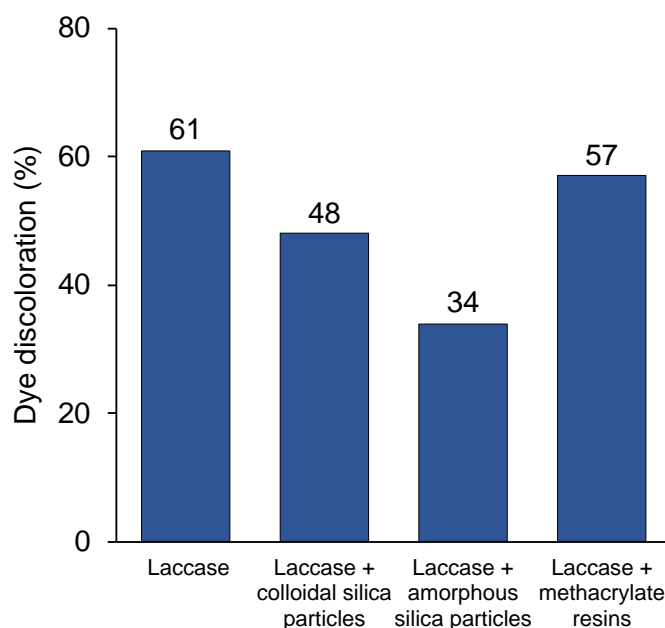


**Fig. 50.** Bemaplex Black dye discoloration catalyzed by laccase enzymes after concentration of the dye into enzyme carriers.

In the considered condition, the methacrylate resin is the best candidate as a dye concentrator. Indeed, the dye discoloration of this sample was comparable to that obtained by the soluble enzyme. The beneficial action of the resin as dye concentrator may be due to the presence of large pores in this material which favor the diffusion of solutions and molecules.

**Conclusions section 6. We have successfully implemented and validated procedures of *supramolecular* engineering applied to obtain 18 engineered enzymes. Morew in details, to date, a total of 29 supramolecular engineered variants from 9 different proteins have been generated and their datasets are available. These proteins are relevant to detergent and textile applications. The complete list of mutants per proteins is detailed below:**

**10 variants EH3**

**4 variants EstLip\_PTEST 1**

**4 variant EstLip\_Dim**

**4 variants FE-Polur1**

**3 variants Lip9**

**1 variant PEH\_Paes\_PE-H-Y250S**

**1 variant EstLip\_TB035**

**1 variant Candida antarctica lipase A (CaLA)**

**1 variant Laccase (*Trametes versicolor*)**

**Three different strategies of enzyme immobilization were applied, namely: the covalent immobilization through an homobifunctional crosslinker, the oriented immobilization through an aminoacidic tag of the enzyme, and the anchoring through the glycans of the enzyme. Different conditions of enzyme shielding were applied by preparing organosilanes mixtures with different compositions and with different ratios of the building blocks. Moreover, different types of carriers were screened (*e.g.*, silica particles and methacrylate resins) in the frame of dye discoloration for textiles manufacturing.**

## 7. New supramolecular engineered enzymes

After successful implementation of *supramolecular* engineering techniques detailed in Section 6, we further implement a method of enzyme stabilisation exploiting the artificial protein chaperone properties of  $\beta$ -cyclodextrin ( $\beta$ -cd) covalently embedded in an ultrathin organosilica layer. Putative interaction points of this

artificial chaperone system with the surface of a selected enzyme, namely the lipase Lip9, were studied in silico using a protein energy landscape exploration simulation algorithm. We found that this enzyme shielding method allows for drastic enhancement of enzyme stability under thermal and chemical stress conditions, along with broadening the optimal temperature range of the biocatalyst. The presence of the  $\beta$ -cd macrocycle within the protective layer supports protein refolding after treatment with a surfactant.

### 7.1. Lip9 protection through $\beta$ -cd supramolecular engineering

We implement a method of enzyme immobilisation and supramolecular organosilica shielding. This method exploits the protein chaperone properties of a novel cyclodextrin building block, Fig. 51. The enzyme selected to establish the proof of concept of this method, a lipase from the *Bacillus* genus, when shielded in CD-containing organosilica, exhibits not only higher thermal stability but also an improved capacity to refold after chaotropic treatment. We expect this method to be versatile in that it can be applied to a range of enzymes for which thermal stability is an issue. This method can eventually contribute to improve the efficiency of industrial biocatalytic processes.

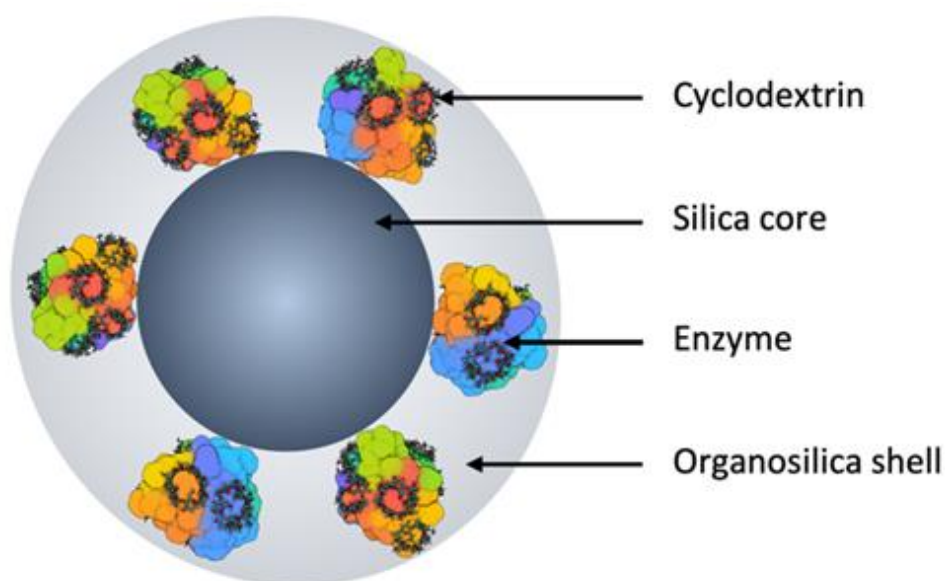
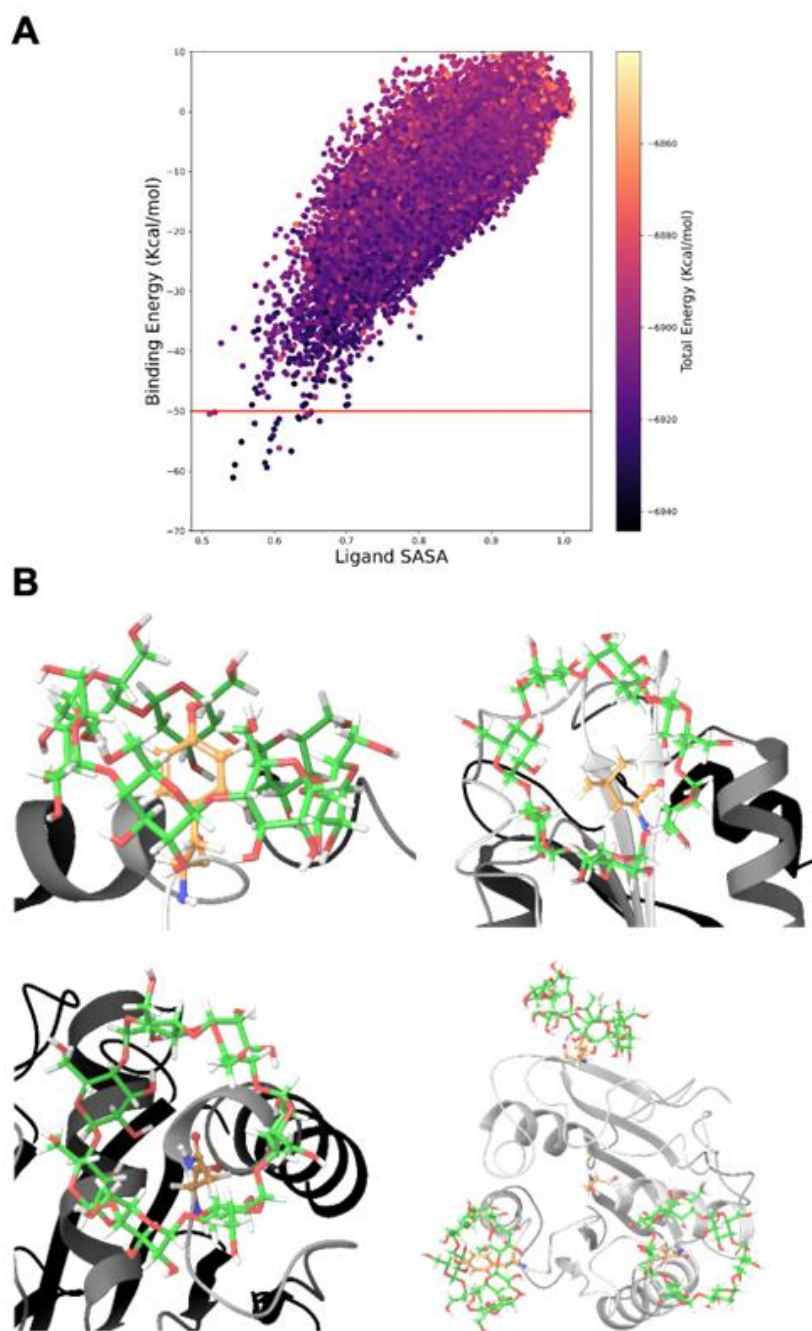


Fig. 51. Schematic representation of chaperone-stabilised enzyme embedded in an organosilica layer.

As model enzyme, we used a lipase enzyme (Lip<sub>MRD9</sub>) from the *Bacillus* genus (WP\_034624255.1), identified by sequence-based metagenomic bioprospecting. First, we studied the possible CD-binding sites at the surface of this model protein. To that end, we employed the SiteFinder PELE protocol. The simulation encompassed 191,000 sampling steps, comprehensively exploring the protein surface. Fig. 52A illustrates the energy profile (created with Matplotlib library) of the Lip<sub>MRD9</sub>-CD interaction, where we monitored the ligand solvent accessible surface area (SASA) versus the protein-CD binding energy. Notably, few binding poses reached energies of -60 Kcal/mol, indicative of a robust interaction between the CD and the protein's surface. Furthermore, the lowest binding energies align with the minimum ligand SASA and minimum total energies of the system, reinforcing the concept of heightened affinity in that specific protein region. A focused analysis was then performed on those poses with the lowest binding energy, based on filtering the CD orientation where secondary alcohols are required to be oriented towards the protein surface.<sup>21</sup> This was justified by the fact that the CD building block produced is modified at the primary rim; this is expected to drastically reduce its ability to bind to the protein surface via the primary rim. Out of the 25 steps with a binding energy lower than -50 Kcal/mol, 9 conformed to the correct orientation. Within these 9 steps, we identified three distinct binding sites (Fig. 52B).



**Fig. 52.** Results for the first round of SiteFinder PELE protocol simulations. Solvent Accessible Surface Area (SASA) vs binding energy (Kcal/mol) for the whole simulation (A). The energy profiles were created with the Matplotlib library. Representation of the top three CD binding sites identified during the SiteFinder PELE simulation; residues inside the CDs cavity and catalytic serine are shown in orange (B).

After identifying the most promising three CD binding sites, a subsequent round of the SiteFinder PELE protocol was initiated. In this phase, the protein bound to the three CDs was considered the receptor, while an additional CD molecule was designated as the ligand. This strategy aimed to comprehensively explore the protein's surface with the three top binding sites already occupied, shedding light on potential tendencies of CDs to bind proteins that were already engaged with other CDs. As depicted in the scatter plot in Fig. 3A, just a few simulation steps managed to surpass the -50 Kcal/mol barrier. However, upon closer examination of the poses exhibiting binding energy below -40 Kcal/mol, a total of 44 structures, we identified 17 accurately positioned, ultimately leading to the selection of 5 distinct binding sites. Consequently, a total of 8 binding

sites were now discernible (Fig. 53B). For each of the identified CD binding sites, a structural analysis was conducted. As depicted in the table, every pose exhibits a minimum of 5 hydrogen bonds between the protein and the ligand, among other interactions. The residues found within the CD cavities comprise Tyr, Leu, Asn and Ile. Three representative poses showcasing these interactions are shown in Fig. 52B. This set of results collectively supported the hypothesis of CDs binding at the protein surface through synergistic hydrogen bonding and hydrophobic inclusion.

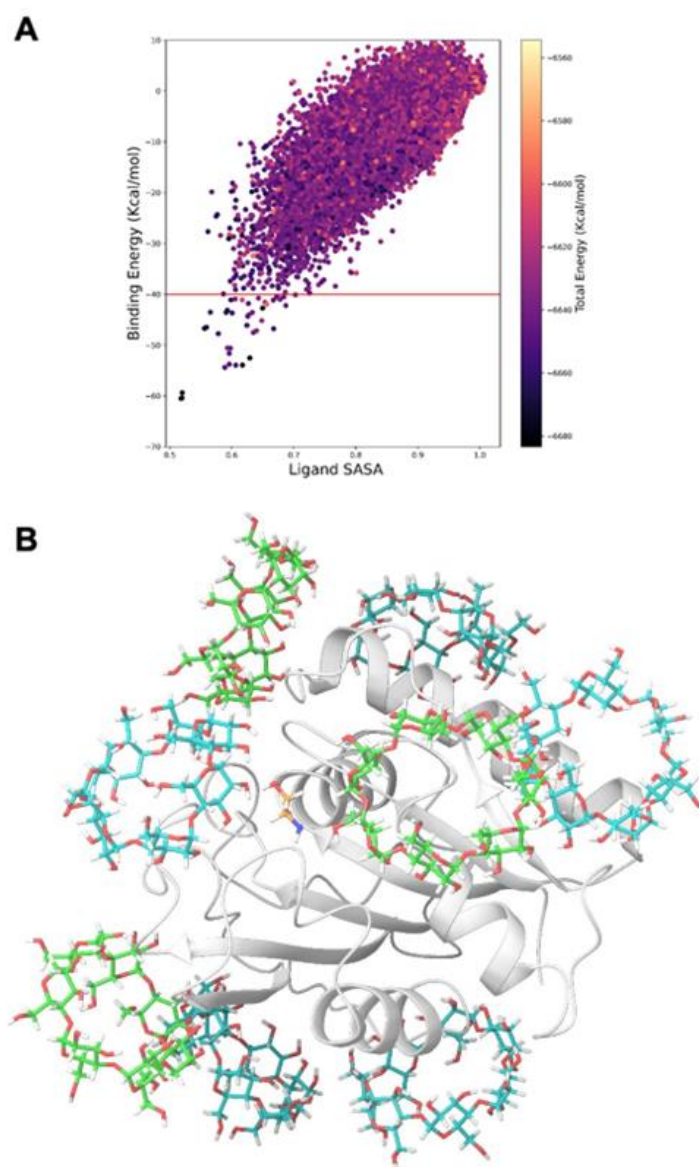


**Fig. 53.** Results for the second round of SiteFinder PELE protocol simulations. Solvent accessible surface area (SASA) vs binding energy (Kcal/mol) for the whole simulation of the protein (A). The energy profiles were created with the Matplotlib library. Visualisation of the LipMRD9 receptor bound to 8 CDs, showcasing the binding sites identified in this subsequent simulation round in cyan, the previously selected in green, and catalytic serine is shown in orange (B).

Considering that shield formation occurs via organosilane self-sorting at the protein surface followed by polycondensation, we decided to produce a CD-derivative that can be used as a layer building block, *i.e.* bearing a tri-ethoxysilane moiety. To that end, native  $\beta$ -CD was reacted with 3-isocyanatopropyl-trimethoxysilane in dimethylformamide (80 °C); Fig. 54. The reaction product, CD-TES, was characterised by means of nuclear magnetic resonance ( $^1\text{H}$  and  $^{13}\text{C}$ ), Fourier transform infrared spectroscopy and mass spectrometry. Collectively, the results confirmed the successful carbamate bond formation with an average of 1 moiety per CD macrocycle.

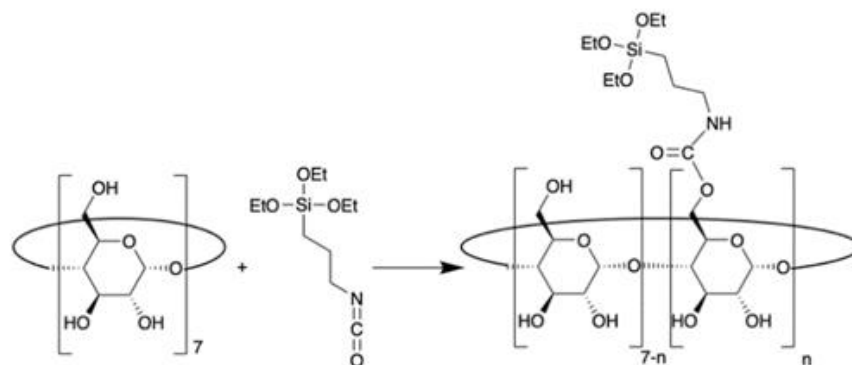


**Fig. 54.** Chemical synthesis of a CD-TES, a  $\beta$ -CD derivative bearing tri-ethoxysilane functions,  $n \approx 1.5$  as estimated by  $^1\text{H NMR}$

Our model enzyme, Lip<sub>M<sub>RD9</sub></sub> (specific activity 19.3 U mg<sup>-1</sup>) was immobilised at the surface of amino-modified SPs (average diameter 290 nm  $\pm$  20 nm). The SPs were further reacted with a mixture of tetra-ethyl-orthosilicate (TEOS), aminopropyltriethoxysilane (APTES) and CD-TES to yield SPs with immobilised Lip<sub>M<sub>RD9</sub></sub> and shielded within a CD-containing organosilica layer, hereafter referred to as SP-Lip<sub>M<sub>RD9</sub></sub>-OS<sub>CD</sub>. Reference particles, SP-Lip<sub>M<sub>RD9</sub></sub>-OS<sub>REF</sub>, were produced by omitting the addition of CD-TES. The particles produced were characterised by scanning electron microscopy (SEM); **Fig. 55**. The micrographs showed, for SP-Lip<sub>M<sub>RD9</sub></sub>-OS<sub>CD</sub>, a close-to-linear increase of the particles' diameter at a rate of *ca.* 6.5 nm/h; **Fig 55E**.

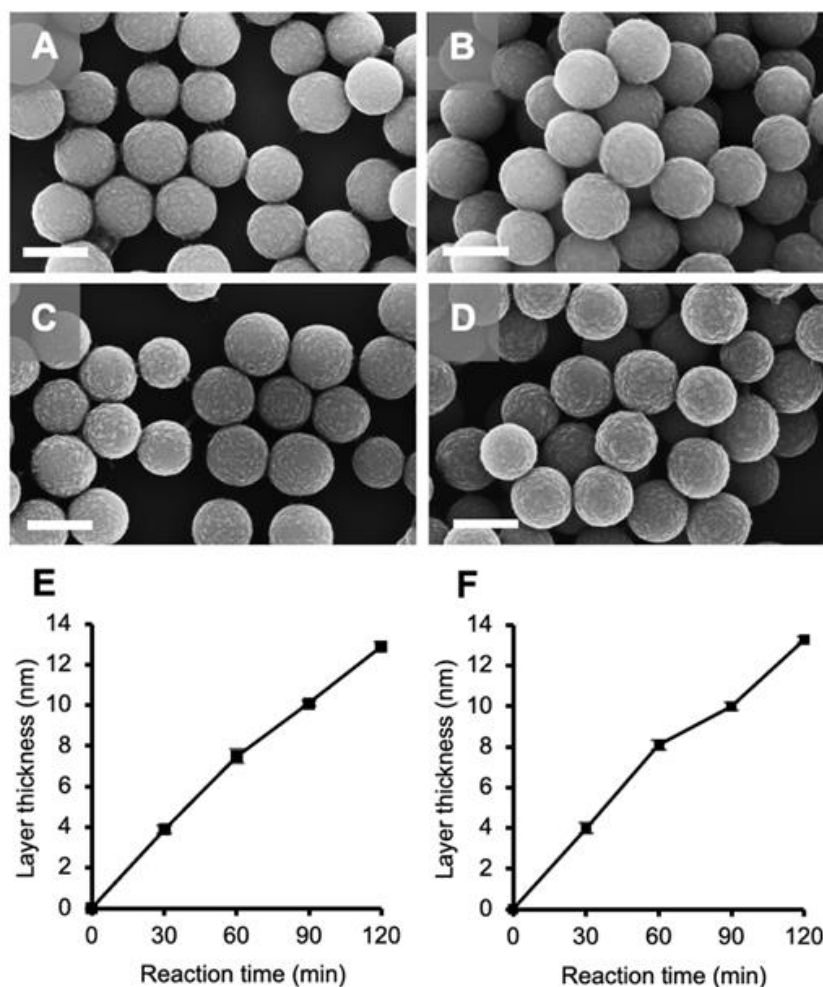


**Fig. 55.** Scanning electron micrographs of SP-LipMRD9-OSCD measured after 30 (A), 60 (B), 90 (C) and 120 (D) min of layer polycondensation reaction. Layer thickness measured via a statistical analysis carried out on at least 100 SPs measured by SEM for

SP-LipMRD9-OSCD (E) and SP-LipMRD9-OSREF (F). Scale bars represent 200 nm. Error bars represent standard deviation measured on at least 100 nanoparticles

It was accompanied by a moderate increase in surface roughness over the reaction duration, without impact on the polydispersity index which remained of 0.005. The layer growth kinetics for SP-Lip<sub>MRD9</sub>-OS<sub>REF</sub> followed a similar trend confirming the lack of relevant effect of CD-TES on the layer growth kinetics; Fig. 55F.

Next, we measured the biocatalytic activity of the immobilised enzymes using an established spectrophotometric assay of *p*-nitrophenyl butyrate hydrolysis; Fig. 56. The specific activity of SP-Lip<sub>MRD9</sub> was measured to be 14.0 U mg<sup>-1</sup>. For SP-Lip<sub>MRD9</sub>-OS<sub>CD</sub>, an activity increase to 127% and 133% (normalized to the specific activity of SP-Lip<sub>MRD9</sub>) was measured for layer thickness values of 4.2 and 8.1 nm, respectively. When the layer was thicker at 10.9 and 14.5 nm, the activity slightly decreased to 118% and 97%. A similar trend was found for SP-Lip<sub>MRD9</sub>-OS<sub>REF</sub>.

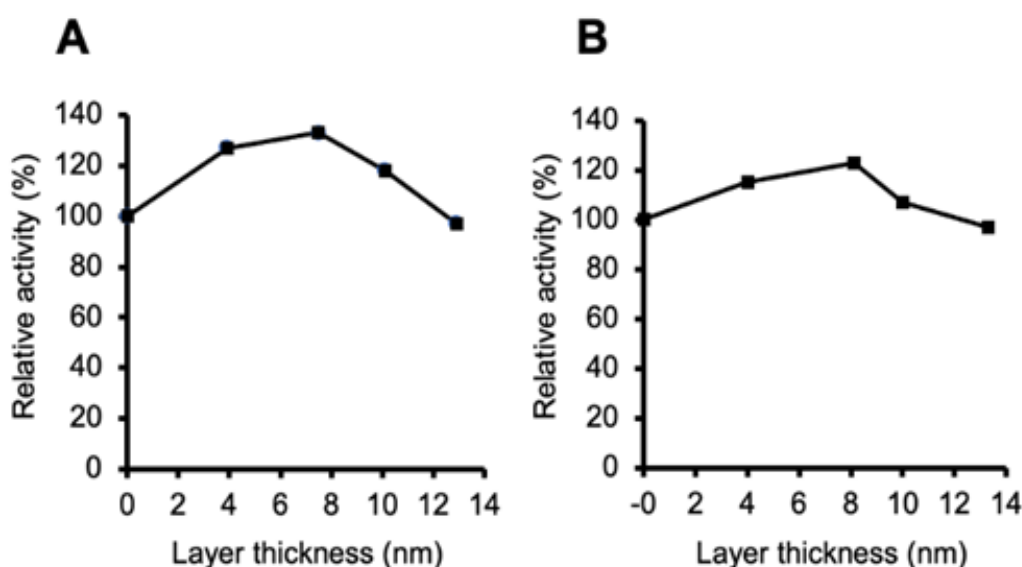
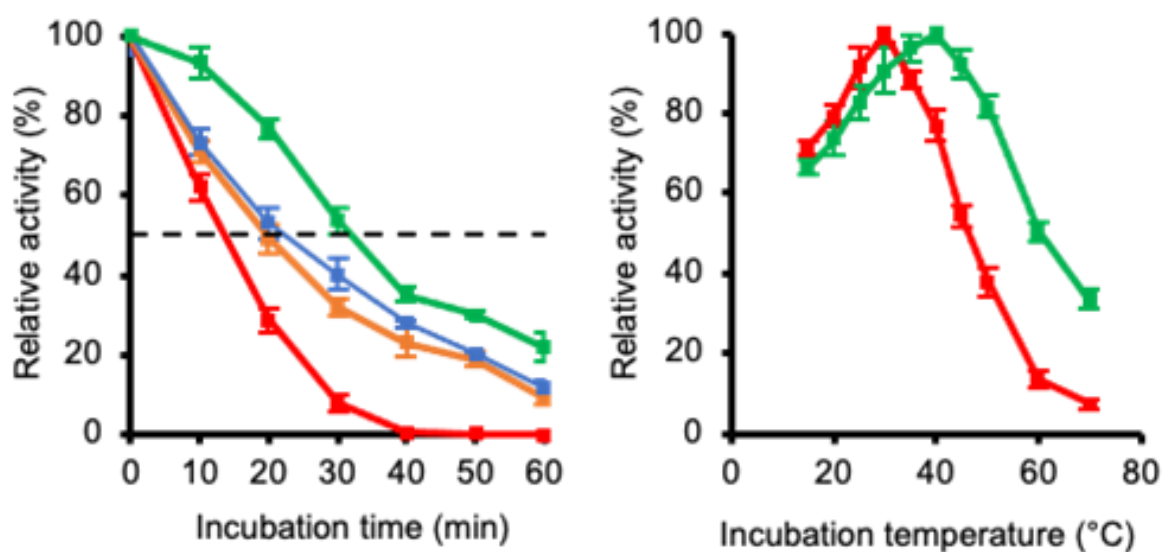


Fig. 56. Enzymatic activity measured for SP-LipMRD9-OSCD (A) and SP-LipMRD9-OSREF (B) Values are normalised with the activity measured in the absence of shielding layer; error bars represent standard deviation measured on triplicates.

Next, we measured the influence of the artificial chaperone building block on the enzyme resistance to thermal stress conditions (Fig. 57A). To that end, the nanobiocatalysts produced were incubated at 50 °C for increasing durations. The soluble enzyme showed a decrease of activity to values of 62.1, 28.8 and 7.8 % after 10, 20 and 30 min of reaction. This corresponds to a half-life of *ca.* 13 min. SP-Lip<sub>MRD9</sub> and SP-Lip<sub>MRD9</sub>-OS<sub>REF</sub> displayed similar trends, with a slightly higher thermal stability than the soluble enzyme, with half-life values of 15 and 17 min, respectively. The stability of SP-Lip<sub>MRD9</sub>-OS<sub>CD</sub>, however, is markedly higher, with values of activity of 93.3, 76.8, 53.6 % after 10, 20 and 30 min of incubation. This corresponds to a half-life of *ca.* 32 min and represent an increase of 246 % when compared to the soluble enzyme. This consistent increase in enzyme stability may be directly attributed to the presence of the  $\beta$ -CD macrocycle in the protective layer. A stronger set of interactions between the surface of the protective shell and that of the protein may contribute to limit the detrimental thermodynamics effects of temperature on the protein conformation. Further, the biocatalytic activity the nanobiocatalysts produced was also studied at increasing reaction temperatures (Fig. 57B). The soluble enzyme, Lip<sub>MRD9</sub>, showed an optimum activity at 30 °C and activity values over 80 % in the range of 25-35 °C. The engineered counterpart, SP-Lip<sub>MRD9</sub>-OS<sub>CD</sub>, showed a maximum activity value at 40 °C and maintained more than 80 % of activity over a broad range of 25-55 °C. The shift in the optimal temperature value and the relevant broadening of the

temperature profile may be attributed to enzyme interactions with the support matrix. Collectively, these results bring compelling evidence of the stabilising effect of  $\beta$ -CD in the engineered organosilica layer.

Thermal and chemical protein denaturation are taking place following different molecular mechanisms involving different thermodynamic pathways. The encouraging results obtained with thermal stabilisation prompted us to test the stabilisation effect of the chaperone-based protective layer against chemical stress conditions. First, we tested the influence of an anionic surfactant, namely sodium dodecyl sulphate (SDS). Lip<sub>MRD9</sub>, SP-Lip<sub>MRD9</sub>-OS<sub>REF</sub>, and SP-Lip<sub>MRD9</sub>-OS<sub>CD</sub> were incubated for 20 min in a buffered solution containing SDS (1%) prior to activity measurements; results are shown in Fig. 58A. The activity of Lip<sub>MRD9</sub> dropped to 3 %; activity values measured for SP-Lip<sub>MRD9</sub>-OS<sub>REF</sub> and SP-Lip<sub>MRD9</sub>-OS<sub>CD</sub> were consistently higher, with values of 15% and 21%, respectively. This demonstrated a moderate positive impact of the  $\beta$ -CD on the protein stability. Additionally, the possibility to refold the enzyme after SDS treatment was tested. To that end, Lip<sub>MRD9</sub>-OS<sub>REF</sub> and SP-Lip<sub>MRD9</sub>-OS<sub>CD</sub> were submitted to centrifugation and resuspended in Tris-HCl buffer. For the soluble enzyme, the surfactant was removed by dialysis against the same buffer. Activity measurements showed that while Lip<sub>MRD9</sub> recovered only 20 % of activity, SP-Lip<sub>MRD9</sub>-OS<sub>REF</sub> and SP-Lip<sub>MRD9</sub>-OS<sub>CD</sub> showed significantly better results with 68 and 84 %, respectively. It was attributed to the capacity of the cyclodextrin macrocycle to strip away surfactant molecule. In the present work, it is more likely that the enzyme recovered its three-dimensional structure owing to the appropriate positioning of the CD moieties in the organosilica matrix.



**Fig. 57.** Enzymatic activity measured at 50 °C during 60 min incubation for SP-LipMRD9-OSCD (green), SP-LipMRD9-OSREF (blue), SP-LipMRD9 (orange), and LipMRD9 (red) (A). Temperature profile for SP-LipMRD9-OSCD (green) and LipMRD9 (red) (B). Error bars represent standard deviation measured on triplicates.

Next, we studied the denaturing effect of urea on Lip<sub>MRD9</sub> and engineered counterparts by measuring the enzymatic activity after 20 minutes incubation with urea solution (6M); as shown in Fig. 58B, SP-Lip<sub>MRD9</sub>-OS<sub>REF</sub>, and SP-Lip<sub>MRD9</sub>-OS<sub>CD</sub> were able to retain 16 and 27% activity after treatment, respectively, while Lip<sub>MRD9</sub> could only retain 7% of its initial activity. This set of results suggest that the organosilica layer surrounding the enzyme supports its refolding as strongly suggested by the activity recovery values measured. While it is expected that the soluble enzyme may undergo irreversible aggregation and that immobilization may prevent that, the significantly enhanced recovery for SP-Lip<sub>MRD9</sub>-OS<sub>CD</sub> brings additional evidence of the stabilising effect of  $\beta$ -CD within the protective layer.

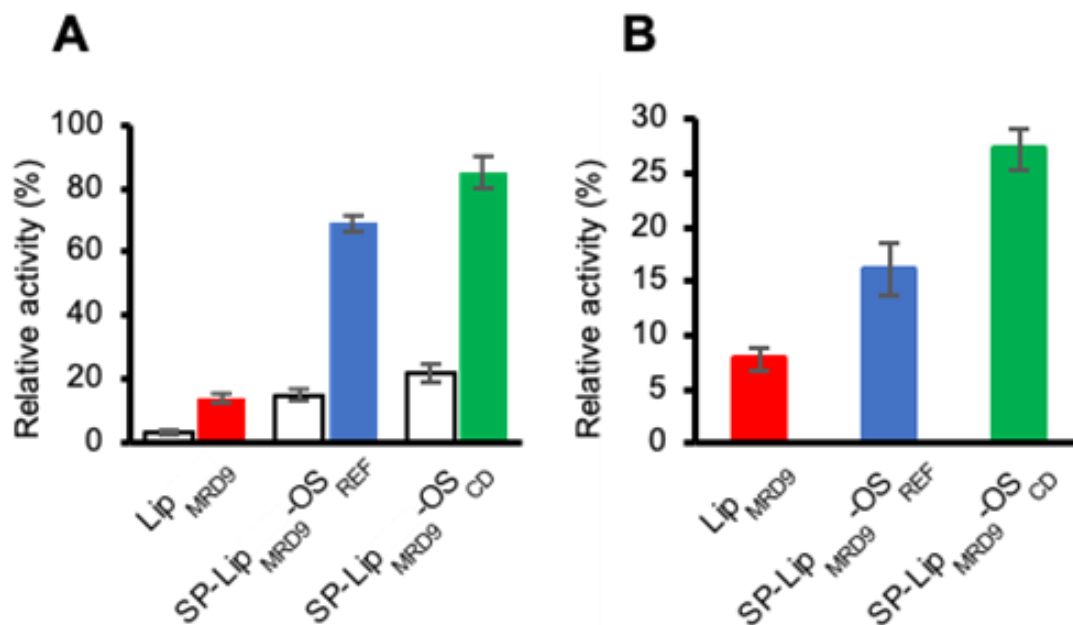


**Fig. 58.** Enzymatic activity measured after SDS (1%) treatment for LipMRD9, SP-LipMRD9-OSREF, SP-LipMRD9-OSCD (white bars), and after further dialysis (red, blue, and green bars, respectively) (A). Enzymatic activity measured after urea (6M) treatment for LipMRD9, SP-LipMRD9-OSREF, and SP-LipMRD9-OSCD (B); error bars represent standard deviation measured on triplicates.

For methodological details, detailed results and datasets (open access), see [Kalourazi et al., 2024](#).

Conclusions Section 7. **In summary, we have demonstrated that the use of a cyclodextrin tri-alkoxysilane derivative in the formulation of an enzyme via organosilica shielding provides the immobilised biocatalyst with improved stability. In silico modelling using a Monte Carlo-based simulation algorithm allowed the identification of putative binding sites, where the macrocycle interacts with the protein through synergistic hydrogen bonding and hydrophobic inclusion. Once immobilised at the surface of SPs and shielded in a CD-containing organosilica layer, the model enzyme exhibited thermal stability markedly higher than its counterparts. Additionally, the range of temperature at which the enzyme is active was broadened. When subjected to chaotropic stress conditions, supramolecularly engineered enzymes exhibited moderately higher stability. The protein's ability to refold in an active state, however, was markedly enhanced. This increased stability suggests that supramolecularly engineered enzymes with artificial chaperone systems could withstand harsh chemical and physical operational conditions. This is expected to provide a longer shelf life and potential for broader applications in biotechnology.**

## 8. Conclusions and outlooks

The Deliverable D5.6 presents several notable conclusions across different sections. Firstly, the PluriZyme strategy has been successfully validated, resulting in the generation of five engineered enzymes with multipurpose functionalities, along with mutants of Fragaecetoxin C for nanosized PET recycling in textile processing waste streams. Secondly, mutants of various enzymes exhibit promise for detergent and textile applications, showcasing improved performance and stability compared to wild-type enzymes. Notable candidates include Lip9 Val161Ser, Lip5W89M/L60F, Lip5lid, PEH\_Paes\_PE-H Y250S, and PET46 A46V. Thirdly, a substantial number of mutants from 35 different proteins relevant to detergent and textile applications have been generated, showing enhanced activities and stability. Fourthly, supramolecular engineering techniques have yielded 18 engineered enzymes and 29 variants from 9 proteins, with strategies of enzyme immobilization and shielding explored to enhance stability and performance. Finally, the use of cyclodextrin tri-alkoxysilane derivative in enzyme formulation via organosilica shielding has shown significant improvements in enzyme stability, thermal resilience, and resistance to chaotropic stress, suggesting broader

applications in biotechnology with extended shelf life. It is to highlight that EstLip\_TB035 (mutant available in which Type II-Sec signal peptide was substituted by a SecI signal peptide sequence) and EstLip-PtEst1 (supramolecularly engineered variant available) have been point in the frame of Deliverable D7.1 as priority targets for full scale wash pre-industrial validation tests. Other enzymes such as Lip9 has been pointed in the frame of Deliverable D7.1 as potential candidate for detergent and textile applications, and thus the higher stable mutant Lip Val161Ser and the supramolecular engineered variant SP-Lip<sub>MRD9</sub>-OS<sub>CD</sub> may be considered for next validation tests. In conclusion, based on the results described in this document, we consider that we have achieved the objectives of **Deliverable D5.6**.

## 9. Final remarks

In light of the comprehensive findings and detailed analyses presented in this report, it is clear that the objectives of the Deliverable D5.6 outlined at the onset of this project have been successfully met. A copy of the submitted Deliverable D5.6 has been recorded in the intranet's project website. See [www.futureenzyme.eu](http://www.futureenzyme.eu) -> login -> private-area -> DELIVERABLES & MILESTONES -> DELIVERABLES -> D5.6\_Datasets of engineered variants. Due to its extensive size, the Tables S1-S4 with datasets are provided in the [www.futureenzyme.eu](http://www.futureenzyme.eu) -> login -> private-area -> Shared data -> Datasets -> Table S1, Table S2, Table S3, Table S4 for D5.6\_Datasets of engineered variants.